Phenomenological Study of Fuel Relocation Behavior and Formation of Debris Bed in Metal-fueled Sodium-cooled Fast Reactor

Hyo Heo

Department of Nuclear Engineering

Graduate school of UNIST

Phenomenological Study of Fuel Relocation Behavior and Formation of Debris Bed in Metal-fueled Sodium-cooled Fast Reactor

A dissertation
submitted to the Graduate School of UNIST
in partial fulfillment of the
requirements for the degree of
Doctor of Philosophy

Hyo Heo

12.19.2018
Approved by

_____

Advisor
Prof. In Cheol Bang

Phenomenological Study of Fuel Relocation Behavior and Formation of Debris Bed in Metal-fueled Sodium-cooled Fast Reactor

Hyo Heo

This certifies that the dissertation of Hyo Heo is approved.

12.19.2018

signature

Advisor: In Cheol Bang

signature

Dong Wook Jerng

signature

Yun-Jae Kim

signature

Seung Jun Lee

signature

Eisung Yoon

Abstract

Metallic fuel has been proposed as one of fuel types in sodium-cooled fast reactor (SFR). The metallic fuel has advantages in terms of safety issues. Especially, it has been known that severe accident for metal-fueled SFR might be terminated earlier due to its safety characteristics. Hypothetical core disruptive accidents (HCDA) are considered as the accident which causes fuel melting and cladding failure in SFR. When cladding bleach occurs in initiating phase of HCDA, molten fuel is relocated debris is formed in fuel assembly. Severe accident consequences are determined depending on these phenomena. Thus, it is necessary to study fuel behavior and solidification phenomena in severe accident. However, the studies related to the metallic fuel in severe accident condition were partly performed. There is still a lack of fundamental knowledge about the severe accident phenomena and related physics. Therefore, the present study focuses on fuel relocation behavior and debris formation phenomena, which is in specific accident scenario, with experimental approaches.

The fuel relocation behavior has been not studied clearly, especially in initiating phase of HCDA. To understand the phenomena and provide physical insights, there were visual studies for various experimental conditions. The studies were performed as a parametric study so key parameters affecting the fuel relocation behavior were selected. The parameter discussed in the experiment are coolant boiling, channel condition, initial melt temperature, and initial melt ejection pressure etc. In the fuel relocation experiments, simulants were used instead of metallic fuel. Wood's metal and gallium were used as the simulant for the metallic fuel in most of experiment. Since the fuel behaviors are driven by force balance, Froude and Weber numbers were compared to investigate similarity. High speed video camera was used to observe the fuel relocation behavior and visual analysis methods were applied on the parameter study. There were two steps to conduct the visualization experiments. Firstly, possible fuel relocation behaviors were observed in small-scaled experimental facility. The experimental facility is called UNIST molten core and coolant interaction experimental facility (UNICORN)-B (baby). From the experiments, it was found that sodium boiling could be powerful driving force for fuel dispersal regardless of channel condition. Then, there were additional visual studies using UNICORN-C (child) which was established considering actual scale of fuel assembly in metal-fueled SFR. As a result, it was clarified that debris bed formation was highly dependent on the fuel relocation behaviors.

Although fuel is ejected into coolant channel, core could be cooled from hydrodynamic point of view. If high porous debris bed is formed, decay heat would be removed using natural circulation flow. UNICORN-A (adult) was established to simulate actual fuel ejection condition in HCDA. Simultaneous occurrence of unprotected transient over power (UTOP) and unprotected loss-of-flow (ULOF) event was selected as a target scenario. A severe accident code SAS4A was used to calculate initial experimental conditions. Radiographic images were obtained to analyze melt relocation behavior. The

experimental results show that melt was not swept out from active core region. Mass fraction of frozen melt was investigated along axial distance. It showed melt was radially dispersed rather than the axial melt dispersal. In addition, most of melt was frozen near cladding failure point where the melt was directly ejected out. Debris bed seemed like agglomerated shape leading to local flow blockage. Since debris bed porosity affects to pressure drop and flow rate of fuel assembly, the porosity was evaluated after the experiment. The porosity was measured with two methods; classical method and post-processing method of radiograph image. The classical method was performed using volume fraction of test section before and after the fuel relocation experiment. Debris bed was measured 0.89 of its porosity with these methods. It could ensure that core has coolability by natural circulation. Thus, it was verified that there was a possibility of early termination of severe accident.

The characteristics of debris bed are mainly determined from physical form of individual debris. Especially, debris bed porosity is affected by debris morphology. In severe accident condition in SFR, metallic fuel had ligament-like shape of debris. This morphology made characteristics of debris bed porosity. The metal fuel had relatively high debris bed porosity. In previous research group, quenching experiments were conducted using molten metal droplet. The debris morphology was analyzed quantitatively. It was insufficient to qualitatively investigate the debris morphology. The present study was performed with experimental works based on theoretical model regarding rapid solidification. It is suggested that debris morphology is attributed to freezing point and instantaneous contact interface temperature between melt and coolant. From rapid solidification experiments, it was shown that high porous debris bed would be formed above porosity of 0.83 based on the reactor accident conditions in ULOF.

Contents

List of figures

List of table

Nomenclature

A	heat transfer area	[m^2]
C_p	specific heat	[J/kg/K]
C_d	drag coefficient	[-]
D	diameter	[m]
g	acceleration due to gravity	[m/s^2]
h	height	[m]
k	thermal conductivity	[W/m/K]
F	force	[kg·m/s^2]
W	work	[kg·m^2/s^2]
T	temperature	[K]

Greek symbols

ρ	density	[kg/m^3]
ε	porosity	[-]
σ	surface tension	[N/m]

Subscripts

fu	fuel
fi	fission gas
so	vaporization of sodium bond
bo	coolant boiling
fr	frictional force by structure
g	gravity
liq,fu	liquid fuel
liq,so	liquid sodium
m	melt
pre	melt ejection pressure
drag	drag force
buo	buoyancy

i	interface between solid and liquid phases
c	coolant

Chapter 1. Introduction

1.1 Background

Metallic fuel has inherent safety characteristics for the mitigation of the accident consequences under design extension conditions (DECs). However, the advantages of the metallic fuel in the transient state have not been enough to solve licensing issues of metal-fueled sodium-cooled fast reactors (SFRs). Although the hypothetical core disruptive accidents (HCDAs) for SFRs with the metallic fuel rarely occur due to its inherent safety and design features, it is needed to clearly evaluate the possibility of an early termination of the transient accident induced by molten metallic fuel-sodium coolant interaction under an initiating phase of the HCDAs, as a part of risk assessment for SFRs. To predict how such accidents progress, the coupled thermal-hydraulic and neutronic phenomena should be identified, but in this study the molten fuel-sodium interaction in terms of only thermal-hydraulics was considered. If the molten metallic fuel is well fragmented by its interaction with the sodium, passive cooling could be expected with guaranteeing effective flow paths for the natural circulation flow. That is a reason why it is should be examined whether the fragmentation of molten metallic fuel occurs inside the subchannel or not[1-15].

After cladding failure, overall severe accident mitigation strategies should be prepared. The metal fueled SFR severe accident scenario needs to be categorized and their mitigation strategies should be established for each phase. As shown in Fig. 1-1, severe accident sequences could be categorized in metal-fueled SFR.

In the initial phase of metal fueled SFR severe accident scenarios, melting of metal fuel and cladding failure are induced with power excursion. After cladding failure, the molten metal fuel shows fragmentation behavior in the core region, which is called the Ex-pin phenomena. Thus, the key safety strategy to mitigate accident progression at this phase, is to discharge melt upwards out of the core. This upward discharge of melt is called as melt levitation. Such melt levitation could ensure early termination of accident progression.

If the early termination of severe accident is not induced in the initial phase, there are two possible explanations. One is that the driving force for the melt levitation is not sufficient, and the other is that the melt falls into a base plate even though the melt was temporarily levitated. In these conditions, the melt may move downward to inlet plenum structure. There could be eutectic reaction between molten metallic fuel and core structure, leading to successive core degradation by eutectic penetration. At UNIST, the eutectic penetration phenomena were visualized using simulants such as gallium and indium as shown in Fig. 1-2. The melt is solidified depending on its behavior and the debris is formed, which is a molten fuel and structure material relocation phase. In general, it is known that debris bed coolability

of molten metal fuel is determined by its conductivity and porosity. There is an experimental database for thermal conductivity of metal fuel and structure materials. On the other hand, the experimental DB for porosity of molten metal fuel debris is insufficient since this debris is formed from unusual reaction, metal-metal reaction. The porosity of molten metal fuel debris is determined by porous structure and this structure depends on quenching of molten fuel and materials properties. Preliminary fragmentation tests in open pool were conducted using simulants at UNIST. In wood's metal-gallium(as a melt and coolant, respectively) reaction, debris surface was somewhat rough, while the debris shape was round and rather smooth in wood's metal-water(as a melt and coolant, respectively) reaction. It showed that the molten material debris was different from the material characteristic. If the coolability of debris bed could be eusured with its high voidage, core decay heat would be removed by natural circulation cooling of sodium. This means that the metal-fueled SFR has coolable geometry even in severe accident scenarios. However, such lab-scaled experiments did not provide reliable data on material characteristic of actual metal fuel.

At the molten fuel and structure material relocation phase, the debris bed could block subchannel exceeding coolability limit. In this case, the relocated molten fuel and structure material would make corium pool locally at the bottom of the reactor vessel, which could threat the integrity of the reactor vessel. This is a long-term cooling phase. To prevent and mitigate these severe cases, innovative passive decay heat removal systems (PDHRS) is required. Korea Atomic Energy Research and Institute (KAERI) has proposed a design measure to mitigate these severe cases, reactor vessel auxiliary cooling system (RVACS). It is a final means to mitigate severe accidents where core region does not have sufficient coolable geometry by any chance. It could passively remove core decay heat by chimney effect during such accident progression.

Fig. 1-3 shows a configuration of initiating phase of HCDA for metal-fueled SFR during an Ex-pin, where pressurized molten metallic fuel is ejected and dispersed into the sub-channel after the fuel pin failure. It is depicted taking into account an unprotected loss-of-flow (ULOF) accident scenario.

Fig. 1-4 represents free body diagram for fuel relocation behavior. The driving forces for melt levitation could be pressurized fission gas in a pin cavity, rapid boiling of sodium bond, coolant sodium boiling caused by a fuel-coolant interaction, and sodium coolant flow. The sodium coolant flow could be neglected in the equation because the severe accident could occur only when unprotected loss-of-flow event should be caused for the metal-fueled SFR. The pressurized fission gas is a key factor in the driving force for the melt levitation among them. The maximum force of each parameter is determined according to accident scenario. If the driving force for melt levitation is less for fully melt levitation which means that all molten fuel is discharged out toward the fuel assembly. The molten fuel which could not be fully levitated fall in fuel assembly, leading to the debris formation. The debris formation, which directly determine coolability in the fuel assembly, is different with the molten fuel behavior. Thus, it is important to obtain physical insight and understanding for molten fuel behavior. After a pin

failure, the molten fuel is fragmented and dispersed with active collision with surrounding structures. The molten fuel behavior includes the successive phenomena and it is highly affected by internal pin pressure which is determined from fission gas and rapid boiling of sodium bond.

1.2 General literature review

A few investigations have been performed to evaluate and investigate fuel relocation phenomena.

Extensive studies regarding fuel relocation behavior in case of the HCDAs under both in-pile and out-of-pile conditions were conducted for metal fuels in the 1960s–1970s, while only few studies of metal fuel relocation behavior were performed because of concerns that the metal fuel could not achieve high burnup due to the irradiation induced swelling problem[16-35]. Following the new metal fuel design development that overcame the swelling problem, experiments regarding thermal hydraulic interaction of molten metallic fuels and liquid sodium have been conducted by several researchers. Nishimura et al.[36, 37] carried out a series of fragmentation experiments using molten metallic simulants in a sodium pool. The simulant materials with quantities ranging from 20 g to 300 g were melted in a crucible with an electrical heater and were dropped into a sodium pool with temperatures from 206 ℃ to 500 ℃. It was reported that the thermal fragmentation originated inside the molten simulants and a solid crust was observed. It was verified that the fragmentation of the molten simulants was attributed to the internal pressure build up by the boiling of sodium, which was locally entrapped inside the molten simulants due to turbulent mixing of the molten simulants and sodium. It was concluded that the superheating and the latent heat of fusion of a molten metal jet were dominant factors governing the thermal fragmentation. The effect of the initial temperature of the coolant sodium on the fragmentation of the simulants was found to be negligible. Most studies that were conducted using metallic simulants in sodium concluded that the molten metals were heavily fragmented after liquid contact and the dominant factors governing the fragmentation were superheating and latent heat of fusion of the simulants[38-44]. Gabor et al.[45-47] conducted experiments using kilogram quantities of various molten uranium alloys in an open sodium pool configuration. They found that the metal fuel fragments created from their pour stream in the open sodium pool were in the form of filaments and sheets with a high bed voidage on the order of 0.9. Their calculation indicated that the debris beds formed by relocated metal fuels in the open pool which is for the coolant outlet. The open sodium pool would be largely coolable by conduction heat transfer. Even under a convective and boiling heat transfer condition, the debris beds were to form for coolable geometry in subchannel. It was found that the debris size was well distributed but the mean size of the debris is about 2-3 mm. That showed the debris size was determined from the experimental condition which means initial melt ejection conditions. Although Gabor et al.'s experiments are useful in evaluating the coolability of relocated metal fuels during the HCDAs in a SFR, they focused on the late phase relocation behavior in which the core material relocates downward through the core support

plate into the inlet plenum where the structures are more open and thus consistent with the open pool configuration. There is still a knowledge gap regarding the initial phase of metal fuel relocation behavior within the core structures in case of the HCDAs. On the other hand, the lead-cooled fast reactor, called LFR, used oxide fuel in general. The characteristics of oxide fuel seem to be different with that of metal fuel. In the steady state, the metal-fueled SFR has asymmetrical temperature profile axially due to the sodium coolant, while there was symmetrical temperature profile in the oxide-fueled LFR. That made the difference of fuel ejection position when the fuel is melted. In transient condition, it is expected that there would be molten fuel behaviors with reactor types. When considering unprotected loss-of-flow (ULOF) event, the fuel dispersion is up to density difference between the fuel and the coolant. The metal fuel is quietly heavier than the sodium, which would lead to its dispersion upward and downward. The fuel motion is more affected the drag force rather than the buoyant force, so the fuel would be levitated and traveled with natural circulation of the LBE, shows the accident mitigation strategy should be prepared to prevent the severe accident.

1.3 Objectives and scope

This manuscript concentrates on 1) direct observation of fuel relocation behavior using simulants like gallium and Wood's metal and 2) investigation of effect of cooling rate on melt solidification.

1) To provide physical insights in fuel relocation phenomena
2) To conduct the parameter study for fuel relocation behavior on melt ejection condition
3) To develop experimental platform to study initiating phase of severe accident for SFR

Chapter 1 introduces fuel relocation phenomena and reviews some studies which were performed for fuel behavior in severe accident.

Chapter 2 shows visual studies for fuel relocation phenomena are described. Using simulant for metallic fuel was introduced to study fuel relocation behavior and its fragmentation phenomena. Melt behaviors was directly observed to investigate the effect of each parameter affecting the relocation phenomena. The dimensionless number such as Froude and Weber were used to compare hydraulic similarity between actual transient condition and experimental condition.

Chapter 3, parametric studies were conducted to assess what parameter is crucial for the fuel relocation behavior. The levitation height of melt, which means melt dispersed upward, was evaluated for predicting a possibility in early termination of accident.

In chapter 4, advanced fuel relocation experiment was conducted considering actual transient condition in metal-fueled SFR. The melt was not swept-out outward active core and frozen in fuel assembly structure. Debris bed porosity after the relocation experiments was analyzed to evaluate core

coolability. The high porous debris bed was formed when the molten metal was rapidly solidified. Debris bed porosity was different depending on debris morphology, especially debris size. Debris size model was developed based on results of quenching experiments.

The conclusions and recommendations are described in chapter 5.

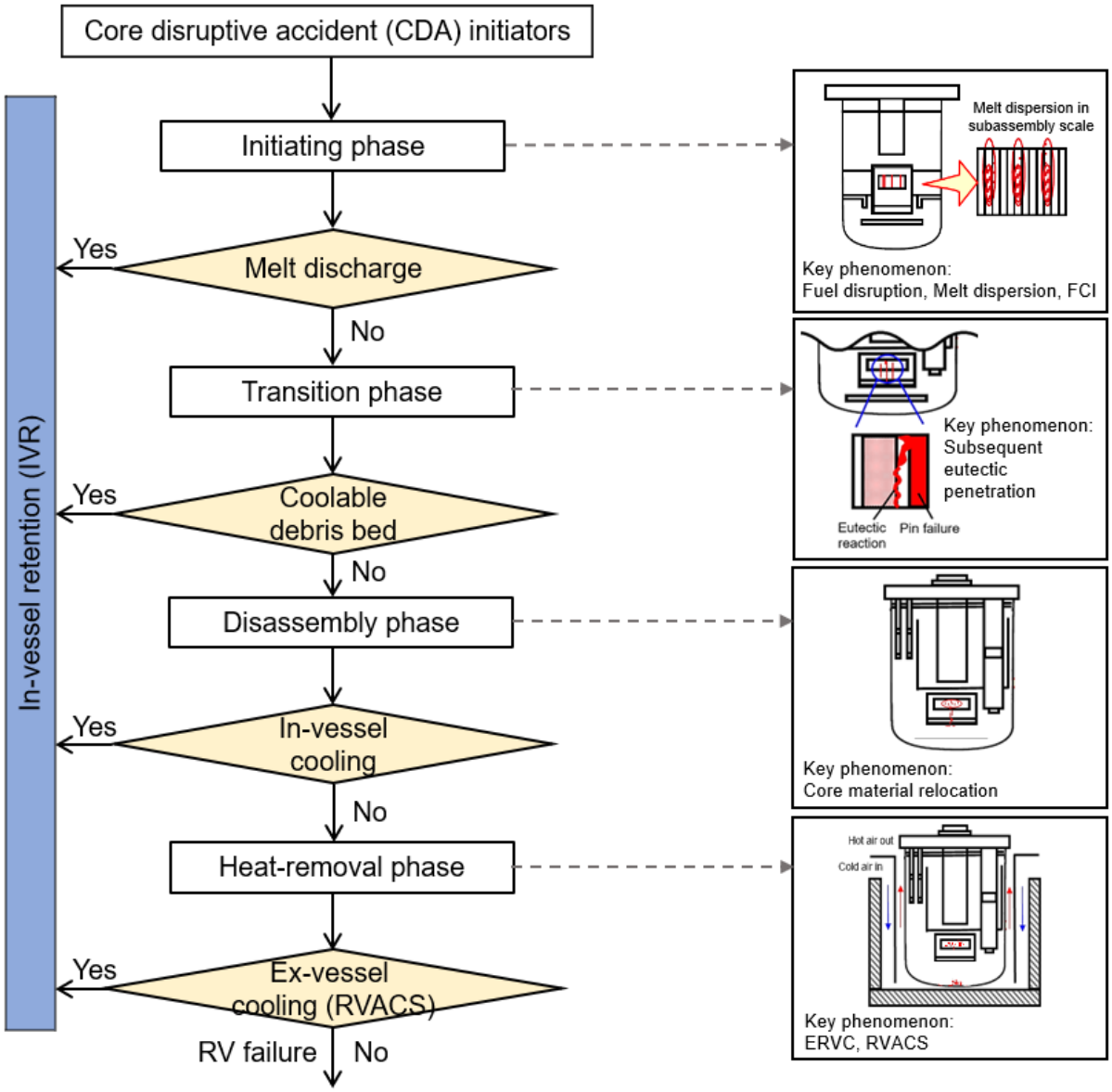

Fig. 1-1 Sequence of severe accident for metal-fueled sodium-cooled fast reactor

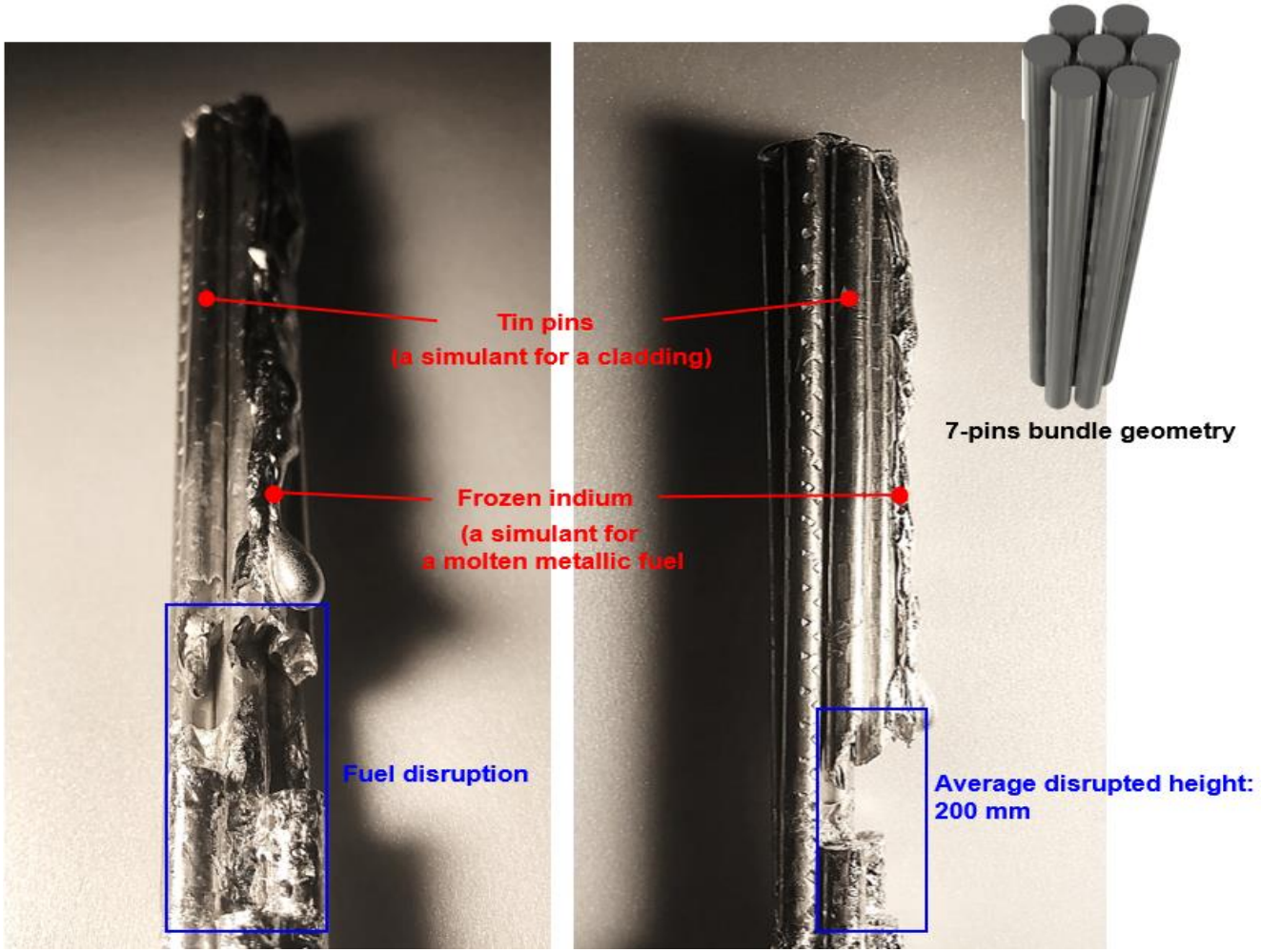

Fig. 1-2 Optical images of eutectic penetration experiments using gallium and indium

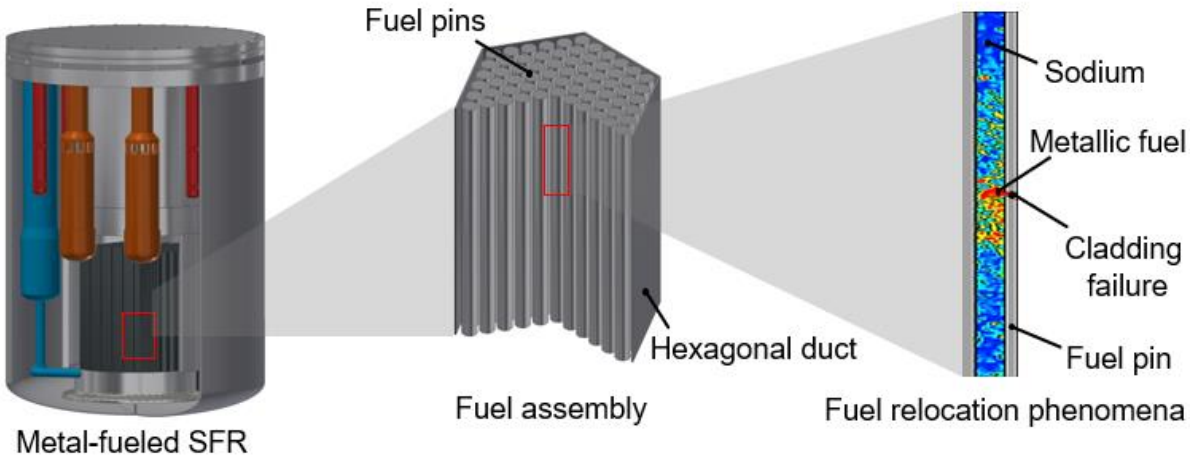

Fig. 1-3 Configuration of initiating phase of HCDA for metal-fueled SFR

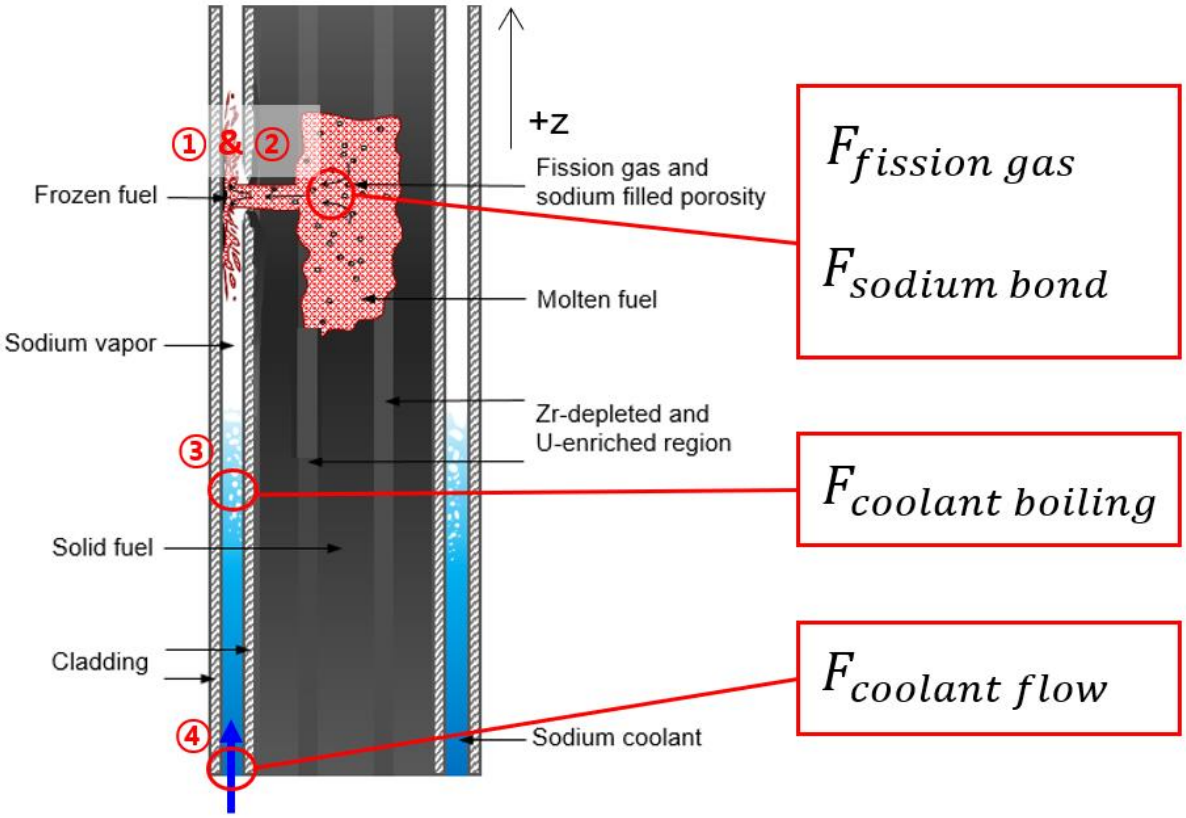

Fig. 1-4 Configuration of free body diagram for fuel relocation behavior

Chapter 2. OBSERVATION OF EX-PIN PHENOMENA

2.1 Introduction

In general, ex-pin phenomena stands for physical phenomena of molten fuel after cladding failure. Since the accident consequence is highly dependent on fuel relocation behavior including its fragmentation and dispersal, the ex-pin phenomena should be clarified. Fuel relocation behaviors, which occurs after cladding failure in metal-fueled sodium-cooled fast reactor (SFR), are complex phenomena with multi-physics and multi-phase flow. To investigate safety characteristics in the severe accident condition, it is crucial to understand fuel dispersion and fragmentation behavior in channel. In addition, these fuel behaviors would determine coolability in active core. If fuel is not swept out without its fragmentation, local fuel blockage might occur. In that case, reactor safety could not be ensured and the accident could be proceeded[48-56].

There are previous studies for the fuel behavior in severe accident for SFR. Most studies focused on the phase where large amount of fuel stream is relocated to reactor vessel. In the present study, the phase is called disassembly phase. The previous research groups conducted fragmentation experiments with pouring fuel or simulant into coolant pool. Nishimura et al.[36, 37] performed the fragmentation experiments using copper, silver, and aluminum. The simulants for simulating fuel were poured into the sodium pool. They revealed the thermal fragmentation as a fragmentation mechanism for metal fuel. In the thermal fragmentation procedure, solid crust at fuel surface is firstly formed and built-up pressure driven by sodium boiling fragmented the fuel particle. Matsuba et al.[57-59] also studied melt fragmentations using aluminum and sodium. It was found that molten aluminum was intensively fragmented due to rapid expansion of sodium vapor and frozen after the fragmentation phenomena. When the mass median diameters of debris were compared to classical fragmentation theory which commonly used in cases of light water reactor, the particle sizes were not well agreed with the theoretical values.

Research interest in initiating phase of severe accident is relatively lower than that of disassembly phase. However, the study for the initiating phase is important since the fuel swept-out could lead early termination of severe accident. In research groups in Japan, fuel assembly with an inner-duct structure (FAIDUS) has been proposed as a mitigation strategy against initiating phase of hypothetical core disruptive accident (HCDA) for oxide-fueled SFR. They performed fuel relocation experiments using horizontal melt ejection. Kamiyama et al.[60-61] conducted fuel relocation experiments using simulant. The alumina was used as the simulant for oxide fuel. To test a design option of FAIDUS, they evaluated driving forces to affect the fuel behavior. Matsuba et al.[57-59] evaluated movement relocated fuel in arbitrarily fuel discharge structure. They showed experimental approach to the fuel relocation behavior in the coolant channel. However, it was There have been not much experimental results about the fuel

relocation phenomena in fuel assembly. It is still insufficient to understand and provide physical insights for the phenomena.

In this chapter, fundamental phenomena in ex-pin for metal-fueled SFR was directly observed. An experimental facility for horizontal melt ejection was designed and established. The experimental facility was used for preliminary experiments, so it was optimized for direct observation of the fuel relocation behaviors. From these experiments, physical understanding of the phenomena was achieved. Finally, the driving force for the fuel swept-out was analyzed from the visual study.

2.2 Experimental setup and procedures

The visual studies were performed with simulant instead of actual fuel and coolant. Gallium, water, and freon were used as simulants, respectively. In the present experiment, possible fuel relocation behaviors were observed in small-scaled experimental facility. The experimental facility is called UNIST molten core and coolant interaction experimental facility (UNICORN)-B (baby). The melt relocation characteristics including its fragmentation and dispersal were clearly observed. Based on the visualization results, anticipated accident consequence was evaluated and driving force to determine the melt behavior was discussed.

2.2.1 Experimental facility

Fig. 2-1 is a schematic diagram of UNICORN-B for simulating fuel relocation behavior. It consists of a coolant channel and a melt injection system. The distance between the upper end of the coolant channel and the melt inlet is 260 mm. The coolant channel was designed as a square channel to maximize the visualization of the melt behavior with 15 mm of its internal equivalent diameter. The melt ejection point was set at 1/3 of the reference point of the lower end of the coolant channel, and the inner diameter of the melt ejection point was 3.7 mm. The melt was ejected from the melt injection system into the coolant channel. The melt injection control was achieved by a ball valve. The injection amount of melt was obtained by hand calculation of the mass flow rate of the melt. The initial temperature and pressure of the melt were measured with a thermo couples and pressure transmitters in the melt injection system. The melt injection system was designed to determine the pressure of the melt with controlling noble gas. The melt behavior was observed through a transparent window, and visualization results were obtained using a high-speed camera (800 fps). The high-speed camera used was Phantom's v9.1 model and the time resolution during visualization was 0.02 s.

2.2.2 Test procedure and experimental methods

The visual experiments for ex-pin phenomena were manually conducted. The experimental pro cedures are as follows.

- A certain amount of melt is injected in the melt injection system.
- Initial melt temperature and pressure are set in the melt injection system using induction heater and noble gas.
- Fill the coolant channel with coolant depending on experimental conditions.
- Pressurized melt is continuously ejected into channel with open of ball valves.

- During the process, the melt relocation behavior and fragmentation phenomenon are obtained using a high-speed camera.
- Repeat the procedures depending on the experimental conditions and investigate what parameters affects the relocation behavior and the fragmentation.

In the fuel relocation experiments, simulants were used instead of metallic fuel. Gallium was used as the simulant for the metallic fuel. In the experiments using UNICORN-B, gallium was selected as a simulant with a low melting point, and water and R-123 were used as the coolant. There were two coolant materials to simulate accident sequences caused by coolant boiling condition. R-123 is a kind of freon which has a boiling point of 28 ℃ which is very low at atmospheric pressure. The coolant boiling condition can be simulated using R-123. On the other hand, in the case of water, the boiling point was 100 ℃ under the atmospheric pressure condition. In this experiment, the water condition was used as coolant non-boiling condition. The gallium has melting point of 30 ^{o}C and it was ejected with the temperature of 50 ^{o}C in the experiment. Thus, the coolant boiling condition could be simulated using R-123 and water. Table 2-1 shows the physical properties of the melt and coolant materials in the experiments.

In initiating event for HCDA in SFR, there are some events like unprotected transient over power (UTOP) and unprotected loss-of-flow. The accident sequence is highly dependent on conditions of the initiating event. It means that the fuel could be relocated in voided or un-voided coolant channel. When sodium boiling occurs before the fuel relocation, the channel would be occupied with sodium vapor as voided condition. On the other hand, the fuel is directly contacted with the liquid sodium if sodium is not boiled. The fuel fragmentation and solidification are affected by these channel condition. Coolant boiling is also considered in the experiments. The metal fuel is relatively low melting point and the eutectic alloy between metal fuel and structures might have more lower temperature. Especially, sodium would not be boiled when the fuel is interacted with remaining in bottom of voided channel. In addition, coolant boiling could be one of promising force to discharge the fuel outward from core. The structure of fuel assembly is so compact and complex. The fuel rod has wire-wrapped structure unlike a typical fuel rod structure. The fuel movement might be disturbed by the structural characteristics. Finally, the critical phenomena where the fuel is relocated without its fragmentation were visualized. It might be occur when fuel is loaded with significant crack on cladding. With these parameters discussed so far, the ex-pin phenomena which might occur in actual transient condition were observed. The test matrix for ex-pin phenomena experiment is listed in Table 2-2.

To conduct the melt injection experiment using the simulants, it is necessary to evaluate hydraulic similarity between actual and simulant materials. Since the fuel behaviors are driven by force balance, dimensionless numbers related to physical force balances were compared to investigate similarity. If the hydraulic similarity is satisfied between two materials, the melt behavior under actual SFR transient

condition will be evaluated quantitatively. In the experiment, the Froude and the Weber number are considered for the similarity analysis. The Froude number represents the ratio of the inertial forces to the gravity forces, and the Weber number represents the ratio of the disruptive hydrodynamic forces to the stabilizing surface tension force. These dimensionless numbers indicate which forces are dominant for the behavior of melt dispersion. Also, these dimensionless numbers yield insight into the underlying physical phenomena. Thus, it is possible to satisfy the hydraulic similarity with the Froude and Weber number. The Froude number and Weber number are respectively defined as

$$Fr = \frac{{V_m}^2}{gD_m} \tag{2-1}$$

$$We = \frac{\rho_c \left\| \overrightarrow{V_m} - \overrightarrow{V_c} \right\|^2 D_m}{\sigma_m} \tag{2-2}$$

where V_m and V_c are the melt and coolant velocities, respectively; g is the gravitational acceleration; D_m is the diameter of the melt injection nozzle; σ_m is the surface tension of the melt; and ρ_m and ρ_c are the melt and coolant densities, respectively.

To calculate the Weber number, it is necessary to evaluate the interfacial velocity between the melt and the coolant. However, the interfacial velocity is difficult to measure and control under the experimental conditions. Thus, the interfacial velocity is assumed to be the initial relative velocity between the melt jet and the coolant. The initial relative velocity is determined by the velocity difference between the melt and the coolant which means the vector difference between the two velocities. The initial relative velocity between the two fluids is directly related to the interfacial momentum of the materials determining the melt behavior and fragmentation.

Table 2-1. Physical properties of melt and coolant for fuel relocation experiments using UNICORN-C

	Actual materials		Simulant		
	Metallic fuel (U-10Zr)	Sodium	Gallium	Water	R-123
Density [kg/m^3]	14100	966	6095	998	1460
Surface tension [N/m]	0.57	0.20	0.74	0.07	0.02
Viscosity [mPa·s]	$5 \cdot 10^{-3}$	1.13	$1.89 \cdot 10^{-3}$	1.00	0.45
Melting / Boiling point [^{o}C]	1077 / -	- / 881	30 / -	- / 100	- / 28

Table 2-2. Experimental conditions for fuel relocation experiments using UNICORN-C

Test no.	1	2	3	4	5	6
Melt / Coolant material [-]	Gallium / Water	Gallium / Water	Gallium / Water	Gallium / R-123	Gallium / Water	Gallium / R-123
Melt temperature [^{o}C]	50	50	50	50	50	50
Coolant temperature [^{o}C]	22	22	22	22	22	22
Melt injection mass [g]	1170	1310	1220	1610	1240	1360
Initial melt pressure [bar]	1	1	1	1	1	1
Coolant flow velocity [m/s]	0.5	0.5	0	0	0	0
Coolant saturation [-]	Unvoid (coolant-occupied)	Unvoid (coolant-occupied)	Unvoid (coolant-occupied)	Unvoid (coolant-occupied)	Void (air-occupied)	Void (air-occupied)
Froude number [-]	165	165	165	243	165	243
Weber number [-]	174	174	173	255	173	255
Remark	Single-pin structure	Multi-pin bundle structure	-	-	-	-

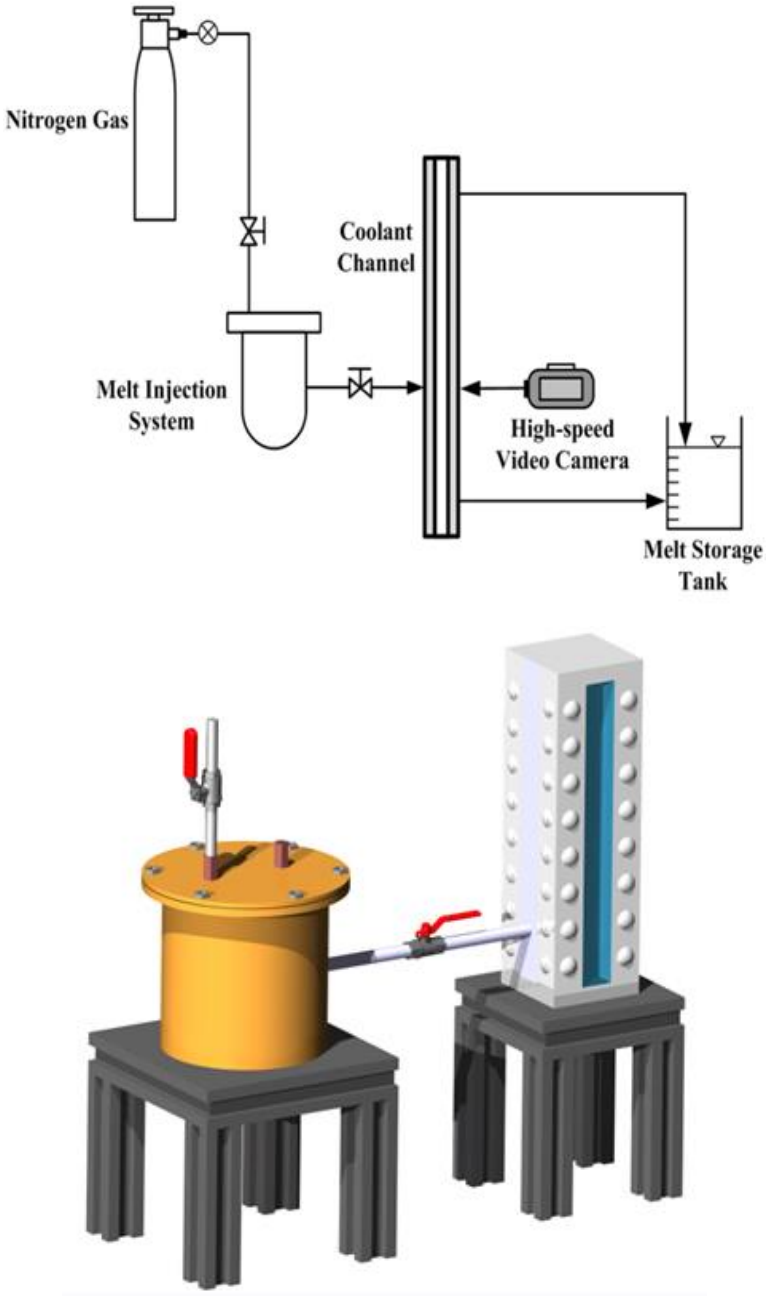

Fig. 2-1 Schematic diagram of UNICORN-C

2.3 Experimental results

The ex-pin phenomena where the fuel is ejected into coolant channel were observed. The experiments were carried out with experimental facilities called UNICORN-C. The melt behavior was investigated on rod bundle structure effect, coolant boiling, channel condition (voided and un-voided condition), and melt ejection velocity. The phenomenological study was performed from the visual results and physical insight to predict accident sequences was discussed.

2.3.1 Physical insights in ex-pin phenomena

In initiating phase of HCDA for metal-fueled SFR, the fuel behavior in fuel assembly is dependent on driving force. There are some dominant forces to determine the fuel behavior; force caused by pressurized fission gas, vaporization of sodium bond, coolant boiling, coolant flow, friction of structure, and gravitational energy. The force balance equation is given by

$$F_{fu} = F_{fi} + F_{so} + F_{bo} + F_{co} + F_{fr} + F_g \tag{2.3}$$

If unprotected loss-of-flow event was considered as an initiating event for severe accident, the coolant flow could be excluded in the experiment. Thus, it is rearranged by

$$F_{fu} = F_{fi} + F_{so} + F_{co} + F_{fr} + F_g \tag{2.4}$$

When fuel stream is assumed as a shape of droplet, energy balance is used to calculate how fuel droplet is swept-out from ejected position.

$$W_{fi} + W_{so} + W_{co} + W_{fr} = \Delta E_g \tag{2.5}$$

The pressurized fission gas and vaporization of sodium bond are factors in pin cavity. Thus, the work by these factors defined by

$$W_{fi\ and\ so} = (PV)_{fi\ and\ so} \tag{2.6}$$

The force by coolant boiling was considered as buoyance force by the sodium vapor.

$$W_{co} = (\rho_{liq,so} - \rho_{so,vap}) g V_{so,vap} \Delta h \tag{2.7}$$

There is frictional force caused by inner structure. The work by frictional force is given by

$$W_{fr} = -\frac{1}{2} c_{d,liq,fu} \rho_{liq,fu} \overline{v_{liq,fu}}^2 A_{sub} \Delta h \tag{2.8}$$

The potential energy by gravitational force is dependent on position of fuel droplet.

$$\Delta E_g = m_{liq,fu} g \Delta h \tag{2.9}$$

The height where the fuel droplet moved is calculated by energy balance equation using Eq. 2.5-2.9.

$$\begin{aligned} &(PV)_{fi\ and\ so} + \left(\rho_{liq,so} - \rho_{so,vap}\right) g V_{so,vap} \Delta h \\ &-\frac{1}{2} c_{d,liq,fu} \rho_{liq,fu} \overline{v_{liq,fu}}^2 A_{sub} \Delta h = m_{liq,fu} g \Delta h \end{aligned} \tag{2.10}$$

Figure 2-2 shows the visualization results for melt behavior in a rod structure. During initiating phase of metal-fueled SFR severe accident, the fuel is directly ejected and dispersed into small gap between fuel rods. Since design of SFR fuel rod has wire spacer, the fuel fragmentation and dispersion might be disturbed by the structural characteristics. To observe ex-pin phenomena with rod structure, the experiments were conducted by inserting a wire-wrapped pipe simulating a single rod. The outer diameter of the pipe used was 6.33 mm, and the outer diameter of the wire was 1 mm. The melt is ejected from the left wall which was directly connected to the melt injection system. In the test section, the wall structure stands for cladding in fuel assembly. The melt was continuously ejected to the channel but was not dispersed in the form of a jet breakup. It was broken due to collisions with surrounding structures. Since solidification effect was not considered in the experiment, the melt was repeatedly fragmented and agglomerated. In addition, there was a melt flow which was shifted to the right side. The wire spacer led to melt movement to the right side, which means that the fuel could be intensively fragmented due to the melt dispersal with the rotation direction of the wire wrap. The contact area between the melt and the coolant increased, which could accelerate to disperse and fragmentation of the melt. However, the local flow blockage might occur due to this flow characteristic when the fuel is rapidly frozen in fuel assembly. The experiment was carried out considering coolant flow to clearly observe the melt behavior affected by SFR fuel rod structure.

Figure 2-3 represents the melt fragmentation and dispersion in the channel with multi-rod structures.

It was performed to visualize the effect of multi-rod structure on the melt behavior. The gap between the pipes and pitch was 0.89 mm and 7.22 mm, respectively. The outer diameter of the pipes was 6.33 mm. The values were selected considering design parameters from prototype generation-IV sodium-cooled fast reactor (PGSFR). The molten gallium was ejected from the left wall like previous case. The melt ejected to the gap between the pipes and the melt dispersal occurred instantaneously. The fragments were observed in initial phase after the melt ejection. It seemed like the size of fragment was lower than gap between pipes and its shape was like a sphere. However, as the melt was continuously ejected and dispersed, it was mixed again with a form of stream. The gallium had low melting point compared to temperature of water pool in the experiment. During the melt dispersion, there was not solidification in melt. The melt was discharged with rotational movement according to flow mixing. There were chances to increase contact area between melt and coolant, thus the local coolant could be entrapped by melt. If the coolant boiling was considered, the melt fragmentation would occur by intense vaporization of the local coolant[62-69]. The melt movement behaved uniformly without its shifting. Since the melt was ejected horizontally, the melt flowed initially in radial direction. The inertial force of melt made the most of melt radially distributed. However, the molten gallium eventually dispersed upward due to the coolant flow.

Figure 2-4 and 2-5 show the molten gallium behavior in a channel occupied with coolant. These behaviors could stand for accident situations when sodium is not boiled before cladding failure. Whether or not coolant boiling occurs before the cladding failure is dependent on accident scenarios. In the visual study, there were two experimental conditions to simulate possible ex-pin phenomena; coolant non-boiling and boiling condition. To apply each condition, water and R-123 were used as coolant. R-123 is a kind of freon, which was appropriate to simulate boiling condition because the initial temperature of molten gallium was 50 ^{o}C.

Figure 2-4 reveals the melt behavior in water-occupied channel. The water is fully filled in the test section to reflect un-voided coolant channel. As molten gallium collided against wall standing for surrounding cladding, it started to spread in vertical direction. The fragmented particle was formed around the collision region due to molten gallium spreading by horizontal flow. A melt-coolant mixing zone was formed in the region near the melt ejection point as the melt was continually ejected from the melt injection system into the channel. There was no driving force for discharging the melt to the top side in coolant non-boiling conditions. The coolant boiling phenomenon did not occur at the melt–coolant interface, because the boiling point of water was higher than the melt temperature. However, thereafter the melt was just moved in the direction of gravity. Since gallium is a liquid metal with a high density, the melt fell down in lower part. During the melt injection, the melt was continuously injected into the coolant channel, so a part of the melt seemed to move upward by its inertia. However, most of the melt moved downward without the occurrence of refreezing phenomena, owing to its good fragmentation. The fragmented particles were of various shapes, from sphere-like to flat-sheet-like. The

shapes of the particles were determined by surface solidification and the contact conditions between the two fluids. The fragmented particles were not agglomerated, and so, the coolant channel was not blocked by the fragmented particles. In this test, 1.22 kg of the melt was injected in the coolant channel, which was equal to the total weight of six fuel pins.

Figure 2-5 shows the melt behavior in the coolant boiling condition. In this experiment, it was observed that void volume of coolant was generated. There was a two-phase flow regime where the melt fragments were dispersed upward along with the coolant vapor. The void volume increased with continuous melt ejection. In addition, the vapor columns were created by this process and grew enough to fill the inside of the coolant channel at a certain time. The melt was fragmented and discharged to the upper side of the channel with the growth of the vapor column, leading to melt sweep-out. It is deduced that the driving force of the melt dispersal is due to accumulation of the vapor pressure. When the melt was ejected into the coolant, an interface between the melt and the coolant was formed and a coolant vapor pressure was created through the interface. The growth of the vapor column caused the buildup of the vapor pressure, and the melt was discharged to the upper part of the channel when the vapor pressure exceeded. Although the coolant flow velocity was zero, the melt was dispersed upward against gravity. This implies that the melt will move toward the outside of the core region even under a zero flow condition if sufficient vapor pressure is built up within the coolant channel. Through the experiment, the possibility of the melt sweep-out was examined even in the absence of the coolant flow. In addition, it was confirmed that the driving force of melt sweep-out mechanism is the accumulation of the coolant vapor pressure due to the active reaction between the melt and the coolant. The amount of melt injected in this experiment is 1.61 kg, which corresponds to mass of 8 fuel pins based on prototype generation-IV sodium-cooled fast reactor (PGSFR) fuel.

In the initiating phase of ULOF event, the voided coolant channel could be formed in the inner core region. This indicates that the melt fragmentation caused by reaction of the melt with the coolant did not occur. Figure 2-6 shows the visual observation results of the behavior of melt injected into the coolant channel, under the voided coolant condition. The voided coolant region formed around the melt injection point, and the coolant was filled at the bottom of the coolant channel. With the injection of the melt from the melt injection system, the injection pressure in the injection system reduced gradually. The initiating behavior of the melt injection was similar to that in un-voided condition. The melt collided with the wall of the coolant channel. A part of the melt seemed to move upward in the voided region, but most of it moved downward without occurrence of the refreezing phenomena, owing to its high density. When the melt fell to the coolant, which was submerged at the bottom of the channel, melt–coolant mixing occurred on the boundary surface between the melt and the coolant. Through the intermixing of the melt with the coolant, the coolant boiling occurred only in test 6 owing to the low boiling point of R-123. This led to the void development of a coolant from the intermixing point, where the melt and the coolant interacted with each other. The coolant void can be developed only after the

formation of a stable void by a sufficient reduction of coolant subcooling in the coolant channel. Since the vapor pressure was accumulated in the coolant channel, the melt at the bottom of the coolant channel was discharged upward. In addition, the void developed by the coolant vaporization occupied the voided coolant region, and so, the melt in the voided coolant region moved to the upper region of the coolant channel. After the coolant channel was dominated by the void development of the coolant, most of the melt fragments were dispersed upward along with the coolant vapor. Figure 2-6 shows that the melt was discharged upward beyond the coolant voided region, in which the additional driving force was generated by the built-up vapor pressure. It seems reasonable to suppose that the melt can be discharged upward after its dispersion in the voided coolant region.

On the other hand, Figure 2-7 shows the experimental results for the melt behavior under the non-boiling condition, in which 1.24 kg of the melt was injected into the coolant channel. In this test, coolant boiling did not occur when the melt came into contact with the coolant, because of the boiling point of water (100 °C). Because no coolant boiling phenomenon occurred, there was no driving force for moving the melt upward. After the injection of the melt, it was not fragmented and was accumulated at the bottom of the coolant channel owing to its high density. This indicates that the recriticality event may occur if the melt is refrozen and agglomerated in such a case.

Figure 2-8 shows the melt relocation behavior according to the initial melt velocity. Concerning severe accident condition in beginning of cycle (BOC) where the fuel is loaded with cracked cladding, the range of the melt velocity was arbitrarily selected; 5 mm/s, 18 mm/s, 72 mm/s, and 144 mm/s. Figure 2-6 (a) and (b) represent the melt behavior at the initial melt velocity of 5 mm/s and 18 mm/s, respectively. Under these conditions, the melt behavior moved downward without colliding with the inner structure of the channel. The melt is likely to fall directly toward the lower plenum, which has potential leading to flow blockage and recriticality. When the melt was ejected at an initial melt velocity of 72 mm/s, melt was contacted to the channel wall. However, the melt relocation behavior still moved downward. On the other hand, when the initial melt ejection velocity was 144 mm/s, it was observed that the melt fragmentation partially occurred due to the collision between the melt and the channel walls. As a result, it could be concluded that if a melt is ejected into the coolant at a low melt velocity, this would proceed severe accident sequence without early accident termination. To predict actual melt behavior in the metal-fueled SFR severe accident, the present study applied the Froude number and Weber number to evaluate the hydrodynamic similarity. As a result, Froude number in the actual reactor case was found to be considerably larger than that in the experimental case. It is considered that the metallic fuel does not move downward immediately to the lower plenum in actual transient cases.

The upward dispersion of melt as observed visually and evaluated by considering the molten fuel discharge under several experimental conditions was discussed. The built-up vapor pressure is proposed as a major cause of the upward dispersion of the melt. Sufficient reduction of the coolant subcooling can be achieved under contact with the coolant. As a result, the void development of the coolant can be

achieved at an earlier stage under the coolant boiling condition. From the viewpoint of thermodynamics, the magnitude of buildup of the coolant vapor pressure is related to the coolant vapor generation rate, which in turn is dominated by the mixing ratio of and the contact interface area between the melt and the coolant, as well as their temperature difference. The visual observation results showed that the coolant pressure buildup occurred under the coolant boiling condition both in the voided and the unvoided coolant channels. In addition, the upward dispersion of melt occurred under the zero flow condition of the coolant. Here, it should be noted that when it is assumed that the coolant pressure can be built up in the coolant channel, the melt is dispersed to the outside of the core region even in the ULOF initiating phase scenario. Therefore, if the reactor condition is a certain condition similar to the experimental condition in the present study, it will be possible to generate sufficient coolant vapor to lead to coolant pressure buildup under the reactor conditions. In other words, in such a situation, the molten metal fuel can be dispersed upward toward the outside of the core by the coolant pressure. Consequently, the experimental results provide the critical physical insight of fuel relocation where accumulation of the coolant vapor pressure would be one of the driving force for fuel sweep-out.

To conduct the melt injection experiment using the simulants, it is necessary to evaluate hydraulic similarity between actual and simulant materials. Since the levitation height and debris bed porosity are determined from the behavior of fuel stream, the hydraulic similarity should be secured. If the hydraulic similarity is satisfied between two materials, the melt behavior under actual SFR transient condition would be evaluated quantitatively. In the experiment, the Froude and the Weber number are considered for the similarity analysis. The Froude number represents the ratio of the inertial forces to the gravity forces, and the Weber number represents the ratio of the disruptive hydrodynamic forces to the stabilizing surface tension force. These dimensionless numbers indicate which forces are dominant for the behavior of melt dispersion. Also, these dimensionless numbers yield insight into the underlying physical phenomena. Thus, it is possible to satisfy the hydraulic similarity with the Froude and Weber number. The Froude number and Weber number were used to represent the overall behavior of fuel stream and the fragmentation of molten fuel, respectively.

Table 2.3 shows comparison of Froude and Weber number between actual transient condition and experimental conditions. The ranges of the Froude and the Weber number in experimental conditions were included in the actual transient condition for metal-fueled SFR. It means that the actual fuel behavior and fragmentation in beginning of equilibrium cycle (BOEC) was simulated in the present study. It was found that the powerful driving force for the fuel levitation was built-up vapor pressure by instantaneous coolant boiling in the BOEC. Especially, the melt was strongly discharged upward and swept-out regardless of coolant channel condition like void and un-void condition. The physical insight could give severe accident mitigation strategy for the metallic fuel in SFR.

Table 2-3. Comparison of Froude and Weber number between actual transient condition and experimental conditions

	Actual transient condition for metal-fueled SFR	Experimental condition
Froude number	435.3 – 10278.6	165 – 2130
Weber number	562.6 – 10962.1	173 – 2253

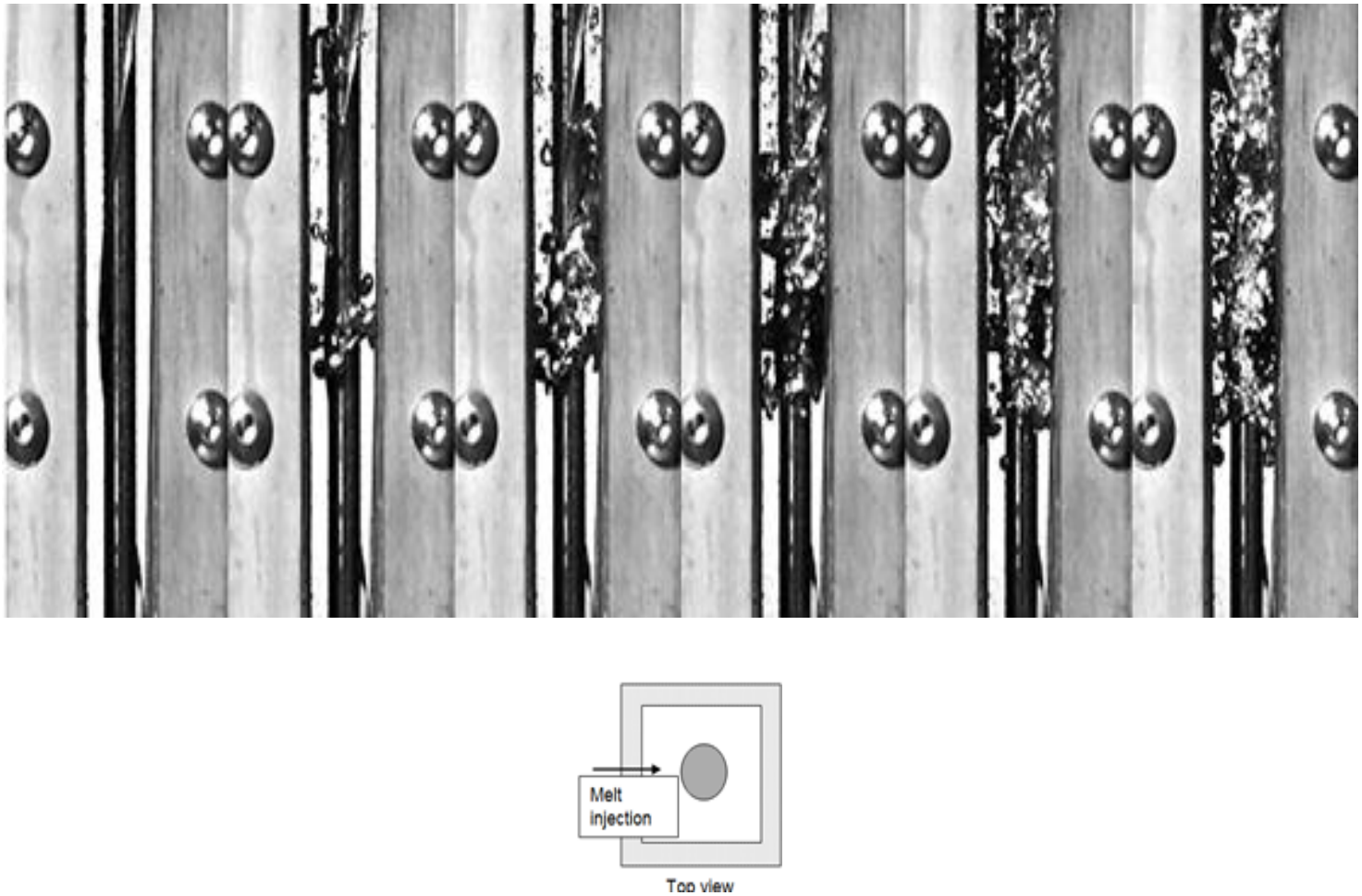

Fig. 2-2 Optical images of melt relocation behavior in a channel with a wire-wrapped rod

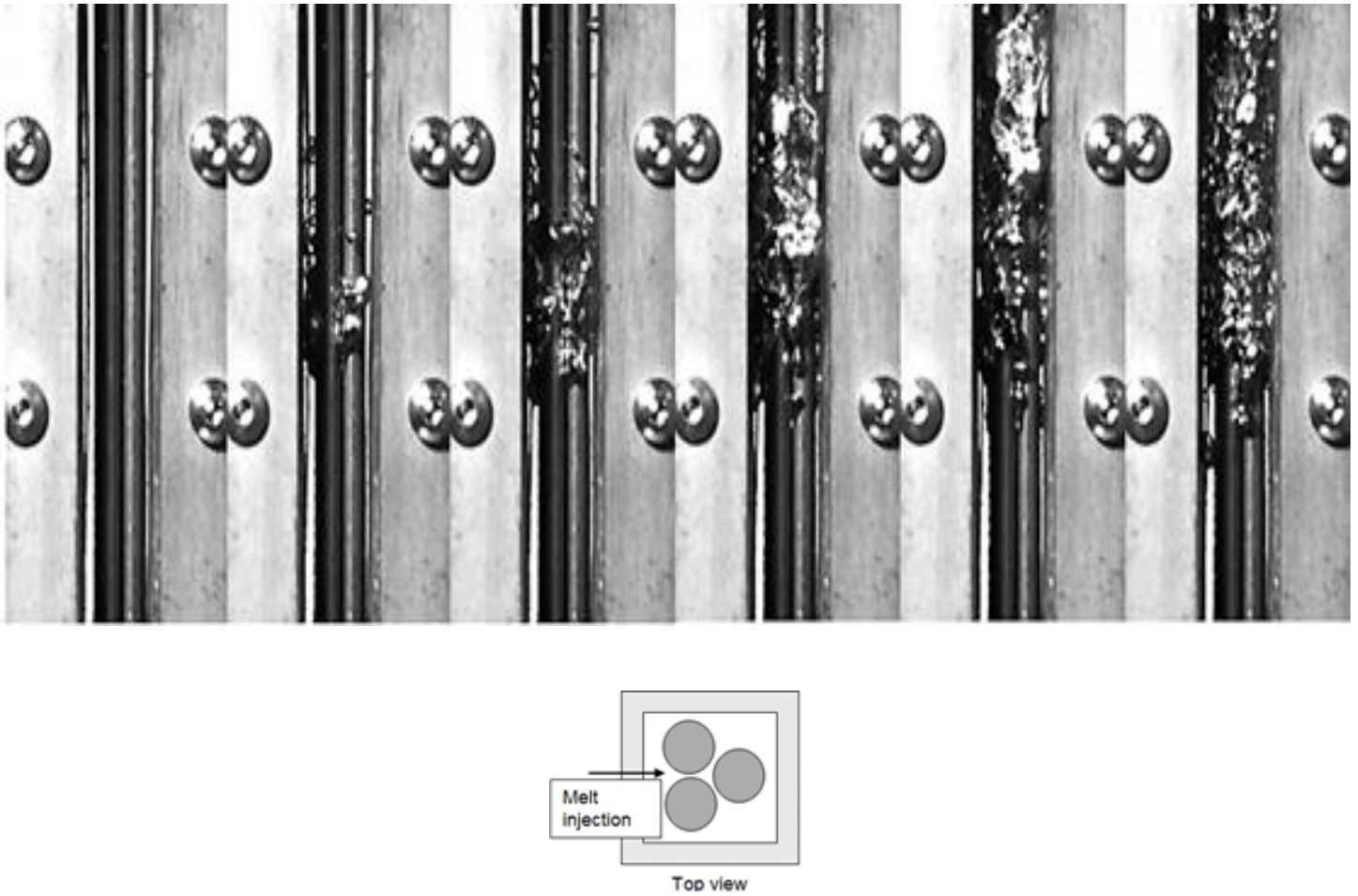

Fig. 2-3 Optical images of melt relocation behavior in a channel with multi-rod bundle

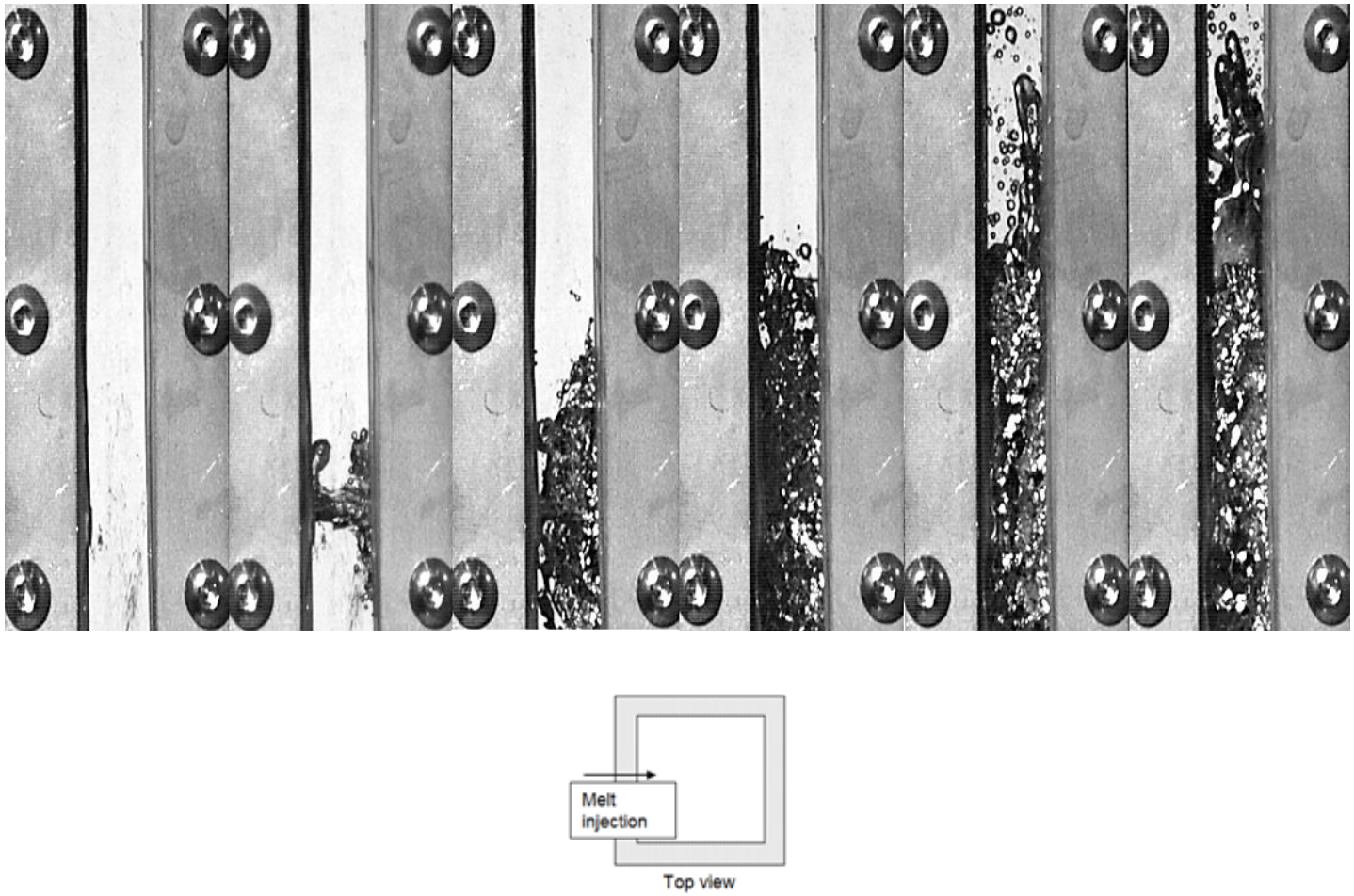

Fig. 2-4 Optical images of melt relocation behavior in an un-voided channel under coolant boiling

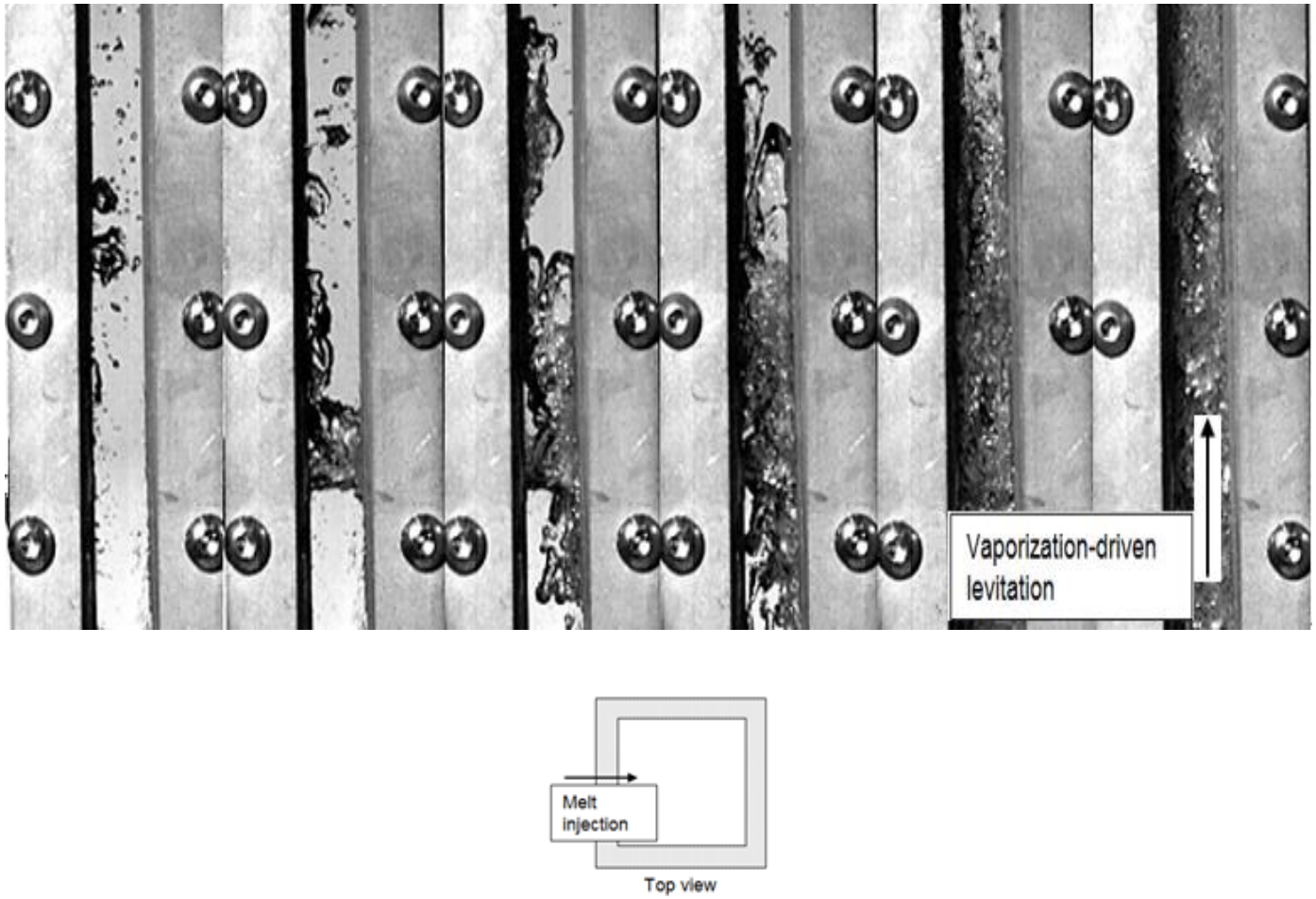

Fig. 2-5 Optical images of melt relocation behavior in an un-voided channel under coolant non-boiling condition

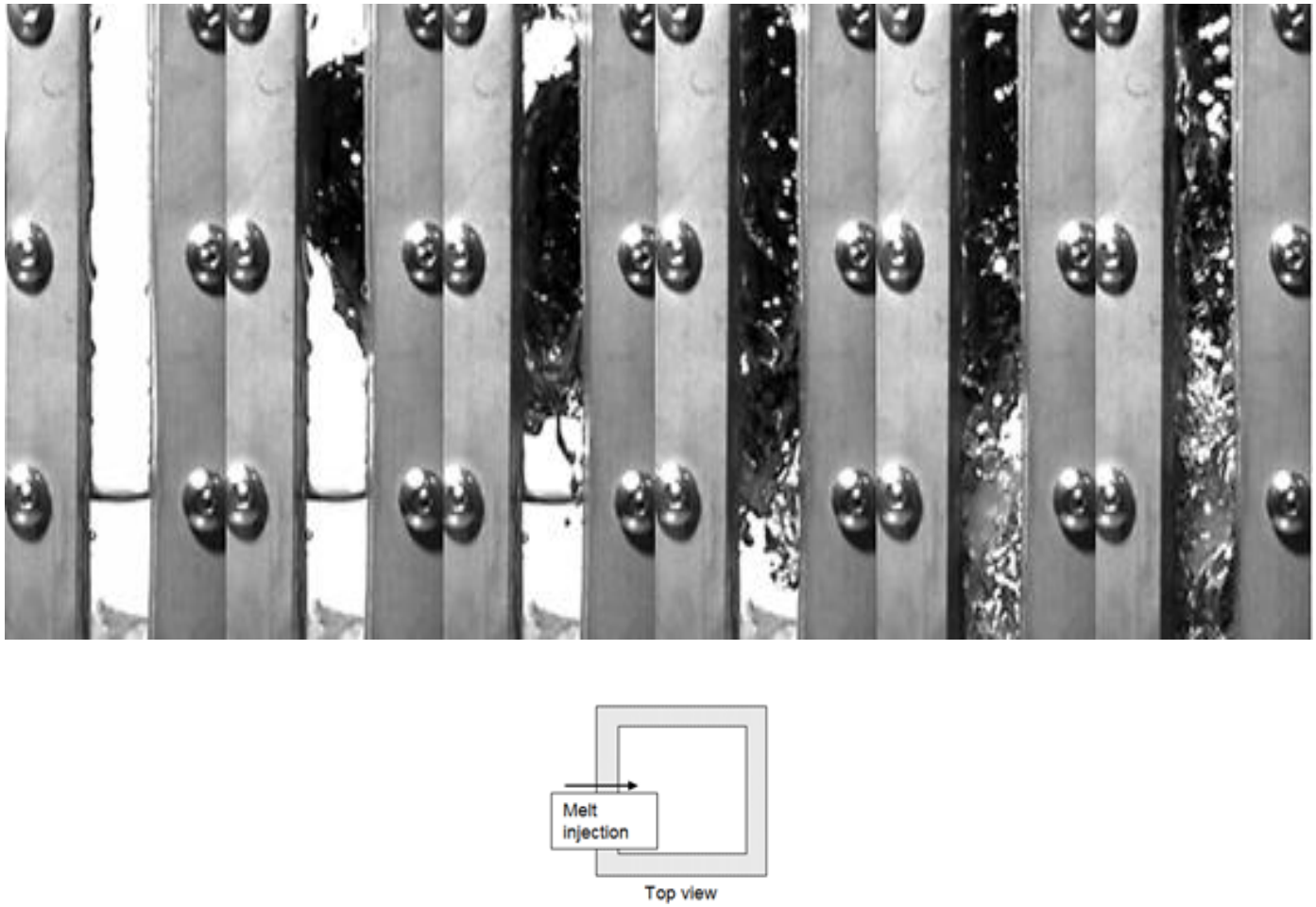

Fig. 2-6 Optical images of melt relocation behavior in a voided channel under coolant boiling

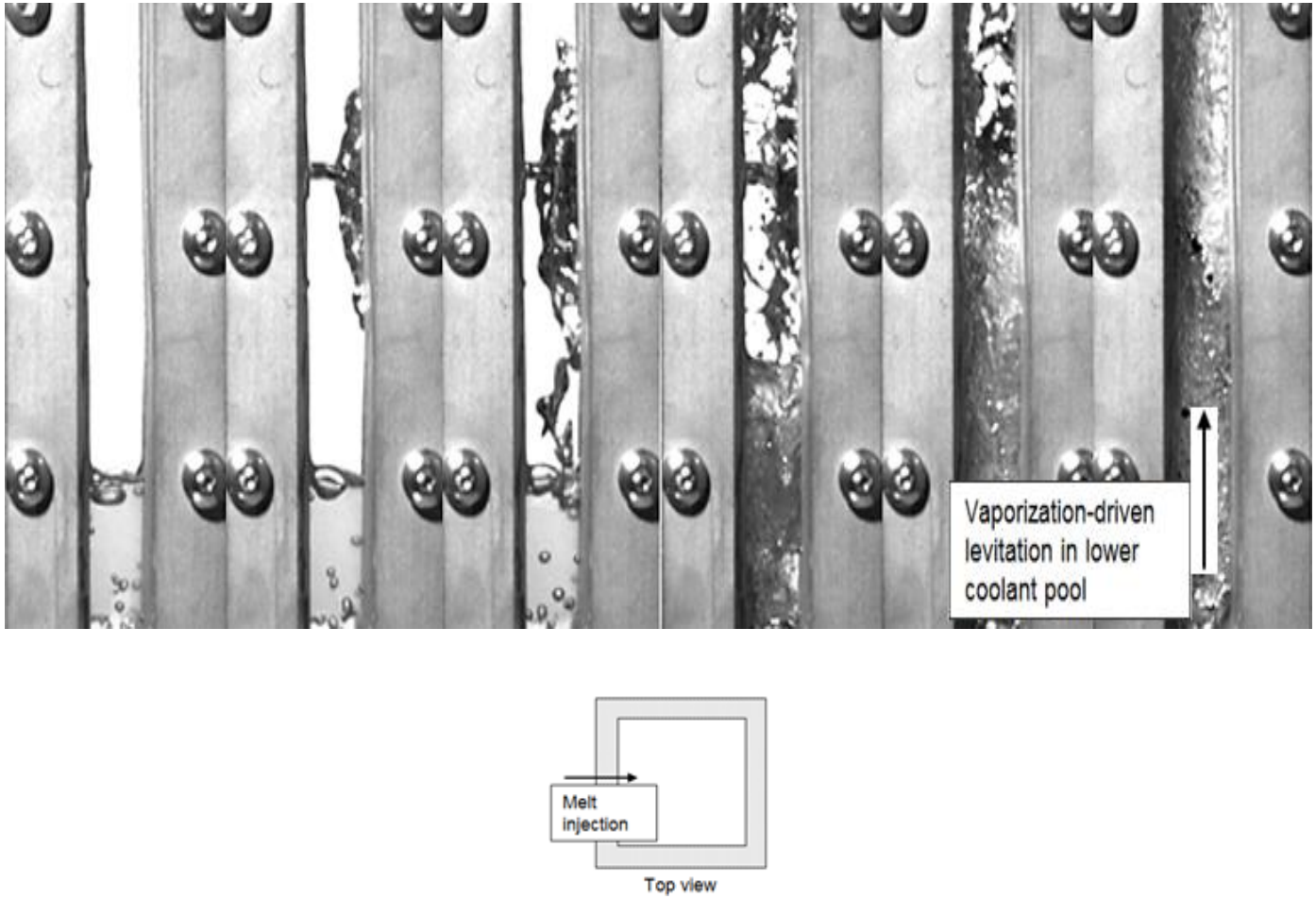

Fig. 2-7 Optical images of melt relocation behavior in a voided channel under coolant non-boiling condition

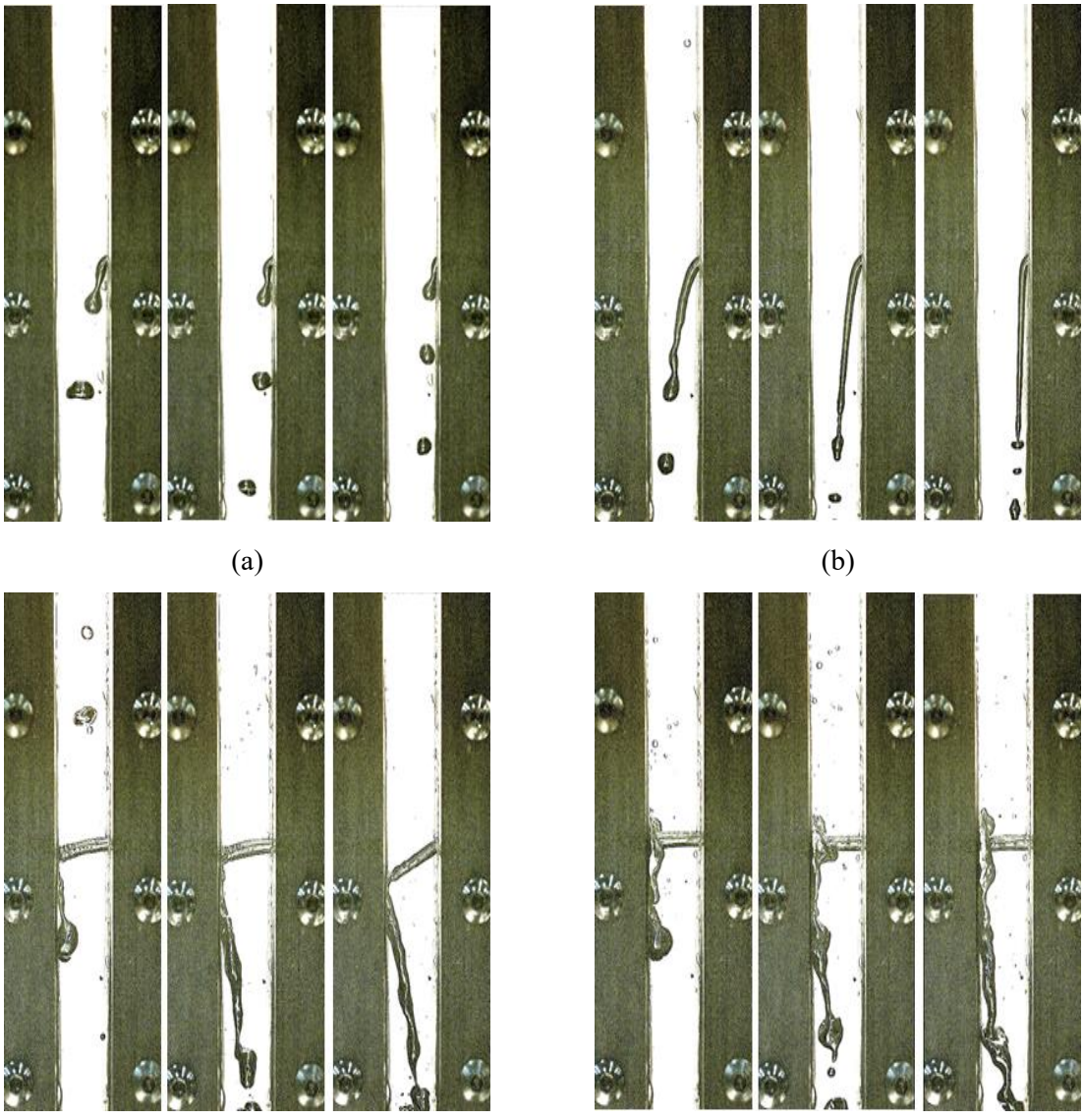

(a) (b)

(c) (d)

Fig. 2-8 Optical images of melt relocation behavior with initial melt velocity of (a) 5 mm/s, (b) 18 mm/s, (c) 72 mm/s, and (d) 144 mm/s

Chapter 3. FUEL RELOCATION EXPERIMENTS

3.1 Introduction

A hypothetical core disruptive accident (HCDA) of sodium-cooled fast reactor (SFR) has been considered as one of the critical issues associated with its inherent safety. In case of metal fuel under this HCDA condition, it has been known that fuel is well discharged upward from core. With axial fuel elongation, the fuel sweep-out would give negative reactivity feedback and eliminate possibility of recriticaility. In addition, it could prevent flow blockage caused by melt agglomeration and debris bed with low porosity. The melt fragmentation behaviors are closely related to a formation of debris shape. The debris shape is formed through the fragmentation and solidification. If the coolant channel does not sufficient coolability by the melt debris, the early termination of accident would not be expected. Thus, it is important to examine the extent of fuel relocation behavior and levitation height of fuel after cladding bleach.

The issue of negative reactivity insertion by fuel relocation was experimentally discussed in Transient Reactor Test Facility (TREAT)-M series tests. In the TREAT-M tests, overall fuel relocation characteristics before and after cladding failure were investigated. The 4 times of overpower was exponentially inserted for 8 seconds under normal flow condition. After the tests, the transient conditions were terminated to analyze failure shape on cladding and debris shape. In the TREAT-M series tests, the five fuel pins in the fifteen pins was broken and the molten fuel was ejected into the coolant channel. The molten fuel at transient state where the fuel has high pressure and temperature is intensively ejected into coolant channel of low temperature and low pressure as soon as the cladding failure occurs. The ejection timing of fuel is the same as that of the cladding failure, so the ejection timing is dependent on fast neutron, coolant temperature, and flow rate. The amount of fuel ejected into the channel was analyzed using axial mass distribution of fuel and fuel relocation behavior. The axial mass distribution was measured using hodoscope. Since the purpose of the TREAT-M series tests were to observe fuel relocation before cladding failure which is called in-pin phenomena, there was few experimental database for ex-pin phenomena. The reactivity feedback by fuel relocation was calculated from axial mass distribution. The amount of fuel mass which was ejected was determined from pressure difference between inside of fuel pin and coolant channel. The pressure difference was dependent on fuel type and burnup. In case of high burnup condition, a large amount of molten fuel corresponding to 2/3 of the initial mass was relocated into the coolant channel. On the other hand, about 1/2 of the initial mass was ejected in the case of the low burnup case. That is, the fuel relocation motion in which the molten fuel is ejected into the coolant channel has advantageous in the high burnup condition, leading to insertion of significant negative reactivity feedback. In addition, binary fuel generated relatively small amounts of fission gases compared to ternary fuel. It also affected to pressurize the inside of fuel

pin. The tests were meaningful to conduct in-pile tests for transient condition of metal-fueled SFR. However, fuel relocation behavior and levitation height of fuel after cladding bleach was not analyzed in detail[38-44].

Recently, ANL has resumed experimental research on severe accident for metal-fueled SFR. T. Kim et al.[43-44] carried out fuel relocation experiments using metallic fuel. They dropped vertically molten uranium to single-pin core structure filled with sodium. They found that the cladding was deformed and sodium boiling occurred during the fuel relocation. There were numerous voids in frozen debris, which means that local sodium entrapped by the fuel stream was instantaneously vaporized. The fuel fragments formed during the fuel relocation, but the shape and morphology was irregular. To compare their results with other researches, they used instantaneous contact interface temperature between fuel and coolant. T. Kim et al. also performed fuel relocation experiments in multi-pin bundle core structure. There were 19 fuel cladding tubes with wire wrapped spacer. The depleted uranium was ejected vertically to the test section filled with sodium. The initial uranium temperature was 1374 and 1537 ºC and the initial sodium temperature was 635 and 676 ºC, respectively. The ejected mass of uranium was 768.3 and 772.5 g. As a result, the uranium was fragmented due to local sodium boiling. They discussed that the freezing point of fuel was crucial to determine its dispersion behavior. From these fuel relocation experiments conducted in ANL, it was observed that the fuel was frozen in the core structure without fuel discharge outward.

In the chapter 3, behavior characteristics of fuel relocation and height where fuel is discharged upward were investigated using a simulant like Wood's metal. It was conducted as parametric studies using some parameter which were selected from previous ex-pin experiments. New experimental facility was developed for the experimental study. Fundamental understanding of the fuel behavior characteristic was achieved and levitation heights of melt which was measured in the experiments was discussed with comparison of theoretical results.

3.2 Experimental setup and procedures

The key parameters which could affect to fuel relocation behavior were deduced from lab-scaled ex-pin experiments; initial fuel temperature, initial coolant temperature, fuel mass, initial fuel pressure, and coolant condition (voided or un-voided channel). To understand physical effect of the parameters on fuel relocation behavior and assess levitation heights of fuel, the fuel relocation experiments were conducted. More advanced experimental facility than the one introduced in previous chapter was used. In this part, the advanced experimental facility was introduced. In addition, simulant material used in the experiments and test matrix are explained.

3.2.1 Experimental facility

Fig. 3-1 shows a schematic diagram of UNIST molten core and coolant interaction experimental facility (UNICORN)-C (child). It is also composed of a melt injection system and coolant channel. The height of the coolant channel was 2230 mm, reflecting the core height of metal-fueled SFR including gas plenum and active core region. The hydraulic diameter of the UNICORN-C without the rod bundle structure is 50 mm. It is quite different from hydrodynamic diameter of design values for actual reactor. However, the experiments are expected to reflect the phenomenological characteristics of melt relocation in detail. To investigate the melt behavior and observe its dispersal and fragmentation, most of experiments were conducted without rod bundle structure. However, the structure effect which affects melt relocation phenomena was also evaluated. The hydraulic diameter of melt ejection point was 10.4 mm. The operating method to control pressure is same in between UNICORN-B and UNICORN-C. The melt ejection system was designed to control the temperature of the melt and the melt ejection pressure to achieve the experimental conditions. Here, the ejection pressure of the melt was controlled by pressing or depressurizing noble gas. The initial temperature and pressure were measured with thermocouples and pressure gauges, respectively, before the melt injection. The dispersion behavior of the molten wood's metal in the coolant channel was observed using a high-speed video camera (1000 fps).

3.2.2 Test procedure and experimental methods

The fuel relocation experiment focused on fuel ejection and its spreading and fragmentation in channel. To simulate the physical phenomena, there was a coolant channel where the coolant was ejected and crucible. To control experimental conditions, the melt was pressurized and heated in the melt crucible. The experimental procedures in detail are as follows.

- A certain amount of melt is injected in the melt injection system.
- Initial melt temperature and pressure are set in the melt injection system using induction heater and noble gas.
- Fill the coolant channel with coolant depending on experimental conditions.
- Pressurized melt is continuously ejected into channel with open of ball valves.
- During the process, the melt relocation behavior and fragmentation phenomenon are obtained using a high-speed camera.
- Repeat the procedures depending on the experimental conditions and investigate what parameters affects the relocation behavior and the fragmentation.

Table 3-1 lists the physical properties of the employed molten materials and coolants in the experiments. The experiments were conducted to observe the fundamental fragmentation behavior of the melt in the coolant channel. Molten wood's metal was selected as the simulant material of the metal fuel. The molten material was injected into water which was used as simulant of the coolant. The physical properties of the metal fuel are used based on the composition of U-10Zr. The materials were selected appropriately because the present study considers the melt fragmentation. Since the experiment is conducted by using the simulants, similarity analysis is crucial to obtain the reliability of the experimental data. To calculate the Weber number, it is necessary to evaluate the interfacial velocity between the melt and the coolant. However, the interfacial velocity is difficult to measure and control under the experimental conditions. Thus, the interfacial velocity is assumed to be the initial relative velocity between the melt jet and the coolant. The initial relative velocity is determined by the velocity difference between the melt and the coolant which means the vector difference between the two velocities. The initial relative velocity between the two fluids is directly related to the interfacial momentum of the materials determining the melt fragmentation behavior.

Table 3-2 shows experimental conditions for fuel relocation experiments using UNICORN-B. To investigate effect of initial melt temperature on fuel relocation behavior, the initial melt temperature of 90 and 550 ^{o}C were selected. The coolant temperature might affect fuel fragmentation and dispersion as well as the fuel temperature. Thus, initial coolant temperature 22, 42, and 52 ^{o}C were considered as experimental conditions. Since the melt and coolant temperature changes with interaction between melt and coolant, the experimental conditions were selected considering initial states. Single or multiple pins could be failed and relocated under actual reactor conditions. The fuel relocation experiments were performed depending on melt mass, especially 180 and 1400 g. When fuel is ejected into coolant, the burnup determines the pressure in the fuel cavity. The initial melt pressure of 10 bar was considered to confirm changes of melt relocation behavior with initial melt pressure. Finally, void channel condition was simulated using air and vapor-occupied channel.

Table 3-1. Physical properties of melt and coolant for fuel relocation experiments using UNICORN-B

	Actual materials		Simulant	
	Metallic fuel (U-10Zr)	Sodium	Wood's metal	Water
Density [kg/m^3]	14100	966	9383	998
Surface tension [N/m]	0.57	0.20	~ 1.00	0.07
Viscosity [mPa·s]	$5 \cdot 10^{-3}$	1.13	$1.90 \cdot 10^{-3}$	1.00
Melting / Boiling point [^{o}C]	1077 / -	- / 881	72 / -	- / 100

Table 3-2. Physical properties of vapor properties

	Sodium vapor	Water vapor	Air
Density [kg/m^3]	0.39	0.59	1.19
Thermal expansion coefficient [10^{-3}/K]	1.44	2.68	3.37
Viscosity [μPa·s]	1.13	$1.90 \cdot 10^{-3}$	1.00
Specific heat [kJ/kg/K]	2.51	2.07	1.01

Table 3-3. Experimental conditions for fuel relocation experiments using UNICORN-B

Test no.	1	2	3	4	5
Melt / Coolant material [-]	Wood's metal / Water	Wood's metal / Water	Wood's metal / Water	Wood's metal / Water	Wood's metal / Water
Melt temperature [°C]	90, 550	250, 256, 248	250, 252	252	251
Coolant temperature (air or vapor temperature) [°C]	24, 22	22, 42, 52	22, 21	25	(48, 46)
Melt mass [g]	180	180	180, 1400	180	180
Initial melt pressure [bar]	1	1	1	10	10
Coolant flow velocity [m/s]	0	0	0	0	0
Coolant saturation [-]	Unvoid (coolant-occupied)	Unvoid (coolant-occupied)	Unvoid (coolant-occupied)	Unvoid (coolant-occupied)	Void (air, vapor-occupied)
Froude number [-]	248	248	248	2130	2130
Weber number [-]	262	262	262	2253	2253
Remark	Initial melt temperature	Initial coolant temperature	Melt mass	Initial melt pressure	Air and vapor-occupied channel

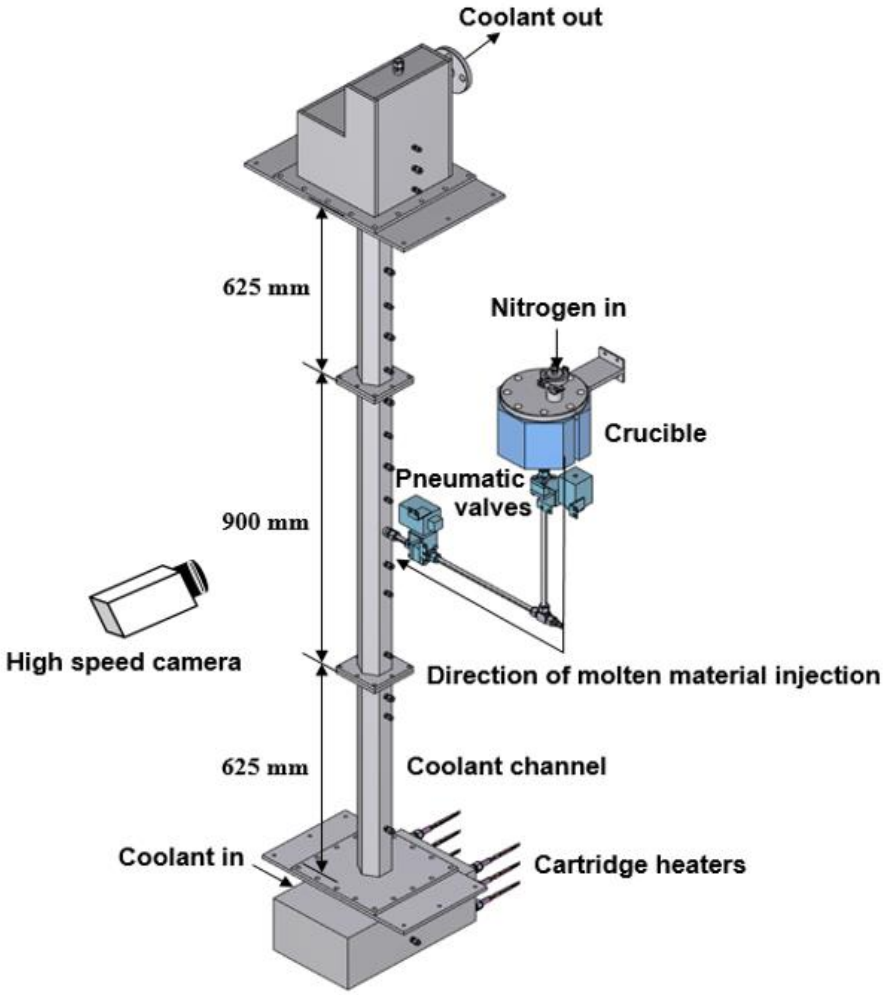

Fig. 3-1 Schematic diagram of UNICORN-B

3.3 Experimental results

There are key parameters affecting fuel relocation behavior, which is deduced from visual study using UNICORN-C. They are as follow; (1) initial melt temperature, (2) initial coolant temperature, (3) amount of melt mass, (4) melt pressure, and (5) void channel condition. To understand the fuel relocation phenomena in metal-fueled SFR, the parameters should be investigated. In the present experiment, parametric studies were carried out using Wood's metal in UNICORN-B.

3.3.1 Fuel relocation behavior

The initial melt temperature was determined by considering superheat temperature of the U-10Zr fuel in hypothetical core disruptive accident (HCDA) condition for metal-fueled SFR. The melt relocation experiments were performed with the initial melt temperature of 90 and 550 °C.

Fig. 3-2 and 3-3 shows the melt relocation behavior at the initial melt temperature of 90 and 550 °C, respectively. The melt reacted immediately with the coolant to promote its dispersion and fragmentation. It is known that melt jet fragmentation occurs due to the relative velocity difference between the melt and the coolant. However, the gap between the melt ejection point and the channel wall is 50 mm. Thus, in the present experiments, the melt collided with the channel wall immediately after melt ejection and melt was fragmented during the procedures. The hydraulic diameter in subassembly for metal-fueled SFR is about 3 mm. The smaller the gap where the melt is relocated, the more the melt fragmentation would occur due to the collision between the melt and the wall surface of the channel. In addition, it was observed that coolant was boiled in a local region due to continuous melt ejection and vapor column was partially generated. However, there was little difference in the fuel relocation and fragmentation behavior with change of initial melt temperature.

Fig. 3-4 represents the debris which was formed after the experiment. The debris shape seemed like ligament-like shape overall. There was no significant difference in the shape and characteristics of debris according to the initial melt temperatures.

Then, the fuel relocation experiments were conducted in initial coolant temperature of 22, 42 and 52 ℃. The initial coolant temperature applied to the experiment was chosen based on the temperature range of sodium considering transient conditions for initial phase of HCDA in metal-fueled SFR.

Fig. 3-5 shows the visual observation results of melt fragmentation behavior with initial coolant temperature of 22 ℃. The condition was highest subcooling compared to other conditions. In early phase of the experiment, gas mushroom dominates the behavior of melt injection. The gas mushroom was composed of air and nitrogen gas in crucible. The air was supplied from the intermediate pipe tubes between the crucible and the test section. After injected in the channel, the gas mushroom moved upward due to pressure difference. Thus, the backflow of melt may not occur at the melt injection point.

The melt was continuously injected into the coolant channel and collided to the channel wall. With multi-combined combined physical mechanisms, the melt was fragmented in the channel. Melt fragmentation occurred partly at the channel wall. It was driven by the inertia force of the melt. The inertia force of the melt activated the melt fragmentation and dispersed the melt debris. In addition, these physical phenomena generated vorticity in specific area around the melt jet. With the continuous melt injection, the vorticity grew strong and made the melt to be fragmented. Also, this vorticity stirred and collapsed the lower end of gas-occupied region. In these procedures, there were evaporations of coolant locally. The generated vapor made the melt to be in instable state. However, such vapor build was insufficient to discharge upward the melt. On the other hand, other melt fragmentation occurred due to hydrodynamic breakup. The breakup was induced by the relative velocity difference between the melt and coolant. Before the collision between the melt and channel wall, the hydrodynamic breakup was shown at the interfacial surface between two ambient fluids. The debris was formed after several combined melt fragmentation and moved downward owing to its high density.

Fig. 3-6 reveals the behavior of melt fragmentation with initial coolant temperature of 42 ºC. Before the melt injection into the channel, the gas mushroom was formed in the channel. The gas mushroom did not affect melt to be fragmented. With continuous melt injection, the lower part of the gas mushroom was collapsed. A part of the melt moved upward in the air-occupied region, but most of it moved downward generating vorticity. This bi-directional dispersion was developed due to the inertia force of melt. However, all melt moved downward after several seconds. It means that there was lack of melt levitation. Although there were evaporations of coolant in the channel, the vapor was not built up sufficiently. The generated vapor was concentrated at the channel wall because the melt moved left side continuously. Thus, the melt was more actively fragmented and dispersed at the channel wall.

As shown in Fig. 3-7, there was the fragmentation behavior of melt with initial coolant temperature of 52 ºC. Like previous cases, the gas was injected into the coolant channel in early phase of the melt injection. The melt was injected to coolant channel after the air injection. The melt fragmentation occurred at the interfacial surface between the melt and the coolant. This fragmentation behavior was clearly observed in Fig. 3-7. The inertia force of the melt dominated the instantaneous movement of the debris. In addition, the inertia force kept the collision of the melt jet with the channel wall. Through this collision with the wall surface, the melt fragmentation was accelerated. The fragmented melt was redistributed by the vorticity without the melt solidification. This melt redistribution phenomenon prevented the melt from taking place flow blockage and induced downward dispersion of the debris. There were two potential possibilities to examine this experimental result. One was the melt redistribution phenomenon, which circulated the flow to agglomerate the melt. The other was that the subcooling of the coolant was different. The different subcooling of the coolant caused the different quenching mechanism so that the debris would increase. In this case, the built-up vapor pressure was also insufficient to levitate the melt upward.

Fig. 3-8 shows debris after melt relocation experiments in initial melt temperature of 22, 42, and 52 ºC, respectively. In case of initial temperature of 22 ºC, there was a melt agglomeration to channel wall. Most melt were fragmented, solidified and dispersed through the collision between the melt and channel wall. The melt with superheat of 150 ºC was instantly quenched in the interfacial surface. The debris bed which was stacked on the bottom plate of test section. The debris did not have consistent shapes and sizes. The debris shape was various from flat sheets to droplet. The debris size also was different in wide range. After the melt injection, a part of melt was agglomerated to the channel wall. Some melt were agglomerated not dispersed. This melt agglomeration was cooled and solidified at the channel wall. The surface of melt agglomeration was like a cluster of fragmented melts. In addition, overall shape of the agglomeration was long and narrow. However, under the actual PGSFR subchannel structure, these agglomerations could prevent the core region from forming a coolable geometry.

Fig. 3-8 (b) shows the debris on bottom of test section. Small debris was concentrated and stacked on center of the debris bed. However, the debris did not have consistent tendency in terms of its shapes and sizes. Melt was also agglomerated at the channel wall in initial coolant temperature of 42 ºC. Overall shape of melt agglomeration was similar with case of initial temperature of 22 ºC. The melt agglomeration was also long and narrow at corners of channel. However, this agglomerated melt was clearly different from the previous case. The agglomerated volume decreased as the coolant subcooling decreased. In addition, the blocked area occupied by melt agglomeration decreased. The agglomerated area blocked the coolant flow path in the channel, so the melt agglomeration could accelerate the accident progression under severe accident condition.

Fig. 3-8 (c) the debris bed in initial coolant temperature of 52 ºC which was stacked on the bottom plate of test section after the melt injection. The debris did not have consistent shapes and sizes. The debris size also was different in wide range. This agglomeration was formed through the quenching of center of the melt jet at the channel wall. Once the center of the melt was quenched, the melt agglomeration was expanded with continuous melt injection. The position of melt agglomeration was slightly higher than melt injection point. In this test section, it did not matter to remain coolability of coolant channel. If the pin structure had considered in the experiments, it may not be able to ensure the coolability of coolant channel.

Fig. 3-9 shows the visual observation results of melt fragmentation behavior with 180 g of melt injection mass. This amount of melt injection means that the melt is injected into the coolant channel under single pin failure condition. The early behavior of the melt injection was dominated by air mushroom. The air mushroom made the coolant channel to the voided channel. The air was supplied from the intermediate pipe tubes between the crucible and the test section. After air injection, the melt was injected into the coolant channel and collided to the channel wall. During the melt injection process, the melt fragmentation behavior was determined from several combined physical mechanisms. Firstly, the melt fragmentation occurred in interfacial surface between melt and coolant. The melt with 150 ºC

superheat was instantly quenched in the interfacial surface and fragmented from the melt jet. That is, the hydrodynamic breakup which was caused by the instability wavelength occurred. However, the center of the melt jet was not quenched and collided to the coolant channel wall as a liquid phase. This collision was caused by the melt inertial forces and it made impact force to fragment remaining melt jet. The impact force induced significant melt fragmentation and dispersed the debris which was formed through the melt fragmentation procedure. In addition, these physical phenomena generated vorticity in specific area around the melt jet. With the continuous melt injection, the vorticity grew strong and activated the procedure of the melt fragmentation. Also, this vorticity stirred and collapsed the lower end of air-occupied region. Due to the collapse of voided region, coolant inflow was accelerated from relatively high position to melt-coolant interaction zone. Though the initial temperature difference between the melt and the coolant was about 230 ºC, the built-up vapor pressure was not sufficient to discharge the melt upward. The debris was formed after multi-combined melt fragmentation and moved downward owing to its high density.

The visual observation results of melt fragmentation behavior with 1400 g of melt injection mass, as shown in Fig. 3-10. The melt amount of 1400 g was equal to the total weight of eight fuel pins based on the fuel requirement of the PGSFR. Like a case of single pin failure, the air was injected into the coolant channel in early phase of the melt injection. The amount of air was irregular so that size of air mushroom was different at each experiment. The melt was injected to coolant channel after the air injection. The melt fragmentation occurred at the interfacial surface between the melt and the coolant. This fragmentation behavior was clearly observed in Fig. 3-10, which was explained by hydrodynamic instability theory. With continuous melt injection, the debris formed by the hydrodynamic instability moved to the channel wall. The inertia force of the melt dominated the instantaneous movement of the debris. In addition, the inertia force kept the collision of the melt jet with the channel wall. Through this collision with the wall surface, the melt fragmentation was accelerated. A part of the melt moved upward in the air-occupied region, but most of it moved downward generating vorticity. The vorticity collapsed air-occupied region and activated the melt fragmentation procedure. Also, the vorticity made the coolant channel covered with the fragmented melt. This behavior seemed as if flow blockage occurred. However, the fragmented melt was redistributed by the vorticity without the melt solidification. This melt redistribution phenomenon prevented the melt from taking place flow blockage and induced downward dispersion of the debris. Also, the melt redistribution increased the debris size.

As shown in Fig. 3-11 and 3-12, the debris formed in early phase of the melt injection was small than the debris formed in last phase of the melt injection. It was improved from that the debris was stacked on the bottom region of the test section. There were two potential possibilities to examine this experimental result. One was the melt redistribution phenomenon, which circulated the flow to agglomerate the melt. The other was that the subcooling of the coolant was different because the coolant was heated through continuous melt injection. The different subcooling of the coolant caused the

different quenching mechanism so that the debris would increase. In this case, the built-up vapor pressure was also insufficient to levitate the melt upward.

In addition to the visualization test, additional experiments were carried out in a hexagonal channel to simulate the hexagonal duct of fuel assembly in metal-fueled SFR. The experiments were performed to ensure geometrical similarity to the SFR channel. The experimental results are shown in Fig. 3-13. Thus, the necessity of critical melt amount leading to the flow blockage was suggested, and the coolable capacity after the fuel relocation was discussed.

Fig. 3-13 (a) represents frozen Wood's metal in the hexagonal channel using X-ray measurement. After melt injection experiment under single pin failure condition, a part of melt was agglomerated to the coolant channel wall. This agglomeration was formed through the quenching of center of the melt jet at the channel wall. Once the center of the melt was quenched, the melt agglomeration was expanded with continuous melt injection. The position of melt agglomeration was slightly higher than melt injection point. This agglomeration area was 15% of inner cross section of the hexagonal channel, which means that the melt agglomeration partially blocked the coolant channel. In this test section, it did not matter to remain coolability of coolant channel. If the pin structure had considered in the experiments, it may not be able to ensure the coolability of coolant channel. The debris did not have consistent shapes and sizes. The debris shape was various from flat sheets to droplet. The debris size also was different in wide range. It was hard to get experimental repeatability because a few change of test conditions could make different results. It means that debris evaluation methodology is limited. To evaluate the debris coolability qualitatively, the noble evaluation methodology for debris coolability is required.

Fig. 3-13 (b) shows debris in case of 1.40 kg melt injection mass using X-ray measurement. The debris was significantly agglomerated compared to the case of single pin failure. The melt was able to be agglomerated after melt the fragmentation because the amount of injected melt increased. The more melt injection mass increases the reaction time of the melt in a liquid phase so that blocked site by the melt agglomeration was different. The area agglomerated by the melt was 65% of inner cross section of the hexagonal channel, which mean that the melt agglomeration blocked most of the coolant channel. If multi-pins structure had involved to the experimental conditions, it would not ensure the coolability of coolant channel. The position of melt agglomeration was lower than melt injection point. The debris bed which was formed on the bottom plate of test section was also observed. The average debris size was larger than that of the case of single pin failure. In case of multi-pins failure, the debris did not also have consistent tendency in terms of its shapes and sizes.

In actual metal-fueled SFR transient conditions, the pressure of the cavity in the molten fuel increases up to a maximum of 100 bar. It is also known that the driving force that induces the discharge of the outer part of the melt is the pressurized environment by the fission gas in the fuel cavity or the rapid evaporation of the sodium bonded inside the pin. To reflect this, parameter study for melt pressure was conducted. In order to understand the characteristics of the ejection behavior of the melt according to

the ejection pressure of the melt, UNICORN-B was used a horizontal melt relocation experiment on the melt at an initial ejection pressure of 10 bar. The selection criterion of 10 bar is the maximum melt ejection pressure that could be controlled by UNICORN-B.

Fig. 3-14 and 3-15 show the melt ejection behavior and experimental conditions at a melt ejection pressure of 10 bar. Fig. 3-14 represents the molten Wood's metal behavior with time. In the initial phase of melt ejection, the melt fragmentated into smaller particles compared to the previous experimental results was confirmed. It means that the physical fragmentation due to the inertial force of the melt during melt ejection is promoted. In addition, it was observed that the discharge of the upper part of the melt occurred at a pressure of 10 bar. It could be seen by accelerating the top discharge behavior of the melt in the later stage of melt ejection. The reason for this phenomenon is that the driving force enough to discharge the melt to the upper part is formed due to the accumulation of vapor pressure due to the locally generated vapors which was for mutual reaction between the melt and the coolant.

As shown in Fig. 3-15, the non-visualization experiment using the hexagonal duct shows that the upper and lower ejection of the melt occurred more actively at the melt pressure of 10 bar than at the melt pressure of 1 bar. However, the melts discharged to the top dropped again to the bottom of the test section by gravity after a certain time. In addition, it was confirmed that the debris mean diameter decreases as the melt ejection pressure increases.

When the fuel is ejected into the channel under conditions where the fuel is molten and relocated, the coolant near the region where cladding failure occurs is boiled and form a void channel region. It is dependent on the SFR severe accident scenario, but the situation of melt ejection in this void channel region would not be totally excluded from the point of view of nuclear safety. From analytical result of metal version of SAS4A (SAS4A-M), the fuel melting occurred within 7 seconds (in case of simultaneous occurrence of unprotected transient over power and unprotected loss-of-flow) with the metal-fueled SFR, and the horizontal ejection of the melt due to the failure of the cladding within 2 seconds. This can lead to sudden increases in the fuel and cladding temperature and induce evaporation of the coolant. Therefore, it is likely that the environment is voided immediately before the melt relocation. To take into account the voided coolant channel, an air-occupied channel was used in the experiment.

Fig. 3-16 shows molten material behavior in the air-occupied channel during continuous melt injection. The channel was filled with air before the melt injection. In early phase of the melt injection, molten wood's metal was not directly fragmented. It was different with that in the coolant-filled channel. In case of the coolant-filled channel, the coolant actively interacted with the molten wood's metal at their interface. It means that the melt was well fragmented, which could have good potential to be dispersed and discharged upward. However, the molten materials were not fragmented but just frozen in the air-occupied channel. Since the water was more viscous medium than the air, there are different interactions when the melt moves through them. The frozen fragments adhered to the channel wall,

which was like the melt behavior itself. Also, there was no air flow generated by a pressure difference between inlet and outlet position of the melt injection nozzle. If this air flow was strong, it may have induced the melt levitation. In actual SFR transient condition, the sodium vapor flow could be formed by its natural circulation or the pressure difference between the molten fuel cavity and the coolant channel. This sodium vapor flow is suggested as one of key factors to levitate the molten metal fuel. In the air-occupied channel, there was no significant driving force for the melt levitation. The melt relocation experiments were conducted in a channel occupied with water vapor as well as with air.

Fig. 3-17 reveals molten material behaviors in the vapor-filled coolant channel. In the condition where Ex- Pin occurs, the sodium around damaged fuel may be rapidly evaporated. To consider such condition, the water in the test section was continuously evaporated using the cartridge heaters. In early phase of melt injection, the molten material was dashed against the channel wall. This behavior of molten material induced direct heat transfer between the molten material and the wall. Thus, freezing of molten material instantly occurred, because the wall temperature is quite lower than compared to that of the molten material. With continuous melt injection, frozen molten material was also added on the wall. This molten material just stuck to the wall, not fell. When considering the accident condition of actual reactor, this phenomenon in the experiment would be melt freezing. If the melt is frozen in the core region, subsequent accident could be induced. That is why the melt levitation is needed to mitigate the severe accident. In the test condition, some molten materials moved upward due to inertia force of the molten material. However, it was just temporary behavior. The molten materials, which were dispersed upward, moved downward after a few seconds. Since the liquid metal as well as the metal fuel has high density, the molten material would fall if there is insufficient driving force to levitate the molten material. The water vapor flow could be one of the driving forces leading the melt levitation. In this experiment, there is little impact on the melt levitation. The experimental results are different from the fact that the thermal expansion coefficient of air is larger than the thermal expansion coefficient of vapor.

In Argonne National Laboratory (ANL), there were experiments which various molten materials were dropped into sodium open pool. They showed that the debris shape would be different depending on the material characteristics. However, if the debris is formed in the voided channel, related fragmentation mechanisms need to be re-examined and improved.

As shown in Fig. 3-18, the debris had shape of the branches in the air-occupied and vapor-occupied channel, respectively. This debris was just solidified after the melt injection and moved downward to the base plate. Most fragments were stuck on the channel wall and others were stacked at the bottom plate. Figure 6 shows fragments frozen on hexagonal channel wall in the voided condition. These results are x-ray images to visualize the inside of stainless steel duct. The hexagonal channel was designed to reflect PGSFR duct shape. After the melt injection, the molten wood's metal was continuously frozen due to cold channel wall. The overall shape of these fragments seemed like the melt behavior during

the Ex-pin phenomena. It could be proved from the visual observation. Most of molten wood's metals were frozen around the melt injection nozzle. It means that the melt started to solidify after first collision with the channel wall. The cooling performance of the melt was dominated by the structure, rather than interaction between the melt and the air. In this case, molten wood's metal was not actively fragmented to particle shapes. The fragments with the shape of branches were formed and stuck on the wall. In case of vapor-occupied condition, most molten material was instantly frozen and it stuck to surface of the hexagonal duct. In side view of the radiography image, it was shown that molten material moved downward due to its high density. When compared to those of coolant-filled channel condition, active melt fragmentation did not occur in the vapor-occupied channel condition. This clarifies that the melt fragmentation depends on phase of coolant. In addition, there is different amount of molten material frozen to the channel wall according to the extent of melt fragmentation. Consequently, there exist differences between un-voided and voided channel results for melt fragments size and shape. In the un-voided channel, most fragments were stacked on a base plate, while they were stuck on a channel wall in the voided channel.

It was appeared that there was not significantly changes of fuel relocation behavior depending on the initial melt temperature, initial coolant temperature, and void channel conditions. The larger amount of melt ejection increased the amount of agglomerated melt in the coolant channel, which could lead to flow blockage in actual accident conditions. It is necessary to acquire analytical technique to evaluate the channel cooling ability when melt agglomerate is formed in the experimental facility. As the melt ejection pressure increased, the average hydrodynamic diameter of the formed debris decreased. This means that debris bed porosity can be formed differently depending on the burnup condition under actual accident conditions.

3.3.2 Fuel levitation

In initiating phase of HCDA for metal-fueled SFR, the accident consequences would be highly dependent on the fuel behavior. However, it is not clear to predict how the fuel would be fragmented and dispersed. If the fuel dummy is frozen at the core, the debris bed would be formed. The local flow blockage might be induced according to porosity of the debris bed. In addition, the core might be under recritical state by relocated fuel in the core. The metallic fuel sweep-out after cladding failure has been proposed as one of physical phenomena for accident mitigation. It could reduce the possibility of occurrence of successive accidents like the flow blockage and recriticaility. In this part, levitation heights where molten Wood's metal was discharged upward were evaluated. The theoretical results for the levitation height also were calculated from energy balance equation. The theoretical equations were induced not considering a function with time, thus average levitation height could be theoretically calculated. The theoretical results were compared with experimental results.

The fuel relocation experiments in the present study were conducted as a parametric study. The parameters which were selected were initial melt temperature, initial coolant temperature, melt mass, initial melt pressure and coolant channel condition. The reference case in the experiments was needed to evaluate effect of each parameter on the levitation height. The experimental condition for the reference case was as follows: initial melt temperature of 250 ºC, initial coolant temperature of 22 ºC, melt mass of 180 g, initial melt pressure of 1 bar, and coolant-occupied channel condition. In the fuel relocation experiments, there were 9 cases of experiments. To effectively compare the levitation height, the reference case was designated as case 1. The levitation height was measured after each experiment based on the visualization results.

Table 3-4 shows levitation heights which were measured in the fuel relocation experiments. The case numbers in the table are classified with the experimental conditions. Case numbers were assigned according to applied parameter based on the reference case. Case 2 and 3 are experiments which decreased and increased the initial melt temperature compared to the reference case. The experiments for effect of initial coolant temperature on the fuel relocation were designated 4 and 5. The effect of melt mass and initial melt pressure on the fuel relocation were also considered in the experiments. They were assigned to case 6 and 7, respectively. Finally, case 8 and 9 means the fuel relocation experiments which were conducted in air and water vapor-occupied channel. From the table 3-4, the levitation height of the case 1 which was reference case was 110 mm. It was already observed that the melt fragments which were dispersed upward fell due to its high density. Thus, there might be uncertainty to measure the levitation height based on the visualization results. The uncertainty was minimized through repeated experiment. The levitation heights were within a similar range in some experimental cases, except for case 7, 8, and 9. Since the thermodynamic effect on the levitation height was not significant, there was little change of the levitation height with initial melt and coolant temperature. In addition, it could mean that effect of coolant boiling on melt sweep-out was negligible in the experiments. The coolant boiling is proposed as one of driving forces to the fuel discharge, but vapor pressure generated by the coolant boiling was insufficient in this case. The flow area is considered as one of factor to determine vapor pressure. To perform visual study of the fuel relocation phenomena, the hydraulic diameter of test section was 50 mm in UNICORN-B. The effect of the coolant boiling on the levitation height was not observed because of relatively large flow area. In case 6, the levitation height was measured as 103 mm. The melt mass also did not significantly affect the movement of melt stream. On the other hand, there was increase of the levitation height with initial melt pressure. The levitation heights for case 7, 8, and 9 were 154, 220, and 218 mm. The melt pressure which stands for pressurized force by fission gas in fuel cavity provided inertial force that allows the melt to be dispersed upward and downward. It was confirmed that main driving force determining melt motion is inertial force of melt itself which was generated by the melt pressure. However, there was difference of the levitation height depending on the coolant channel conditions. The case 7 was performed in coolant-occupied channel, but the other cases

were conducted in air and vapor-occupied channel. The height where the melt traveled upward varied depending on the medium through which the melt passed. There was the height difference of about 65 mm. In case 8 and 9, the air and vapor were used to occupy the channel. The experimental results regarding the levitation were almost same. To measure the average levitation heights in the experiments, the contributors for the melt levitation were investigated from the visual studies. The main contributor was revealed as total ejected volume by the melt relocation. The volume occupied the channel and vigorous mixing was observed in the volume, which induced levitation of debris in the volume. It was reflected total ejected volume and volume addition by evaporation was expressed as volume of air, evaporated steam and debris volume with its porosity. This volume occupied the channel with upward and downward bidirectional expansion. Therefore, total ejected and increased volume were divided by 2 times of the channel area. It was assumed that the debris was homogeneously filled in the channel.

To compare the levitation heights from between experimental and theoretical results, the forces which were applied to melt were investigated. Fig. 3-19 represents free body diagram of melt during fuel relocation phenomena. In the experiment, the initial melt pressure was key driving force to determine the height where the melt was traveled. It was observed that the levitation heights were dependent on the medium. However, the frictional force by structure could be negligible in the study. Since the flow area was relatively large, the melt behavior was not disturbed by the inner structure. When the melt moved upward, the drag forces by the medium was involved in the melt motion. The buoyant force also affected the melt behavior. Finally, the gravitational force should be considered. The force balance equation for the melt is given by

$$F_m = F_{pre} + F_{drag} + F_{buo} + F_g \tag{3.2}$$

When the shape of melt was simply assumed as sphere, energy balance is derived by each force term.

$$W_{pre} + W_{drag} + W_{buo} = \Delta E_g \tag{3.3}$$

The kinetic energy of the melt is generated from the initial melt pressure. Considering vertical velocity of melt, the work by the initial melt pressure is defined by

$$W_{pre} = \frac{1}{2} m \overline{v_m}^2 \tag{3.4}$$

The drag force by medium is regarded with drag coefficient, coolant density, coolant velocity, and surface area of melt. The coolant velocity is equal to the melt velocity due to no flow condition in the experiment. The work by drag force is defined as the product of the drag force and the levitation height.

$$W_{drag} = -\frac{1}{2} c_d \rho_c \overline{v_m}^2 A \Delta h \tag{3.5}$$

where c_d is drag coefficient. The average particle size is calculated from Eq. 3-1 where the shape of melt was assumed to be spherical. Most of fuel relocation experiments were conducted in coolant-occupied channel. Since the melt was submerged, the buoyant force was considered and the work by buoyant force is given by.

$$W_{buo} = \rho_c V_m g \Delta h \tag{3.6}$$

The potential energy of melt was changed by melt mass and levitation height. The change of the potential energy is defined by

$$\Delta E_g = \rho_m V_m g \Delta h \tag{3.7}$$

By using Eq. 3.3-3.7, the energy balance equation is rearranged by

$$\frac{1}{2} m \overline{v_m}^2 - \frac{1}{2} c_d \rho_c \overline{v_m}^2 A \Delta h + \rho_c V_m g \Delta h = \rho_m V_m g \Delta h \tag{3.8}$$

The height where the melt discharged upward could be calculated from the melt velocity, physical properties of melt and coolant.

$$\Delta h = \frac{\frac{1}{2} m \overline{v_m}^2}{\left(\frac{1}{2} c_d \rho_c \overline{v_m}^2 - \rho_c V_m g + \rho_m V_m g\right)} \tag{3.9}$$

Fig. 3-20 shows the levitation heights from between experimental and theoretical results. The theoretical results were calculated using Eq. 3.9. In the void channel, the levitation height was over-estimated since the frictional force was not considered in the theoretical model. However, overall the theoretical model showed good agreement with the experimental results. With increase of initial melt pressure, the levitation height of melt was increased in both experimental and theoretical results. In HCDA condition for metal-fueled SFR, the pressure by fission gas and vaporization of sodium bond is dependent on burnup. The difference of melt ejection pressure in between beginning of end cycle (BOEC) and end of equilibrium cycle (EOEC) has been predicted up to 50 bar depending on accident scenarios. It means that possibility of early accident termination is greater in EOEC than that of BOEC.

Table 3-4. Levitation heights in fuel relocation experiments

Test no.	Initial melt temperature [°C]	Initial coolant temperature [°C]	Melt mass [g]	Melt pressure [bar]	Coolant saturation	Levitation height [mm]
1	250	22	180	1	Coolant-occupied	110
2	90	24	180	1	Coolant-occupied	108
3	550	22	180	1	Coolant-occupied	120
4	256	42	180	1	Coolant-occupied	86
5	248	52	180	1	Coolant-occupied	98
6	252	21	1400	1	Coolant-occupied	103
7	252	25	180	10	Coolant-occupied	154
8	251	48	180	10	Air-occupied	220
9	251	46	180	10	Water vapor-occupied	218

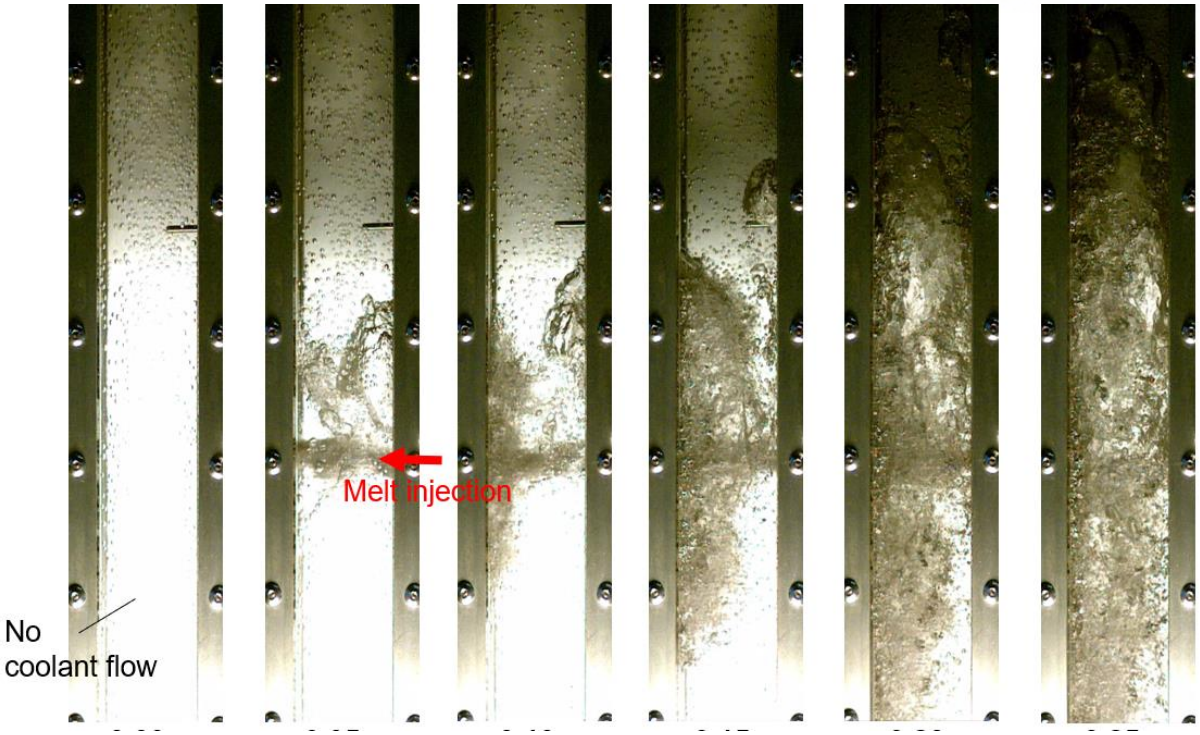

Fig. 3-2 Optical images of melt relocation behavior with initial melt temperature of 90 °C

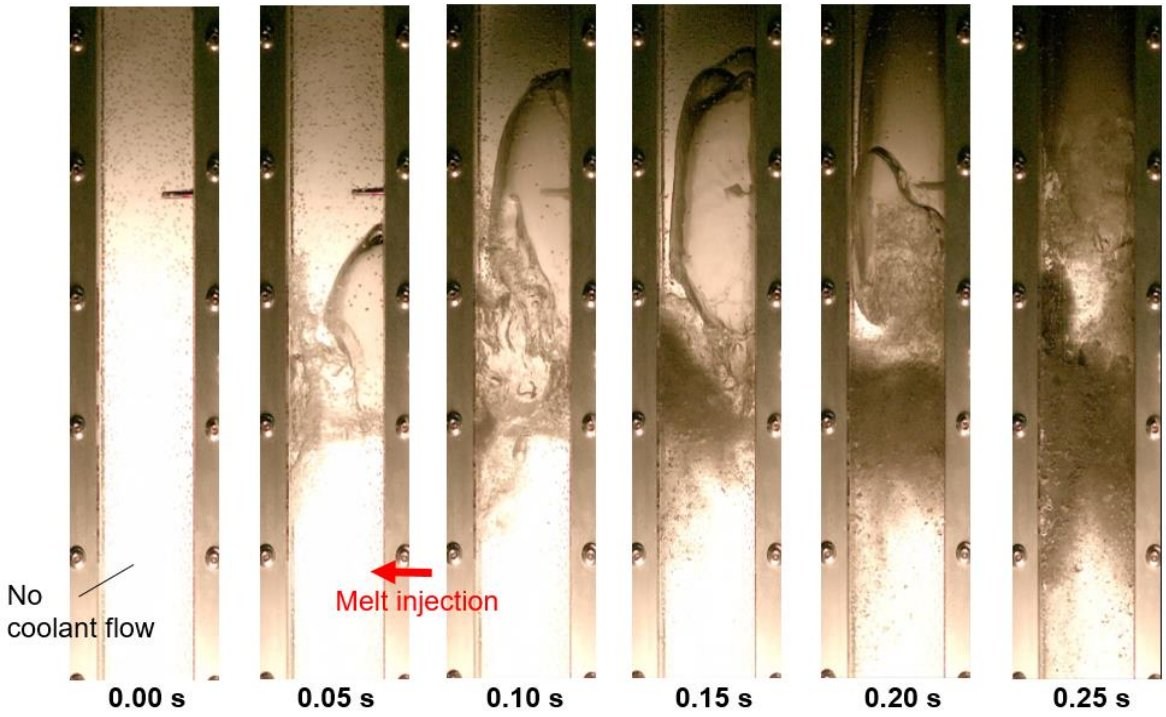

Fig. 3-3 Optical images of melt relocation behavior with initial melt temperature of 550 °C

(a)

(b)

Fig. 3-4 Optical images of debris after melt relocation experiments in initial melt temperature of (a) 90 and (b) 550 ℃

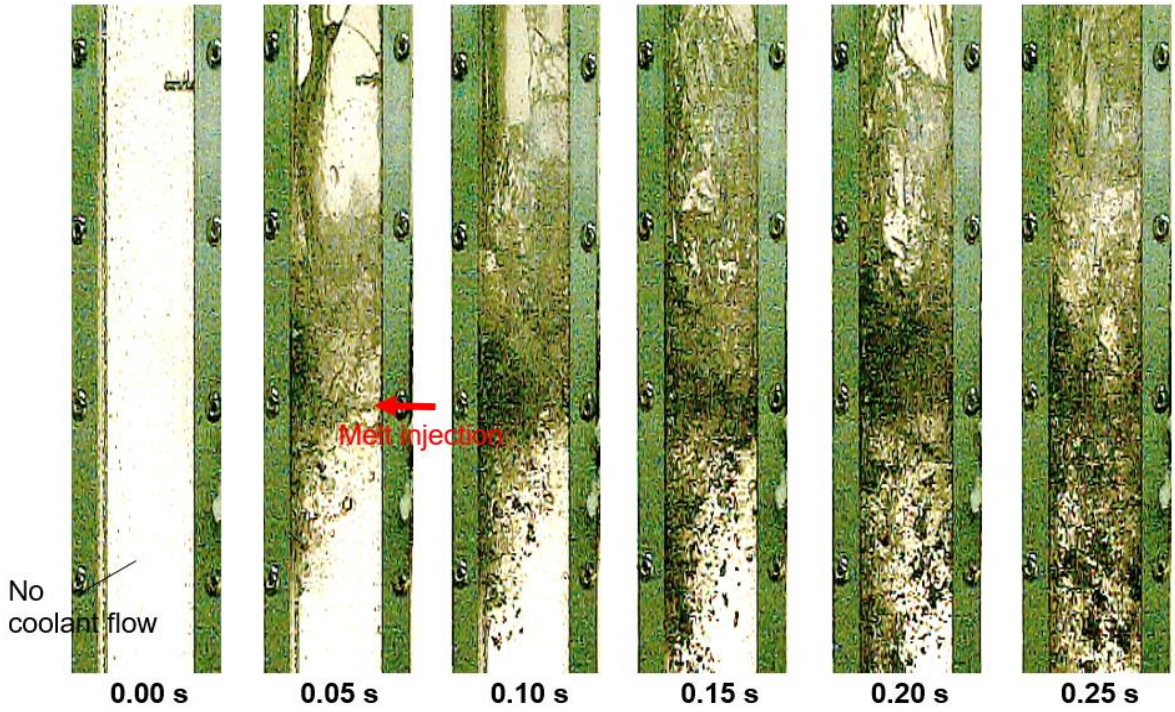

Fig. 3-5 Optical images of melt relocation behavior with initial coolant temperature of 22 ºC

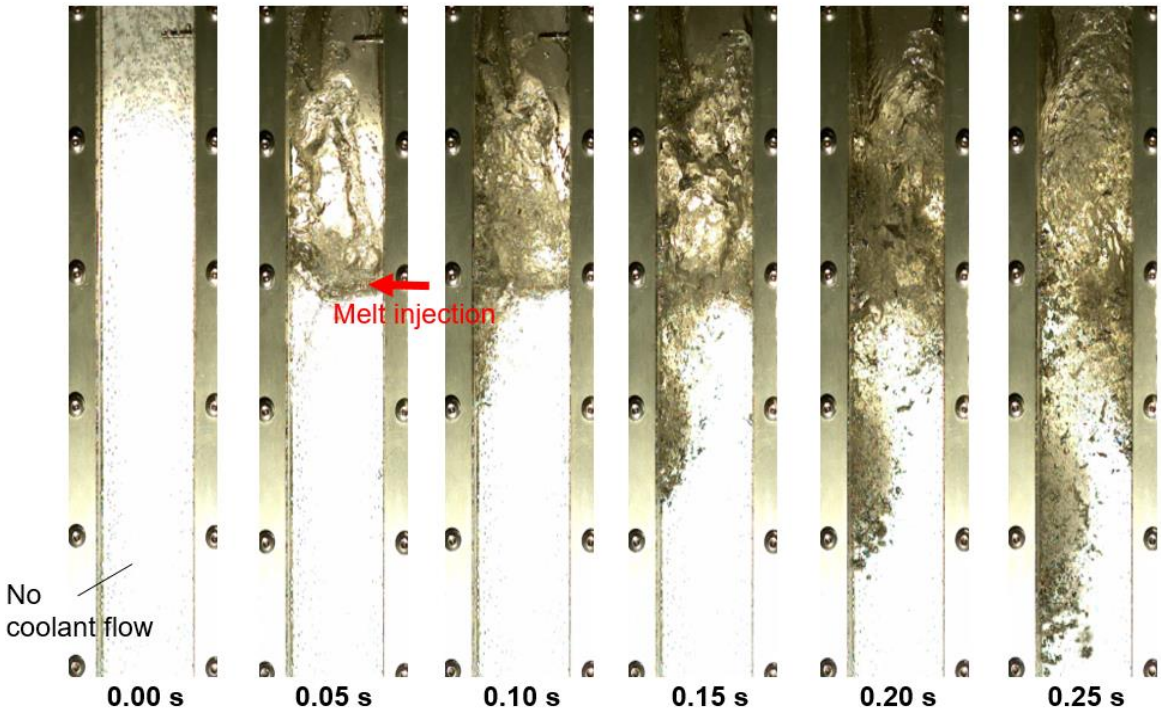

Fig. 3-6 Optical images of melt relocation behavior with initial coolant temperature of 42 ºC

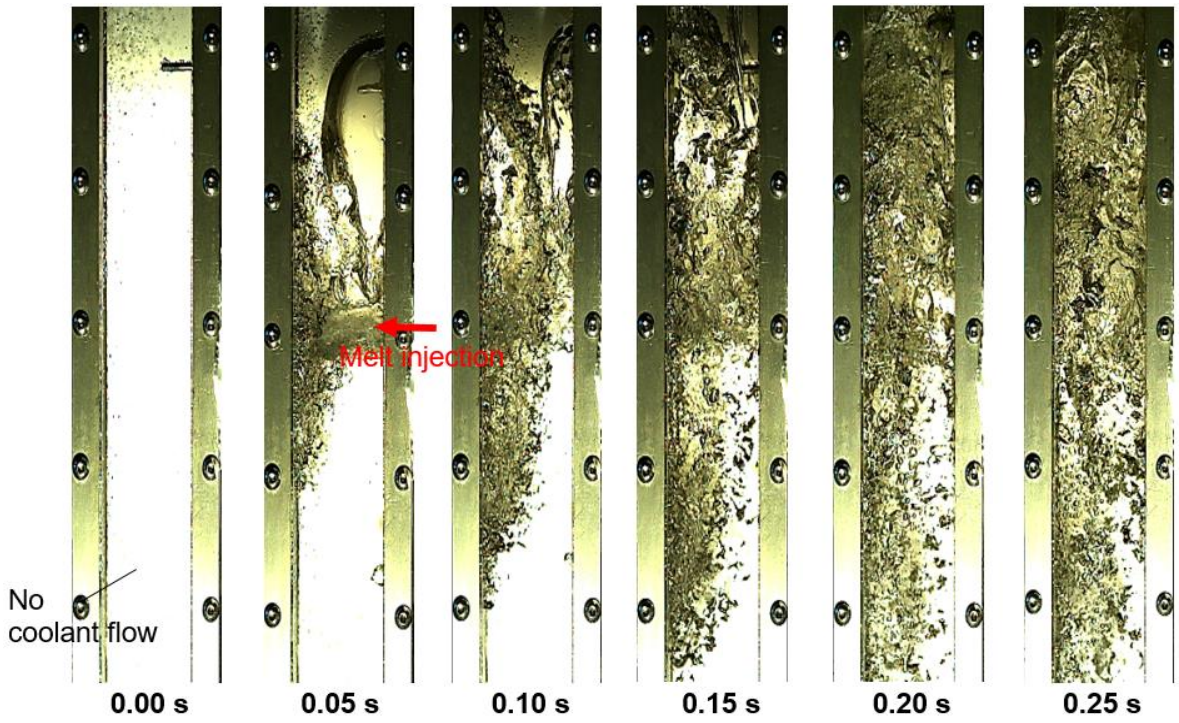

Fig. 3-7 Optical images of melt relocation behavior with initial coolant temperature of 52 °C

(a)

(b)

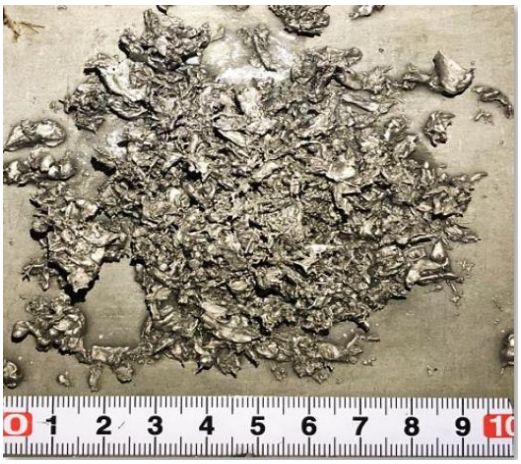

(c)

Fig. 3-8 Optical images of debris after melt relocation experiments in initial melt temperature of (a) 22, (b) 42, and (c) 52 ℃

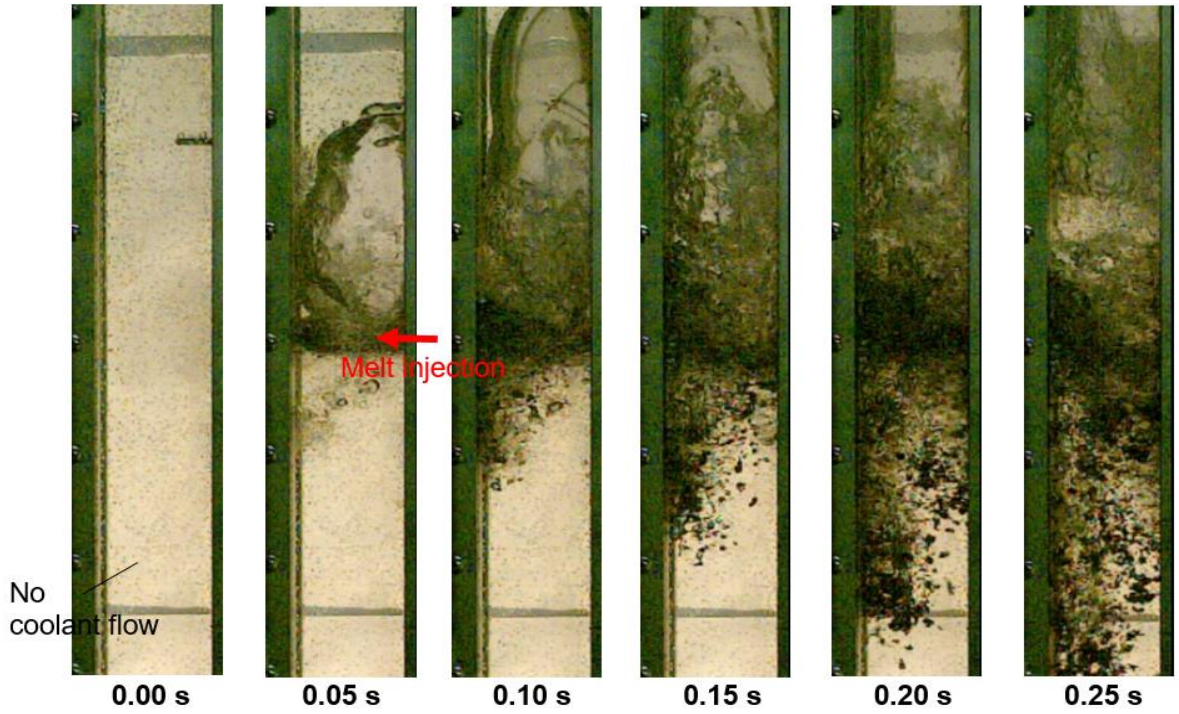

Fig. 3-9 Optical images of melt relocation behavior with melt mass of 180 g

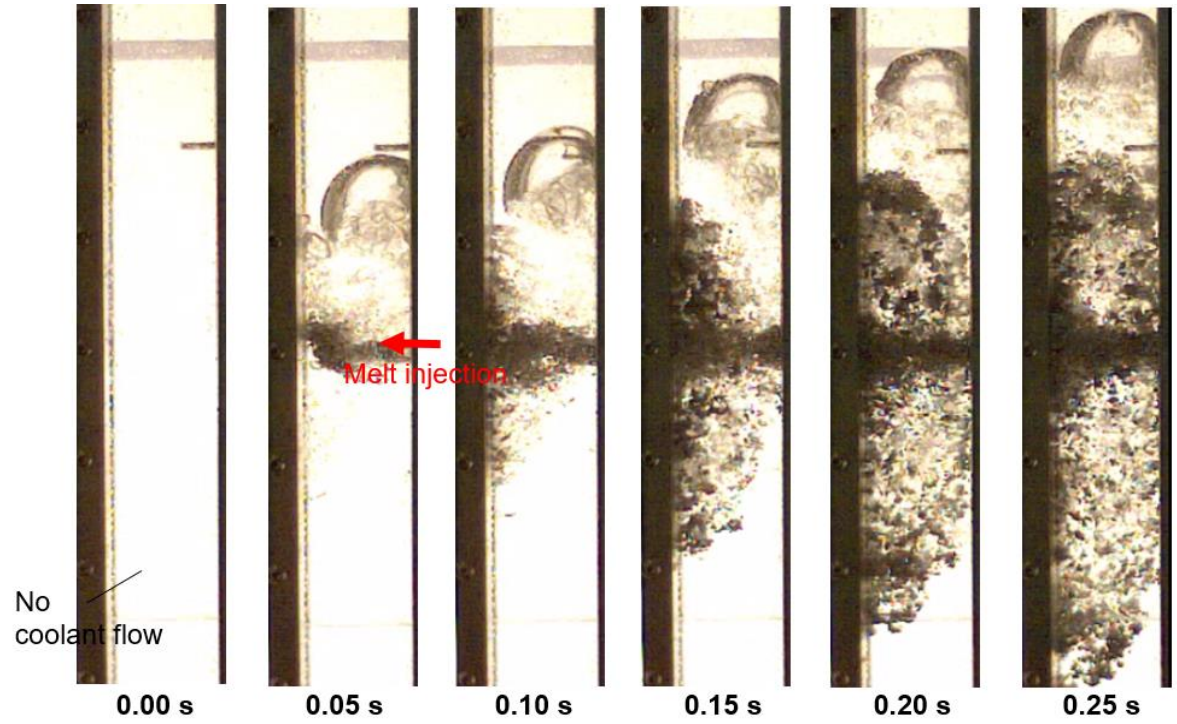

Fig. 3-10 Optical images of melt relocation behavior with melt mass of 1400 g

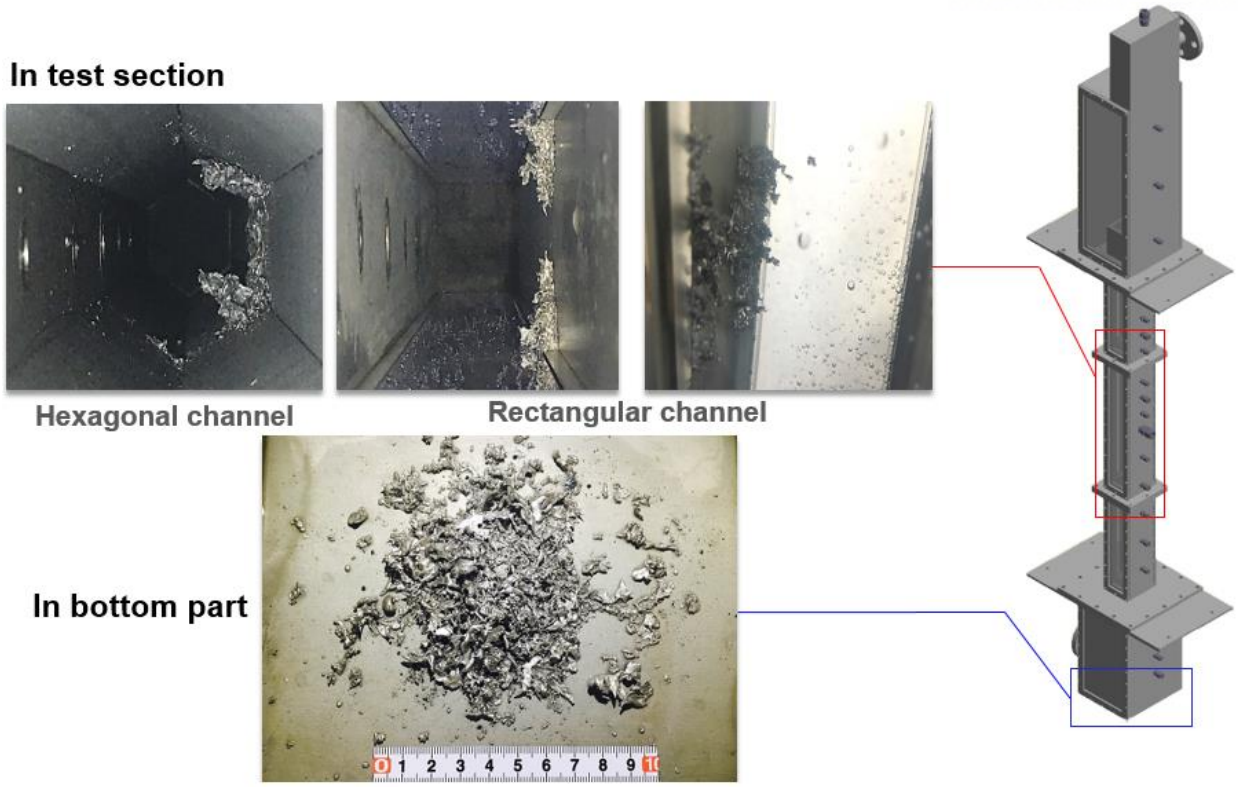

Fig. 3-11 Optical images of melt agglomerate and debris after melt relocation experiment in melt mass of 180 g

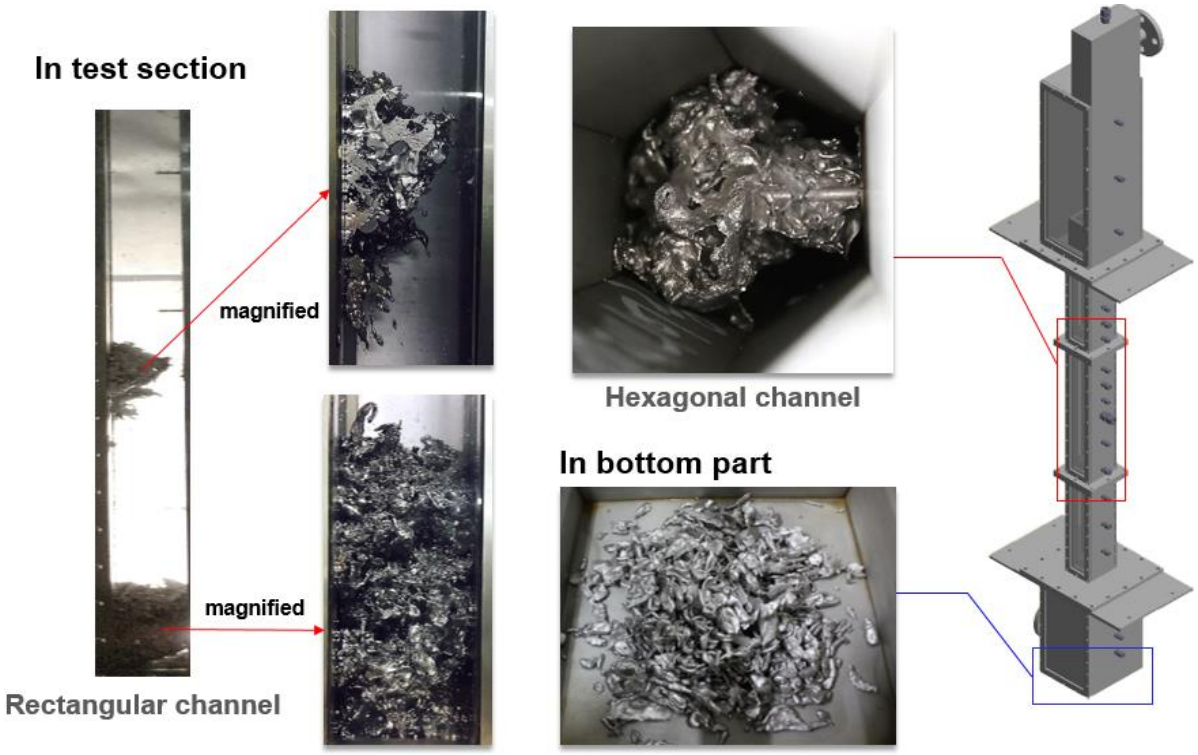

Fig. 3-12 Optical images of melt agglomerate and debris after melt relocation experiment in melt mass of 1400 g

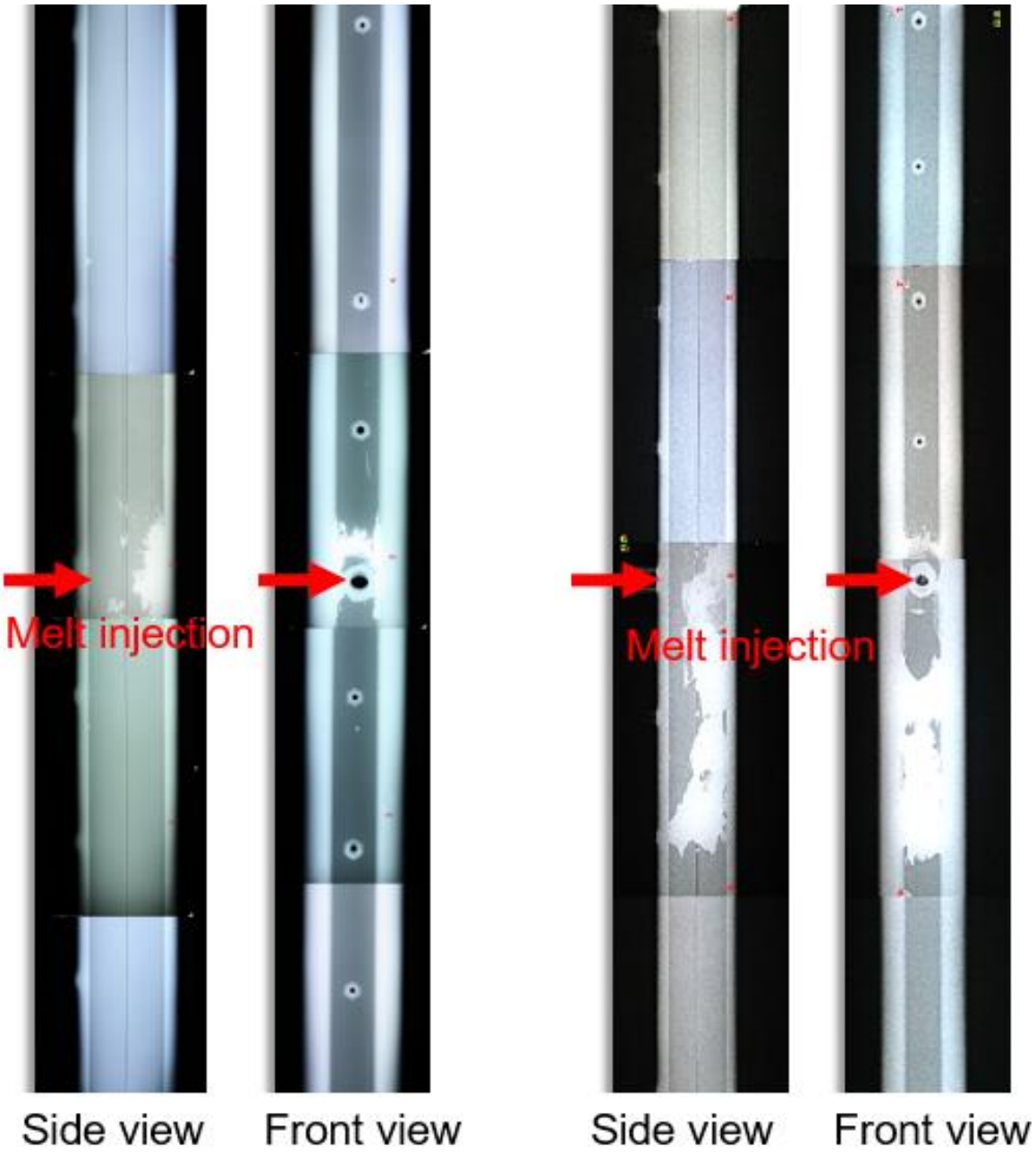

(a) (b)

Fig. 3-13 Radiography images of melt relocation behavior in melt mass of (a) 800 g and (b) 1400 g

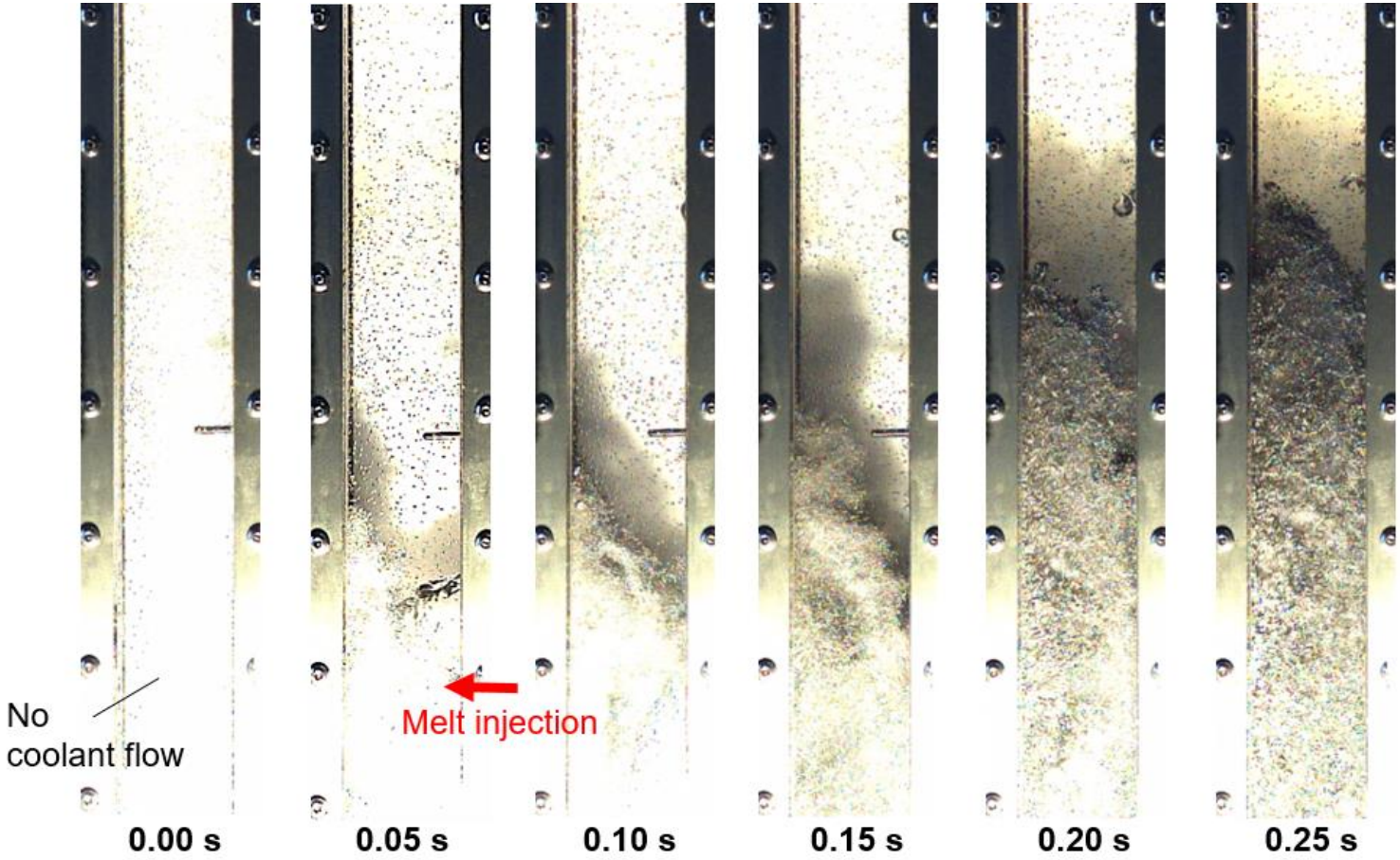

Fig. 3-14 Optical images of melt relocation behavior in melt pressure of 10 bar

Fig. 3-15 Radiography images of melt relocation behavior in melt pressure of 10 bar

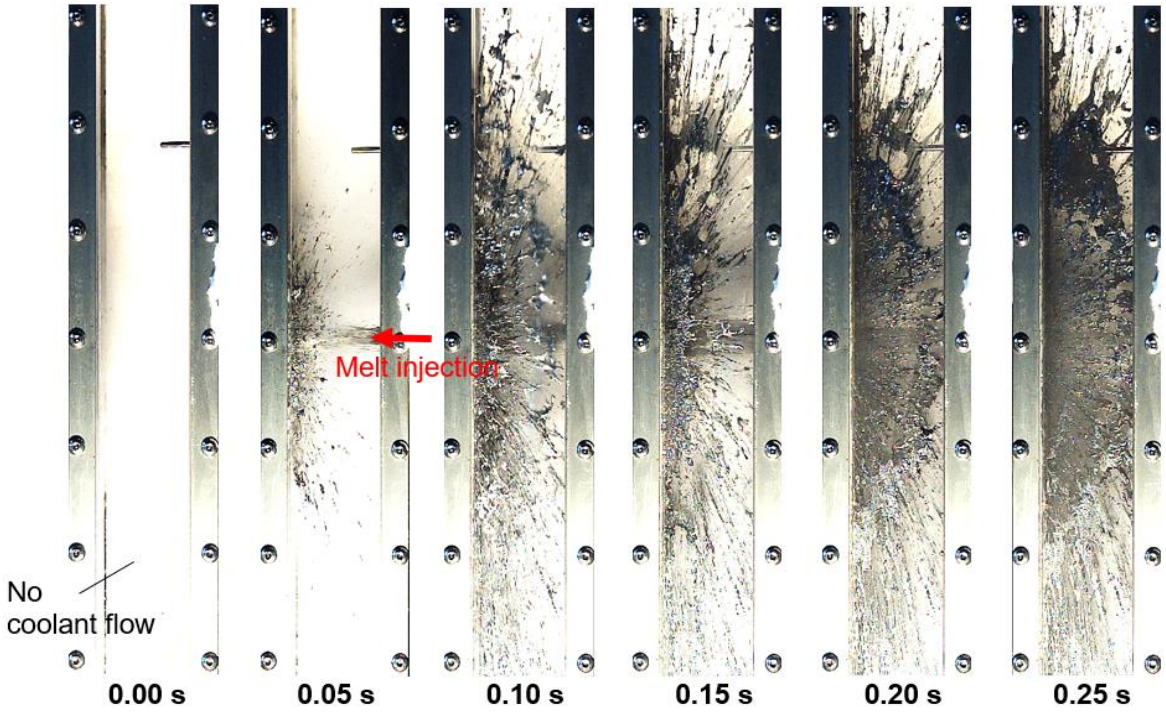

Fig. 3-16 Optical images of melt relocation behavior in air-occupied channel

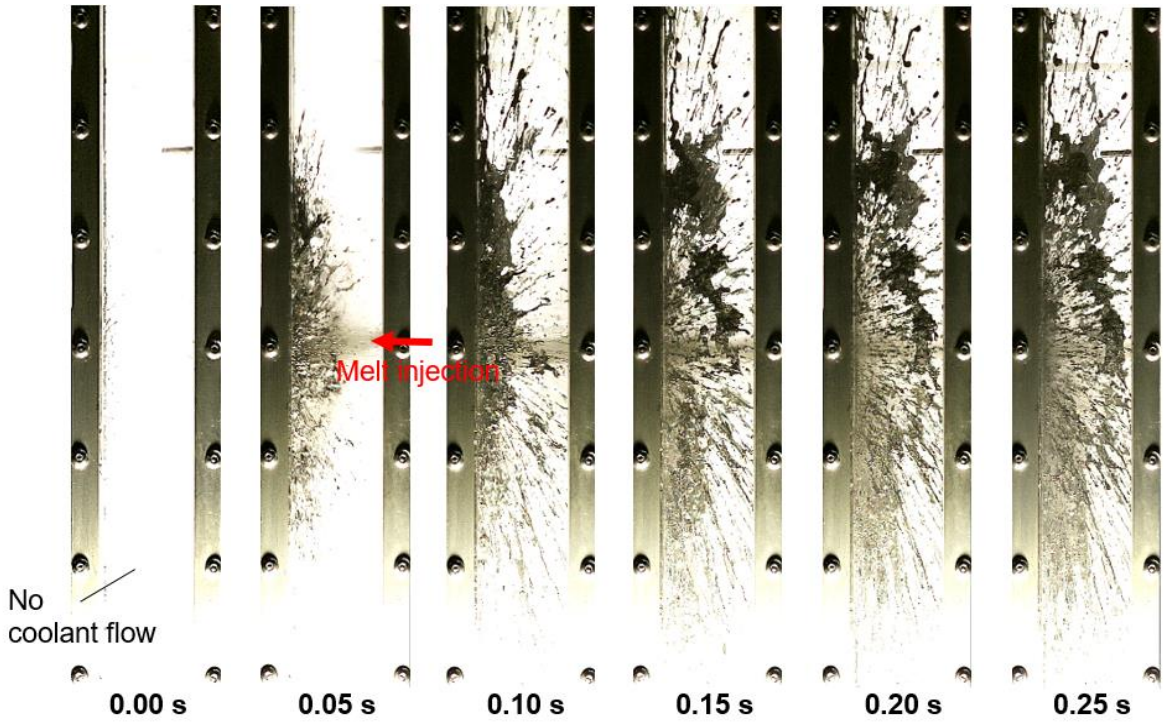

Fig. 3-17 Optical images of melt relocation behavior in vapor-occupied channel

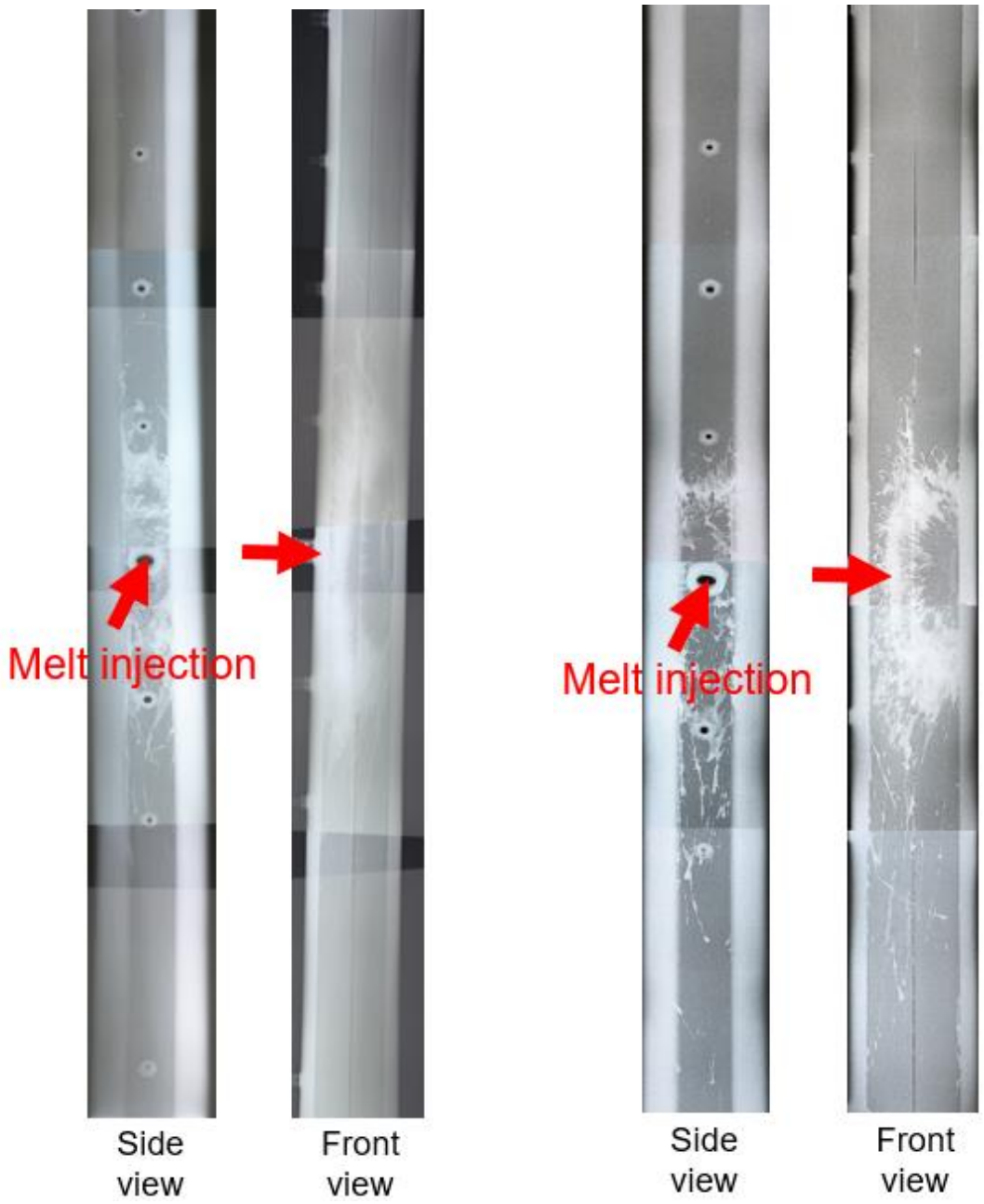

(a) (b)

Fig. 3-18 Radiography images of melt relocation behavior in (a) air and (b) vapor-occupied channel

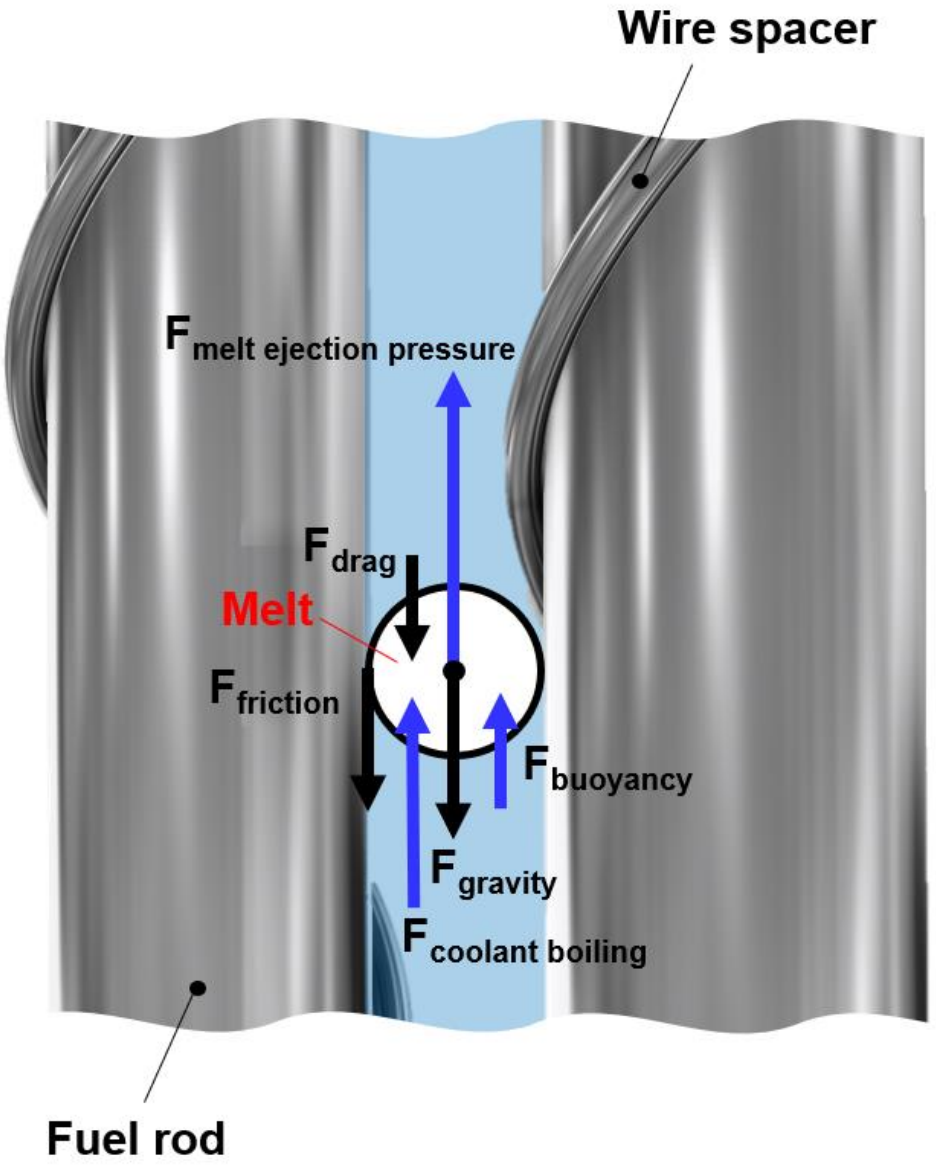

Fig. 3-19 Free body diagram of melt during fuel relocation phenomena

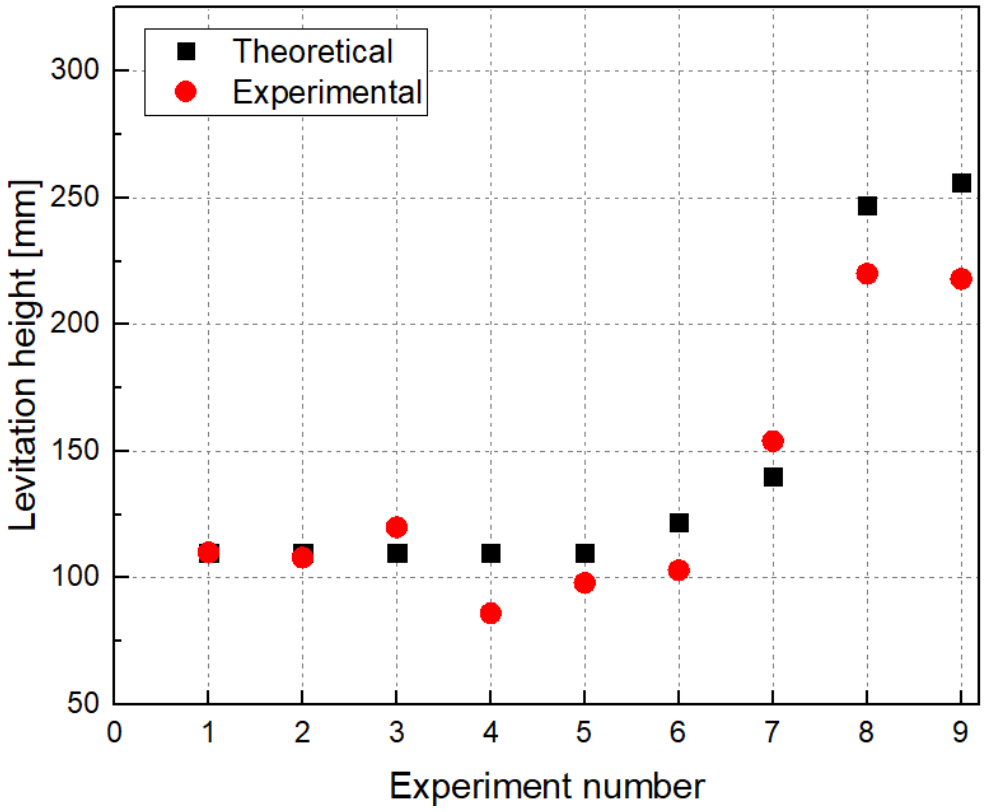

Fig. 3-20 Comparison of levitation heights between experimental and theoretical result in fuel relocation experiments

(Exp. #1 - T_m: 250 °C, T_c: 22 °C, m_m: 180 g, P_m: 1 bar, coolant-occupied

Exp. #2 - T_m: 90 °C, T_c: 24 °C, m_m: 180 g, P_m: 1 bar, coolant-occupied,

Exp. #3 - T_m: 550 °C, T_c: 22 °C, m_m: 180 g, P_m: 1 bar, coolant-occupied,

Exp. #4 - T_m: 256 °C, T_c: 42 °C, m_m: 180 g, P_m: 1 bar, coolant-occupied,

Exp. #5 - T_m: 248 °C, T_c: 52 °C, m_m: 180 g, P_m: 1 bar, coolant-occupied,

Exp. #6 - T_m: 252 °C, T_c: 21 °C, m_m: 1400 g, P_m: 1 bar, coolant-occupied,

Exp. #7 - T_m: 252 °C, T_c: 25 °C, m_m: 180 g, P_m: 10 bar, coolant-occupied,

Exp. #8 - T_m: 251 °C, T_c: 48 °C, m_m: 180 g, P_m: 10 bar, air-occupied

Exp. #9 - T_m: 251 °C, T_c: 46 °C, m_m: 180 g, P_m: 10 bar, water vapor-occupied)

Chapter 4. DEBRIS BED POROSITY EXPERIMENTS

4.1 Introduction

Sodium-cooled fast reactors (SFRs) with metallic fuel have inherent reactivity feedback mechanisms and high thermal conductivity. They provide advantages for an accident mitigation even in an initiating phase of severe accident. The initiating phase means when cladding failure occurs and molten fuel is ejected into coolant. There are complex physical phenomena in the phase. The molten metallic fuel could be swept out above the core or dispersed in subassembly, depending on accident scenarios. In the latter case, the fuel might be fragmented and frozen in the core, leading to local flow blockage[70-79]. It depends on debris bed porosity whether the core has a coolable capability from a natural convection. Since there is a lack of fundamental understanding for the accident consequences, it is necessary to investigate the debris bed porosity in hypothetical core disruptive accident (HCDA) for metal-fueled.

The pour stream experiments were conducted in Argonne National Laboratory (ANL). The purpose of the experimental study was to evaluate the metallic fuel behavior in severe accident of liquid metal reactor (LMR). The key parameters which were considered in the experiments were as follows; Melt superheat, melt ejection velocity, ejection diameter, sodium pool depth, and melt material. They investigated the fragmentation and interaction behavior of the metallic fuel with sodium. In addition, the debris size, shape, and porosity of debris bed were analyzed. From the pour stream experiments, most of the debris shapes were formed in the ligament-like and sheet-like shape. The average size of the debris was about 10 mm, and the debris was stacked on as a debris bed on bottom of interaction vessel. The debris bed porosity was measured using radiography image and there was a high porous debris bed with debris bed porosity of 0.9. The experiments were performed with melt ejection velocities. The experiments at high melt ejection velocities of 10 m/s resulted in small debris formation compared to experiments with low ejection velocities. In addition, the small debris formed the debris bed porosity of 0.84. In the experiment, thermal equilibrium was reached within 2 to 3 seconds immediately after the fuel-sodium interaction. The thermal equilibrium was determined by the energy balance between (1) the temperature rise of sodium in the fuel-sodium interaction and (2) the temperature decrease of the melt including the fuel freezing in which the melt solidified. They concluded that debris shape for the metallic fuel was like ligament and sheet and the debris bed with a high porosity was formed. Even if a debris bed with a thick layer is formed, a debris bed with a high voidage is likely to provide a flow path. Thus, the decay heat could be removed by convection and boiling heat transfer to mitigate the severe accident. In addition, they revealed that debris with high thermal conductivity was also advantageous for decay heat removal.

There were researches to analyze debris characteristics like its morphology and size. Most of studies

focused on the disassembly phase of HCDA. In the phase, significant amount of fuel is ejected into the lower plenum of reactor vessel because the disassembly phase assumed that core is already degraded. Thermal fragmentation has been proposed as one of mechanism to predict the debris shape and size during the physical phenomena. The research groups regarding to the thermal fragmentation performed the experiments where the melt stream or droplet dropped vertically into coolant pool. After the experiment, the debris analysis also was carried out with its size distribution.

The chapter 4 includes two experimental study for debris bed porosity and quenching for debris formation. Firstly, the debris bed porosity experiment was conducted. Using new developed experimental facility, the ex-pin experiments were performed in 19-pin bundle structure. The test section was designed by referring to design parameters of Korean typed sodium-cooled fast reactor (SFR). To simulate actual transient condition, the experimental conditions were deduced from analysis results of SAS4A. The accident scenario was selected with simultaneous occurrence of unprotected transient over power (UTOP) and unprotected loss-of-flow (ULOF). From the ex-pin experiment, the debris bed was observed using radiography image. In addition, the debris shape forming the debris bed was visualized using micro-CT in detail. The debris bed porosity was evaluated from the experiment. To understand how debris bed was formed in terms of debris bed porosity, quenching experiments was performed. As a result, characteristic length concept for debris was introduced and was investigated with instantaneous contact temperature between melt and coolant.

4.2 Experimental setup and procedures

There were two type of experiments in this chapter; ex-pin and quenching experiment. The ex-pin experiment was conducted to evaluate the debris bed porosity after fuel relocation. To simulate fuel ejection from a cladding which are degraded, the fuel ejection method was newly developed. The fuel relocation behavior was investigated using radiography images. The debris bed porosity was analyzed both using classical method and micro-CT. The classical method means that the porosity was calculated using volume fractions. To obtain physical insights of characteristics of debris bed porosity in metallic fuel, the quenching experiments were performed. In the quenching experiments, the levitation coil which was a kind of induction heating was used. In this part, the experimental setup and procedures for the experiments were introduced.

4.2.1 Ex-pin experiment

To predict the debris bed porosity after fuel relocation in metal-fueled SFR, it is necessary to establish a test section simulating actual SFR fuel assembly. In addition, ex-pin experiment should be performed reflecting the actual fuel ejection conditions in initiating phase of HCDA.

In the study, design specifications of fuel assembly in prototype generation-IV SFR (PGSFR) were referred. Table 3-1 shows the design parameters in between PGSFR fuel assembly and newly developed experimental facility. The adult version of UNIST molten core and coolant interaction experimental facility (UNICORN) was established, which is called UNICORN-A. In the test section of UNICORN-A, diameter of fuel pin, pitch, and the spacing between the wire spacers of PGSFR were reflected. The test section is a 19-pin bundle structure and enable to eject melt from a damaged tube which stands for degraded cladding.

In the case of severe accident conditions of PGSFR, it is also possible to derive the melt ejection conditions based on the result of the SAS4A code. The experimental result of the fuel relocation obtained from the melt ejection conditions could be used to validate the related phenomenon modeling. Thus, UNICORN-A was developed and its characteristics compared to the existing experimental facility as follows:

- Reflection of design specification of active core in PGSFR fuel assembly (P/D, L/D)
- Construction of multi-pin bundle structure with wire spacer
- Ejection of melt from degraded rod structure
- Actual melt ejection condition considering SAS4A results

Recently, ANL has been developing a metal fuel version of SAS4A, an early stage analysis code for SFR severe accidents. The existing SAS4A has been developed as an SFR critical analysis code for oxide fuel such as MOX fuel, but it is also developing a metal fuel version of SAS4A reflecting the physical and chemical characteristics of the metal fuel in transient conditions. In the study, the accident scenario was selected to deduce melt ejection condition from SAS4A results. The simultaneous occurrence of UTOP and ULOF event was considered as the accident scenario. It was reasonable from a conservative point of view. According to the safety analysis results using the SAS4A, it was confirmed that the cladding failure occurred in the simultaneous occurrence of UTOP and ULOF event and the fuel relocation phenomenon occurred.

The SAS4A metallic fuel version mentioned above is currently in development and has limited use of non-developer code. Therefore, in this study, the range of experimental conditions is derived by adding the physical properties of the PGSFR metal fuel U-10Zr to the existing SAS4A. One of the major differences between the SAS4A metallic fuel version and the existing SAS4A version is whether or not the cladding failure is simulated by eutectic reaction and Zr migration. In the pin relocation series experiment conducted at the recent ANL, it showed that the metallic fuel was deeply penetrated to the side stream due to the eutectic reaction between the metal fuel and the cladding tube. From the viewpoint of the melt ejection condition, there is a relatively little change of temperature and pressure in the fuel cavity is not large when the cladding failure due to eutectic reaction is greater than the mechanical failure of the cladding tube due to the high pressure in the pin cavity. In other words, the SAS4A analysis using U-10Zr property could generate a larger boundary of melt ejection condition.

In order to simulate the simultaneous occurrence of UTOP and ULOF event for analysis using SAS4A, a positive response of 0.1 $/s is inserted without scram, and half of the flow rate in 0.3 seconds due to the trip of two primary heat transport system (PHTS). The test matrix was selected to reflect the melt ejection conditions derived from the SAS4A analysis.

Table 3-3 reveals the experimental conditions in the ex-pin experiments. The damaged diameter which means size of degraded cladding, melt ejection mass, and melt superheat during ejection were selected to be 3 mm, 15.26 g, and 15 °C, respectively, according to the analysis of the SAS4A for simultaneous occurrence of UTOP and ULOF event. In addition, in the SAS4A analysis, air was used as the coolant as a coolant in consideration of the fact that the portion of the water near the rupture portion of the melt was filled with sodium vapor. In most metallic fuel SFRs, the phenomenon of pin fracture following fuel fusion occurs by eutectic erosion. As a result, in the case of eutectic erosion, the melt ejection pressure is considerably less than the mechanical failure of cladding due to the increase in the pressure inside the pin cavity. Therefore, the melt ejection pressure obtained from the SAS4A analysis and the melt ejection pressure in the TREAT-M series experiment DB were selected as the upper and lower ranges of the melt ejection pressure, respectively. In this experiment, the experimental conditions were selected by selecting the melt pressurization pressure of 7 bar within the range of melt

ejection considering the structural limitations of the fuel relocation simulator.

Fig. 3-1 represents preliminary experimental facility for experiment of debris bed porosity. The experimental facility consisted of 7-pin bundle structure. The fuel ejection method using damaged pin was tested. In addition, effect of the structure temperature on the melt behavior and the debris bed porosity was examined. In the experiment, the structure temperature means the temperatures of surrounding rods near the rod where the melt was ejected. When the fuel relocation occurs, the temperature surrounding fuel rods might be high as well as the fuel rod where the cladding bleach occurs.

Fig. 3-2 shows UNICORN-A (adult) as experimental facility for fuel relocation phenomena. For multi-pin structures such as SFR fuel assemblies, they should be designed to have the same spacing between all pins and pins. At the lower part of the assembly, there is a grid which is fixed at a certain interval to support the structures. The various pins fastened to each grid are kept at the same spacing regardless of the axial direction by the wire spacers. In addition, a total of four cartridge heaters with a maximum output of 1.2 kW were installed at the lower part of the aggregate, so that the temperature of the coolant could be controlled in a future nuclear fuel reloading simulation. The height of the test section excluding the lower part of the aggregate is 1216 mm, which is designed to be higher than 900 mm, which is the PGSFR active core region. This is for analyzing the melt discharge behavior and the axial distribution of the upper discharge. A total of 19 pins were inserted into the test section of the hexagonal duct, and the middle pin was selected as the broken pin to simulate the melt ejection. In addition, the hexagonal ducts were divided into several equal parts in order to easily repeat the experiments based on previous experience. Axial pressure gauges were installed to quantitatively analyze the melt dispersion behavior. The ex-pin experiment was conducted using Wood's metal as simulant for metallic fuel. Table 3-2 shows physical properties of Wood's metal.

There are two types of pin structures: intimate pins, damaged pin. The wire spacers were designed to be equal to the L/D of the PGSFR fuel pins for all pins. The wire was designed to have a diameter of 1 mm and was also designed to simulate wire geometry with PGSFR. For damaged pins, it is designed to be 85 mm higher than unbroken pins. This is because the crucible and the broken pin must be fastened for melt ejection. In the simulation of nuclear fuel relocation, a line heater was installed in the melt injection line between crucible and broken pin to minimize heat loss during melt ejection.

The ex-pin experiments using UNICORN-A were carried out as follows.

- Make the damage pin where the melt would be ejected from crucible.
- Connect the damaged pin to the pipeline connected to the crucible and insert it into the 19-pin assembly.
- Put the wood's metal into the crucible with the mass to be ejected.
- Control the initial melt temperature and pressure in the crucible.

- Eject melt by controlling valves connected between the crucible and the damaged pin.
- After the ex-pin experiment, cool the test section down sufficiently and take radiography of the test section to qualitatively analyze the melt distribution along the axial direction and debris bed porosity.

4.2.2 Quenching experiment

It is crucial to understand how high porous debris bed is formed in metallic fuel after the fuel relocation. In the present study, there was experimental approach to investigate the debris formation using quenching experiment. Fig. 3-3 shows schematic diagram of experimental facility for quenching experiment. The experiment was conducted by dropping the melt droplets into the coolant pool. Since the instantaneous contact temperature of melt and coolant was considered as key parameter on the debris formation, it was important to control the initial melt and coolant temperature. The melt temperature was varied using an induction heater with melt levitation. The copper coil for the induction heating could levitate the melt droplet in the coil. With oscillating electromagnetic fields in the coil, there was a force to levitate the melt droplet. Thus, proper frequency and power were required depending on melt materials. The quartz tube was used to oxidation of melt particle during the heating of melt droplet. After melt was reached at the desired temperature, the melt droplet was dropped into coolant pool which was designed as a rectangular channel with thermocouples. The temperature change of melt was measured in coolant channel. The coolant temperature was controlled with cartridge heaters inserted in the channel. There were two cartridge heaters to control the coolant temperature up to saturation point. In addition, the channel was designed with transparent windows to observe the quenching procedure.

The quenching experiments were performed using following experimental procedures.

- Make the melt droplet according to experimental conditions.
- Control frequency and power in induction coil to levitate the melt droplet.
- Put the melt droplet inside the coil and heat up the melt.
- Drop the melt into coolant pool when melt temperature is reached at desired condition.
- Collect the debris formed in the coolant channel to analyze the debris size and morphology.
- Observe the debris shape and measure the surface area and volume of the debris using micro-CT.

Table 3-4 represents the test matrix for the quenching experiment. The melt droplet was used with Wood's metal since the Wood's metal was eutectic alloy. In initiating phase of HCDA for metal-fueled SFR, the cladding was degraded with eutectic reaction between metallic fuel and cladding material. Although there was effect of hoop stress on the cladding failure, the eutectic reaction was critical

phenomena to degrade the cladding in metal-fueled SFR. When the metal fuel is ejected into coolant, the melt would be a eutectic alloy. To consider quenching performance in the eutectic alloy, Wood's metal was selected as simulant for metallic fuel. The range of initial melt and coolant temperature was achieved for various instantaneous contact interface temperatures. The initial temperature of melt was varied from 100 to 500 ºC. The range of instantaneous contact interface temperature was from 32 to 110 ºC. The range included the freezing point of Wood's metal. Based on experimental results of fuel relocation experiment in chapter 3, it was found that the melt temperature gave significant effect on formation of the debris morphology. However, the effect of coolant temperature on the debris formation seemed to be negligible. Thus, initial coolant temperature was not considered as experimental parameter. The melt formed nominal at diameter of 10 mm spheres in the induction coil before its quenching. To analyze physical characteristics of debris, the debris size and morphology was observed using micro-CT. The micro-CT is an equipment for computed tomography and it was optimized to observe debris shape in the experimental conditions.

Table 4-1. Design parameters between PGSFR fuel assembly and UNICORN-A

	PGSFR	UNICORN-A
P/D	1.14	1.14
L/D	29.86	29.88
P [mm]	8.44	9.12
L [mm]	221	239
D [mm]	7.4	8

Table 4-2. Physical properties of melt and coolant for fuel relocation experiments using UNICORN-A

	Metallic fuel (U-10Zr)	Wood's metal
Density [kg/m^3]	14100	9383
Surface tension [N/m]	0.57	~ 1.00
Viscosity [mPa·s]	$5 \cdot 10^{-3}$	$1.90 \cdot 10^{-3}$
Melting / Boiling point [^oC]	1077 / -	72 / -

Table 4-3. Comparison of SAS4A result and experimental condition

	SAS4A results	Experimental results
Damaged diameter for melt ejection (mm)	2.975	3
Initial melt superheat [^{o}C]	15	15
Melt mass [g]	15.26 g/pin	15.26 (single pin failure)
Initial melt pressure	44.47	44

Table 4-4. Test matrix for quenching experiment

	Experimental results
Initial melt temperature [^{o}C]	100 – 500
Initial coolant temperature [^{o}C]	18
Instantaneous contact Interface temperature [^{o}C]	32 – 110
Melt diameter [mm]	10

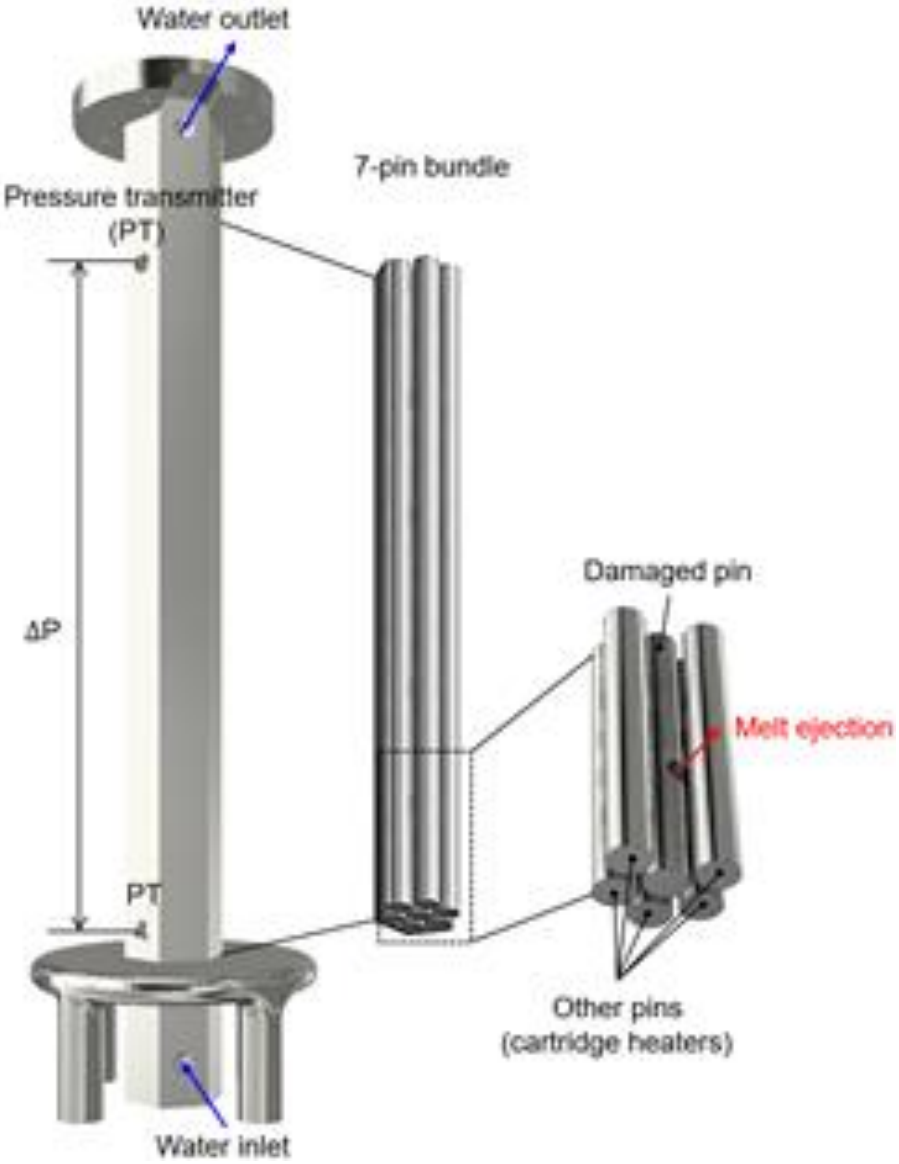

Fig. 4-1 Schematic diagram of experimental facility for fuel relocation in 7-rod bundle structure

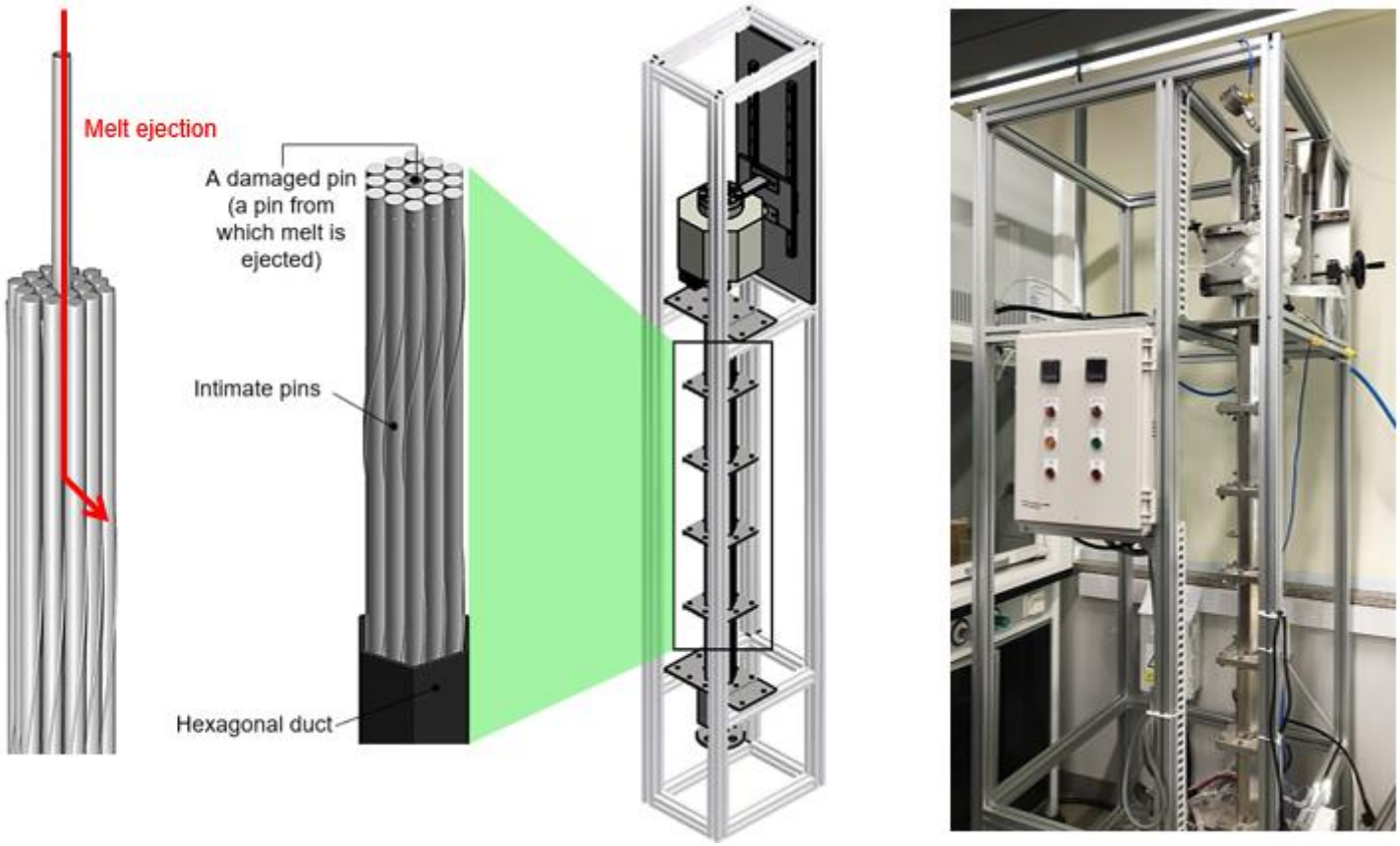

Fig. 4-2 Schematic diagram and optical image of UNICORN-A

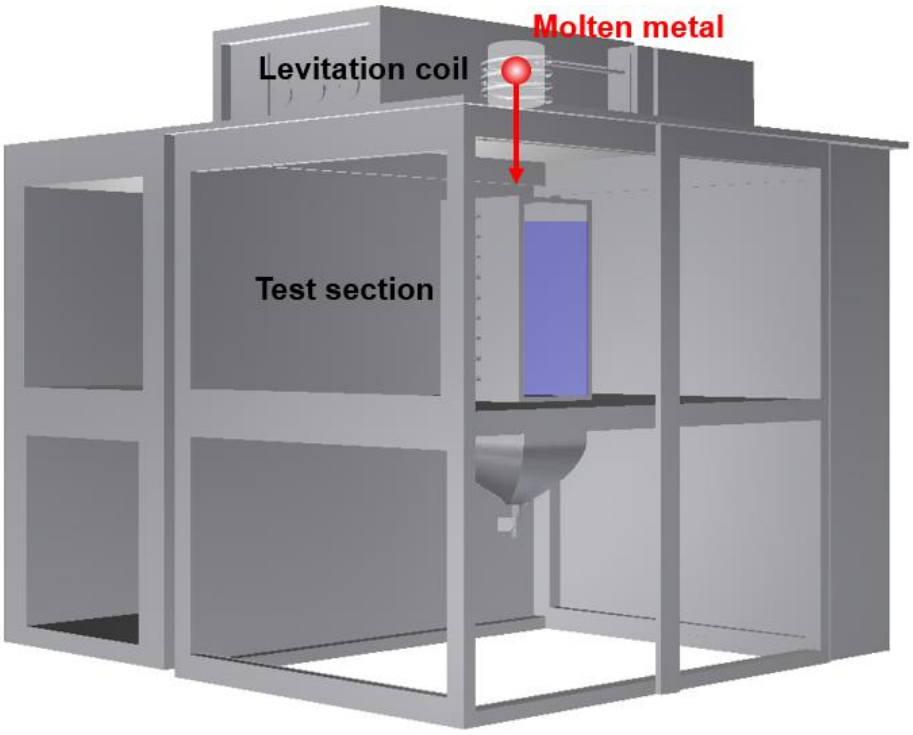

Fig. 4-3 Schematic diagram of experimental facility for quenching experiment

4.3 Experimental results

In this part, debris bed porosity from the ex-pin experiment and characteristic length of debris were discussed. To evaluate the debris bed formation, the ex-pin experiment was firstly performed in UNICORN-A. The debris bed porosity was measured considering simultaneous occurrence of UOTP and ULOF event. Since there are quenching phenomena when fuel is relocated into coolant, the physical relationship between the instantaneous contact interface temperature and debris characteristic was investigated.

4.3.1 Debris bed porosity

Fig. 4-4 represents the test for ex-pin experiment in 7-pin rod bundle structure. In order to reflect the pin diameter and pin-to-pin spacing of the actual PGSFR, a test section considering the multi-rod bundle structure was constructed. In the transient condition, the middle pin among the seven pins with the highest probability of fuel ejection was designed as a damaged pin. A circular shape of 3.7 mm diameter was selected as a fracture shape, and the peripheral pins were designed as a temperature controllable cartridge heater. In addition, a pressure gauge was installed at the top and bottom of the test section to measure the pressure drop after the fuel relocation experiment. This is to measure the pressure drop change due to the melt debris dispersed in the secondary passages after nuclear fuel relocation.

In the fuel relocation experiment, the melt in the crucible was instantaneously ejected into the side stream. Fig. 4-5 shows the change in pressure in the channel during the fuel relocation. From the graph, melt starts to be ejected around 1.4 seconds and has a maximum pressure of about 2.3 bar at 1.9 seconds. It means that all of the melt in the crucible has been ejected into the sub-stream within 0.5 seconds. It was observed that the equilibrium of pressure reached 3.5 seconds after melt ejection.

Fig. 4-6 reveals the result of x-ray photographing of the shape of test part after melt ejection. In the case of Wood's metal, the damping coefficient difference with the surrounding structure is remarkable, so that the dispersion behavior and distribution of the melt in the fuel assembly can be grasped by x-ray photographing. In the case of the 7-pin assembly, it was possible to observe the atomized melt debris after melt ejection. The debris observed here was heterogeneous in shape, and concentrated in the vicinity of the rupture, not integrated, but distributed away from the rupture in several directions.

There are several criteria for evaluating the cooling capacity of the core immediately after the ejection of the melt in the early stage of a serious accident. Here, a method of identifying the pressure drop change due to the debris bed is proposed as one of the criteria for evaluating the core cooling capability. According to previous research results, it is known that metallic fuel has a high porosity of 0.9. In this experiment, the pressure drop was measured on a 7-pin before and after the melt ejection. Fig. 4-5 shows the change in pressure drop in the channel before and after the fuel relocation. The graph

including the debris shows the pressure drop change after the fuel relocation and the graph without the debris means the bare condition before the melt ejection. The graph shows that the debris of the metal type increases the pressure drop compared to the bare condition even if the porosity is high. This is because the pressure drop coefficient due to the debris bed is increased. This tendency was also revealed by CFD analysis. Flow-3D was used to construct the same geometry as the 7-pin assembly test section, and pressure drop experiment was performed by setting the porous media using the porosity and permeability obtained from the experiment. As a result, it is confirmed that the trend is consistent with the pressure drop experiment results.

Figure 4-7 shows the experimental results of the fuel relocation experiment under simultaneous occurrence of UTOP and ULOF event. The visualization results were obtained by X-ray after the fuel relocation experiment. The X-ray damping coefficient difference between the test structural material and Wood's metal, the fuel material, can clearly distinguish the results of the fuel relocation behavior. According to the critical accident scenarios selected in this study, local coolant boiling occurs before nuclear fuel breakdown occurs. This means that the fuel is ejected under void channel conditions. As a result, the metal fuel with high thermal conductivity is quenched after it is relocated in the channel. Therefore, it is physically plausible to deduce the relocation behavior of nuclear fuel through X-ray after the experiment like this experiment.

As shown in Fig. 4-7, the melt was radially dispersed around the rupture of the damaged pin. This is the same as the preliminary experimental results of the fuel relocation in the previously performed 7-pin rod bundle structures. In addition, the following melt distribution and channel behavior can be deduced through the solidified melt distribution. The melt ejected through the rupture part lost its inertial force due to the collision between the pin and the surrounding structures such as the wire spacer, and the dominant melt behavior has the behavior of spreading to the region between the pin and the pin in the radial direction. X-ray photographs showed that the melt was distributed at the shear area of the 19-pin fuel assembly. On the other hand, the melts spread in the radial direction are dispersed upward and downward in accordance with the rotation direction of the wire spacer as the melt ejection continues through the rupture part. Through this series of melt behaviors, the range of the melt discharged to the upper and lower sides of the fracture section was within a radius of about 43 mm and 67 mm. This can be understood in more detail in Fig. 4-8. Fig. 4-8 shows the mass fraction of Wood's metal per axial direction. From the analysis of mass fraction by axial direction, metal fuel has high density so the fuel falls down to solidify when the fuel is relocated. This applies only if there is no upper coolant flow as in simultaneous occurrence of UTOP and ULOF event.

No particulate form of melt debris was observed and the solidified melt in the form of agglomerates could be identified. It is considered that the melt has solidified before the melt atomization due to the collision between the melt and the surrounding pins due to the inherent characteristics of the metal with a large cooling rate in the voided region. The pin shape and the gap between pins of the comprehensive

test apparatus are similar to PGSFR. This suggests that the same ejection behavior and axial distribution as the experimental results will occur under the same accident scenarios in PGSFR.

The simulation results show that there is insufficient driving force to induce the top exhaust after the nuclear fuel breakdown without the coolant flow to the top. As a result, the melt in the nuclear fuel assembly is located in the atomized state. In order to induce the end of the accident after the initial stage of a severe accident, residual heat should be removed by core cooling by natural circulation. The debris bed porosity is an important variable in determining the extent of the accident, since the pressure drop depends on the porosity of the debris bed in the fuel assembly.

Fig. 4-9 shows the debris bed visualization results formed after the experiment. Wood's metal debris bed shape was secured with Micro-CT and debris bed porosity was measured by post-processing. The porosity of Wood's metal debris bed was 0.89. In addition, the porosity also was measured with classical method using volume fractions. From the method, the porosity of 0.83 for the debris bed was measured. Since the debris bed porosity varies according to the accident conditions, the debris bed porosity experiments were conducted and measured the porosity range of Wood's metal debris bed.

As a result, it was confirmed that the porosity was in the range of 0.82-0.89. It is included in the porosity range of the metal fuel debris bed formed after the quenching of the metal fuel (U-10Zr) in ANL's sodium pool in the 1960s. This means that even if the fuel is destroyed, the metal fuel has the safety of early termination of the accident.

4.3.2 Characteristic length of debris

From previous fuel relocation experiments, it was found that the debris bed was formed in the subassembly. There was high porous debris bed when using metal-typed melt. In pouring stream experiment with the metallic fuel, the debris bed with high porosity of 0.8 was formed. It could be strong safety characteristics against HCDA for metal-fueled SFR. The possibility of occurrence of flow blockage would be removed and the core could have coolability by natural convection. However, there is a lack of fundamental knowledge why the metallic fuel has debris bed of debris bed.

Since the fuel is relocated after cladding failure, the intensive heat is transferred from the fuel to coolant or core structure. In thermodynamic point of view, there is a quenching phenomenon when fuel is relocated. Fig. 4-10 shows transmission electron microscopy (TEM) and energy dispersive spectrometry (EDS) image of Wood’s metal in bare condition. The bare condition means Wood’s metal before quenching experiment. Wood’s metal is eutectic alloy with bismuth, lead, tin, and cadmium. The four materials were well mixed in the grain boundary. The microstructures of Wood’s metal were compared between before and after its quenching.

Fig. 4-11 represents TEM and EDS image of Wood’s metal after its quenching. The initial melt temperature is 250 ^{o}C and coolant temperature was 18 ^{o}C. After the quenching, each material consisted

of the eutectic alloy was separated[80-81]. In aspect of classical crystallization theory, crystal growth and morphology formation would occur with separated material. It is a characteristic of eutectic alloy during quenching, which could affect the debris formation. Wood's metal was used to consider this quenching performance of eutectic alloy. In the quenching performance, the surface of separation between the solid and liquid phases is affected by the instantaneous contact interface temperature. To determine the temperature history and rate of progression of the solidification front within the spherical droplet, the Fourier heat conduction equation is solved assuming constant thermophysical properties:

$$\alpha \left[\frac{\partial^2 T(r,t)}{\partial r^2} + \frac{2}{r}\frac{\partial T(r,t)}{\partial r}\right] = \frac{\partial T(r,t)}{\partial t} \tag{4-1}$$

$$T(r,0) = T_m, T(R,0) = T_c \tag{4-2}$$

At the liquid-solid interface (r = a), the two conditions to be satisfied are the energy balance and the continuity condition

$$k\frac{\partial T(r,t)}{\partial r}\Big|_{r=a} = \rho c_p \frac{da(t)}{dt} \tag{4-3}$$

$$T(a,t) = T_i \tag{4-4}$$

The instantaneous contact interface temperature could be calculated from the assumption where there is a no deformation between melt and coolant in semi-infinite geometry. In addition, it is solved as a one-dimensional heat conduction problem. The instantaneous contact interface temperature between melt and coolant is theoretically given by

$$T_i = \frac{T_c + T_m\left(\frac{k_m \rho_m C_{p,m}}{k_c \rho_c C_{p,c}}\right)^{1/2}}{1 + \left(\frac{k_m \rho_m C_{p,m}}{k_c \rho_c C_{p,c}}\right)^{1/2}} \tag{4-5}$$

For a complete description of the problem, specific boundary condition is necessary which describes the surface heat transport process to the coolant. The surface boundary condition can be described in terms of either a heat transfer coefficient for boiling or a constant surface temperature if perfect wetting occurs. Based on a compilation of contact angle measurements between melt and coolant, it was concluded that the interface temperature at the surface of separation could be established like Eq. 4-5.

To investigate the debris size and morphology regarding the debris bed porosity, it is necessary to quantify the debris characteristics. In the present study, concept of characteristic length of debris was proposed. The concept is simply defined using debris volume and surface area. From previous experimental results, it was examined that the high porous debris bed was formed when most of debris had complex shape. The complex shape means ligament-like and flake-like shape. As the debris had complex shape, the surface area would be increased compared to simple debris structure. Thus, the characteristic dimeter of debris was defined by the debris volume over its surface area. When it was assumed that the shape of the debris is uniform as spherical shape with the characteristic length, the debris bed porosity in unit volume would increases as the diameter increases.

The debris after quenching experiments were collected and they were distinguished with initial melt temperature. The instantly contact interface temperature also increased with increase of the melt temperature because the coolant temperature was constant. It was found that the debris morphology was relatively getting complex as the instantly contact interface temperature was increased. Radiograph images for the debris were measured to compare debris shapes in detail. It was clearly confirmed that the debris had ligament-like shape with increase of instantaneous contact interfacial temperatures from radiograph images. Especially, the debris shape was rapidly changed form after initial melt temperature of 300 ^{o}C. Since the instantaneous contact interfacial temperature was over the freezing point of Wood's metal after initial melt temperature of 300 ^{o}C, the complex morphology of debris was formed. When the instantaneous contact interfacial temperature is larger than the freezing point of melt, there was relative long time until thermal equilibrium state between melt and coolant. Thus, the hydraulic force exerted on the melt could affect the shape of melt particle. This force formed debris of complex shape.

In case of the melt ejection condition in simultaneous occurrence of UTOP and ULOF, the instantaneous contact interfacial temperature was lower than the freezing point of Wood's metal. However, the debris bed had high porous structure. Although the debris had simple shape at low the instantaneous contact interfacial temperature, the debris for metal-typed melt had inner pore inside the debris. The inner pore was clearly observed from radiography image using micro-CT. Since the melt was frozen with local coolant vaporization inside the melt itself, the inner pore was formed. Therefore, it is expected that the debris bed of metallic fuel would have high porous debris bed even if the debris shape is simple or the melt is not fragmented. The physical characteristics of metallic fuel ensure coolable state of core with natural convection.

The characteristics of debris bed are mainly determined from physical form of individual debris. Especially, debris bed porosity is affected by debris morphology. In severe accident condition in SFR, metallic fuel had ligament-like shape of debris. This morphology made characteristics of debris bed porosity. The metal fuel had relatively high debris bed porosity. In previous research group, quenching experiments were conducted using molten metal droplet. The debris morphology was analyzed quantitatively. It was insufficient to qualitatively investigate the debris morphology. The present study

was performed with experimental works based on theoretical model regarding rapid solidification. It is suggested that debris morphology is attributed to freezing point and instantaneous contact interface temperature between melt and coolant. As shown in Fig. 4-12, the characteristic dimeter of debris was decreased with decrease of difference between freezing point and instantaneous contact interface temperature between melt and coolant. That means more high porous debris bed was formed with decrease of difference between the two temperatures. Based on rapid solidification experiments, it was shown that high porous debris bed would be formed above porosity of 0.83 based on the reactor accident conditions in ULOF.

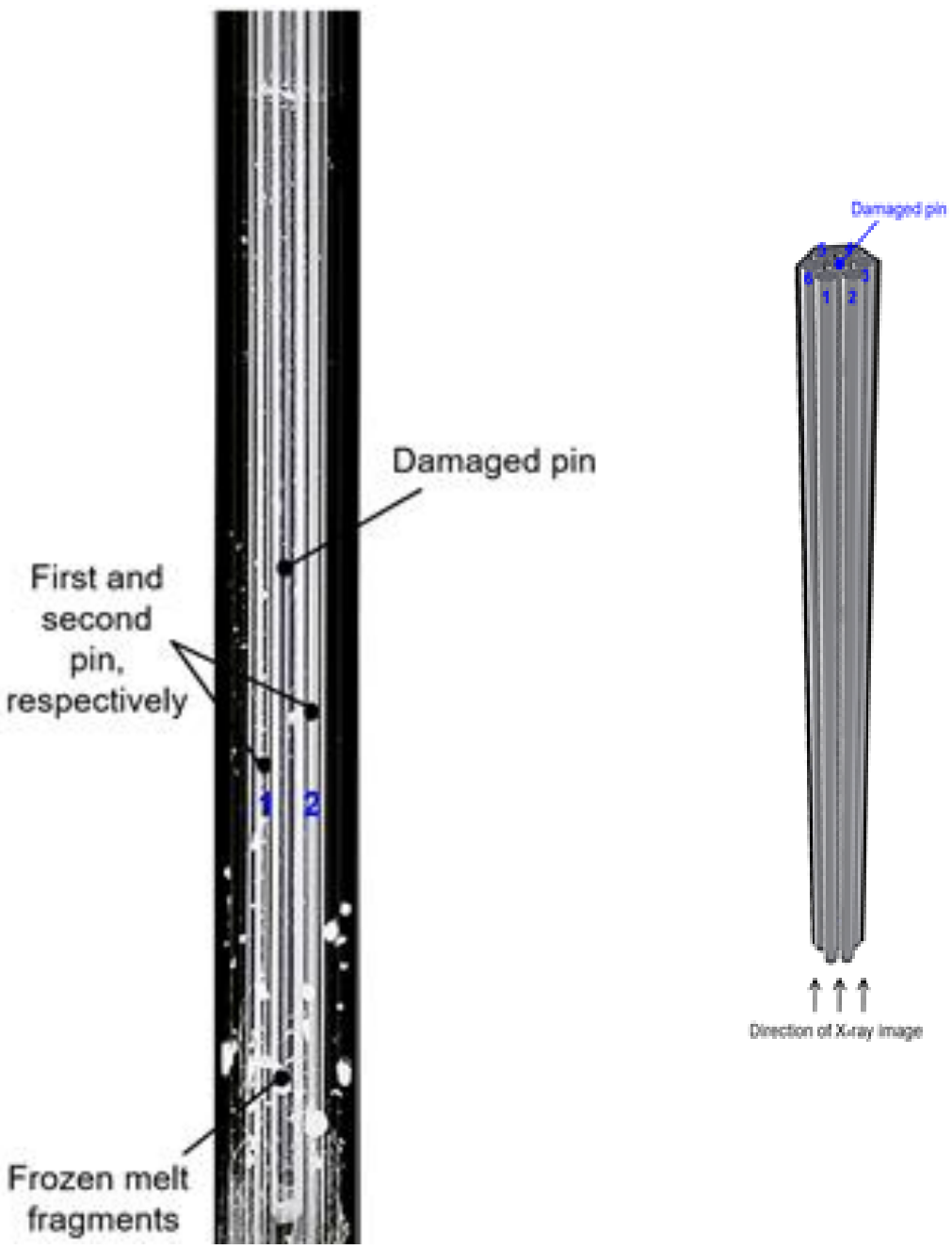

Fig. 4-4 Radiography image of test section after fuel relocation experiment

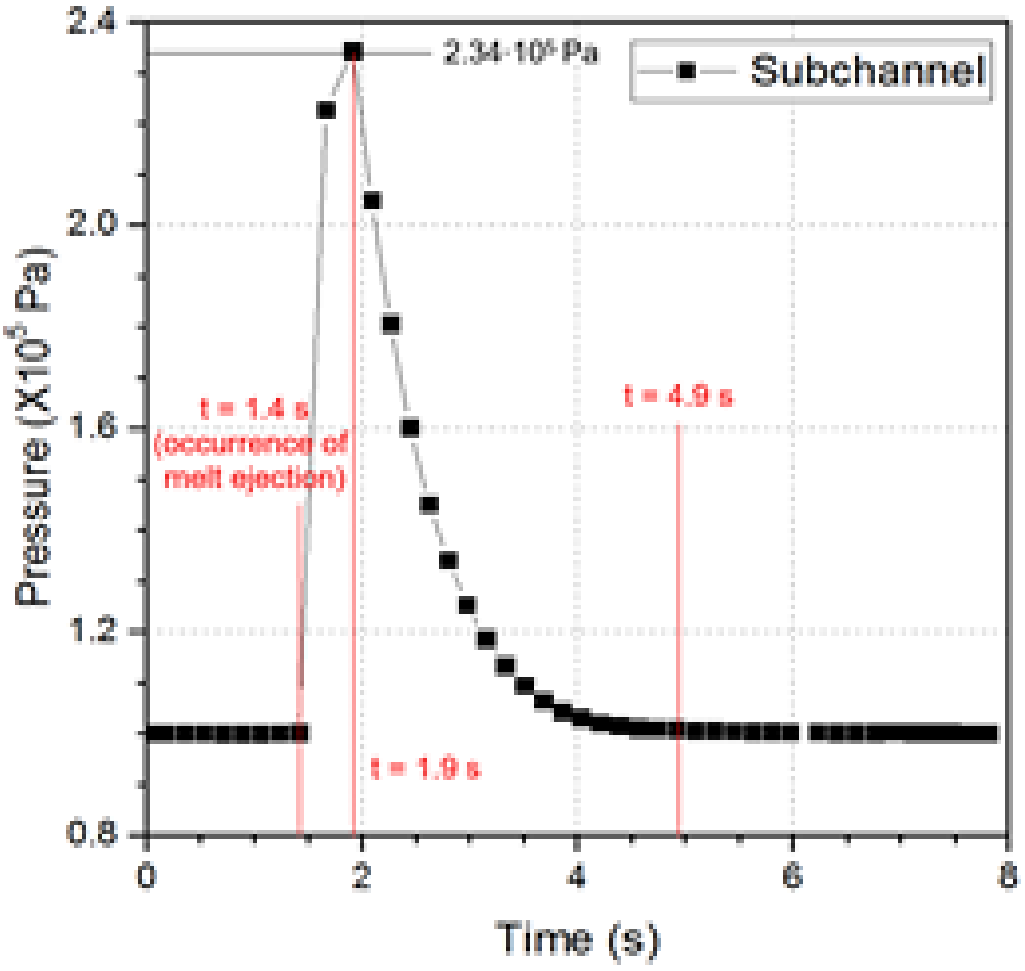

Fig. 4-5 Pressure in test section of preliminary experiment for fuel relocation with time

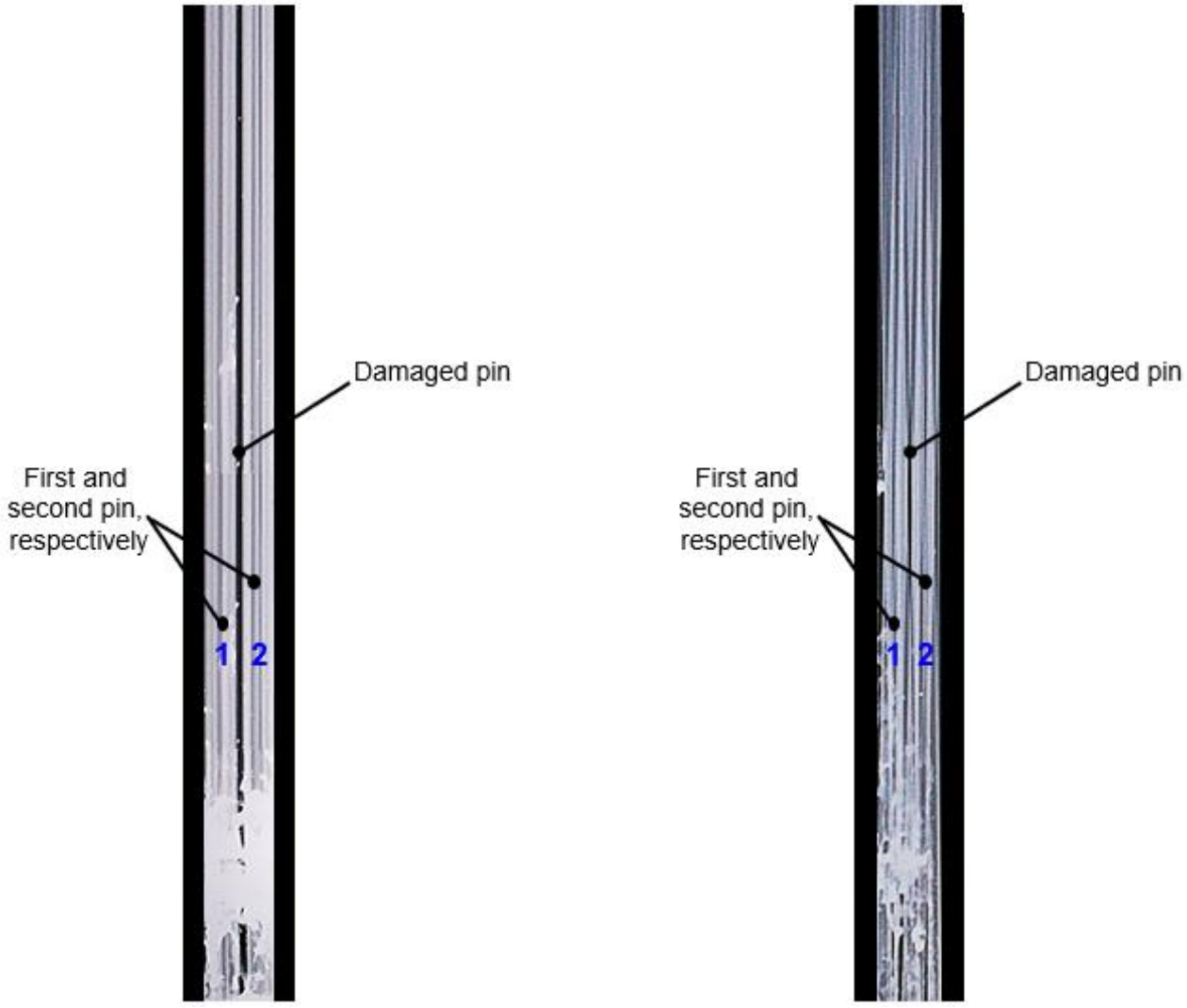

(a) (b)

Fig. 4-6 Radiography image of test section with temperature of intimate pins ((a) $T_{intimate\ pin}$: 21 ºC, (b) $T_{intimate\ pin}$: 90 ºC)

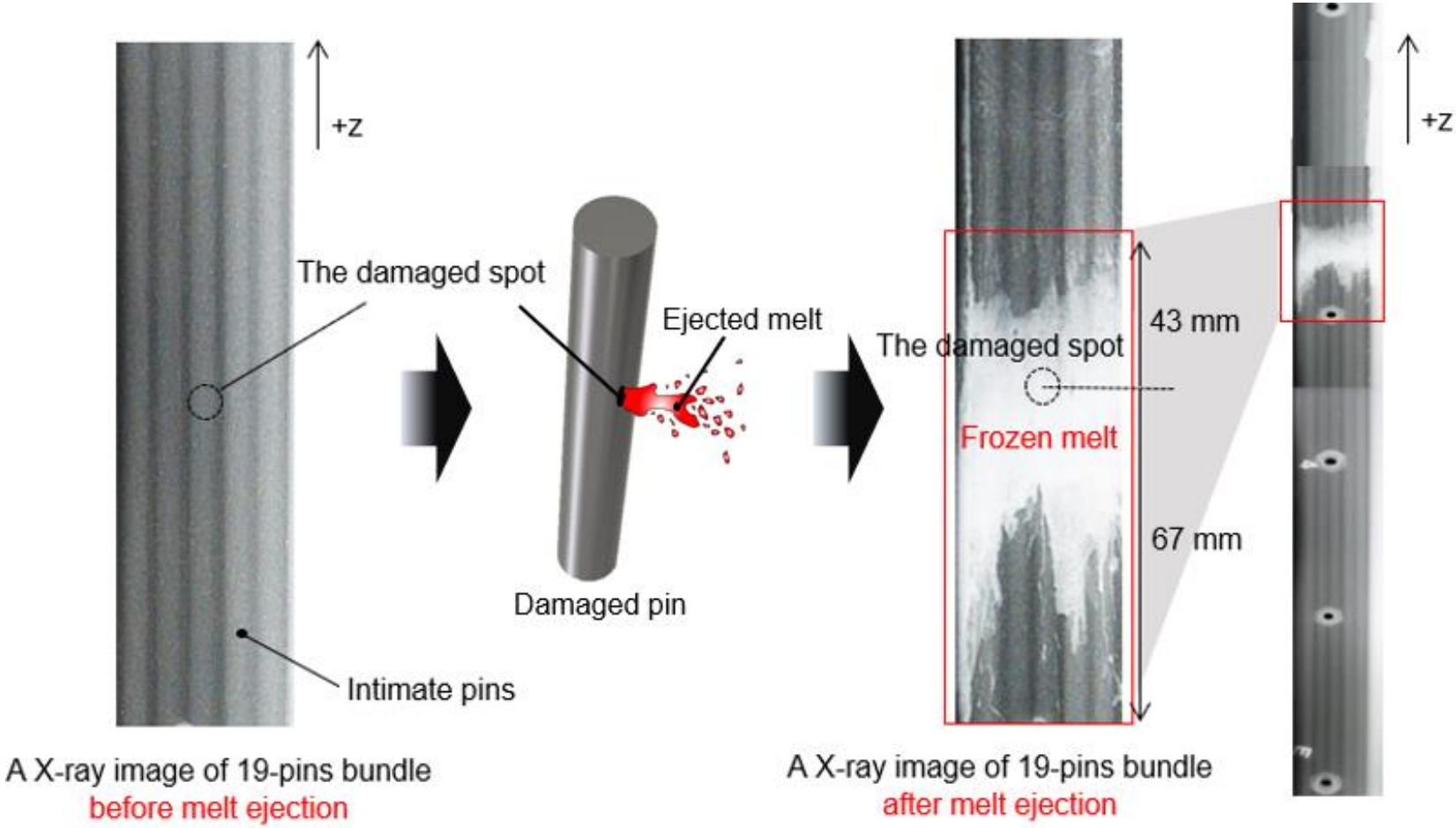

Fig.4-7 Radiography image of melt relocation behavior in simultaneous occurrence of UTOP and ULOF event

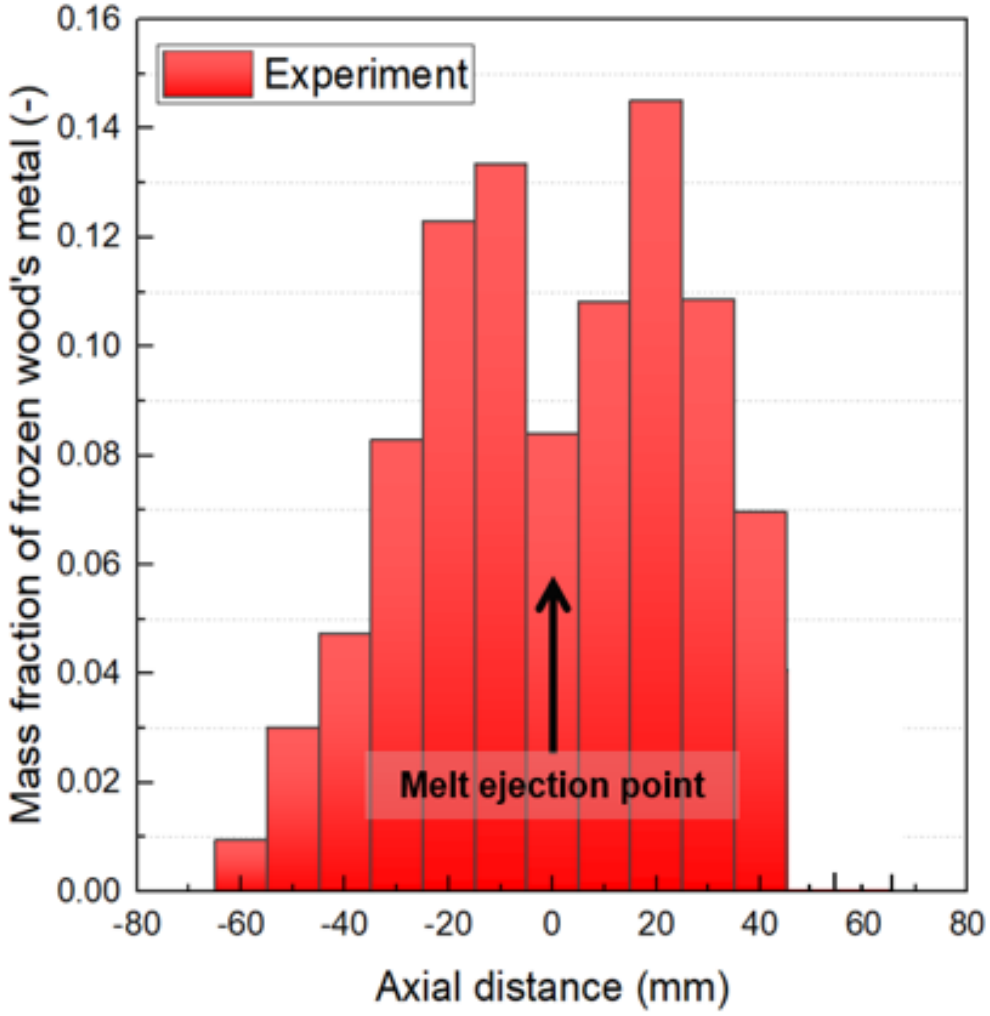

Fig. 4-8 Mass fraction along axial distance in melt relocation behavior concerning simultaneous occurrence of UTOP and ULOF event

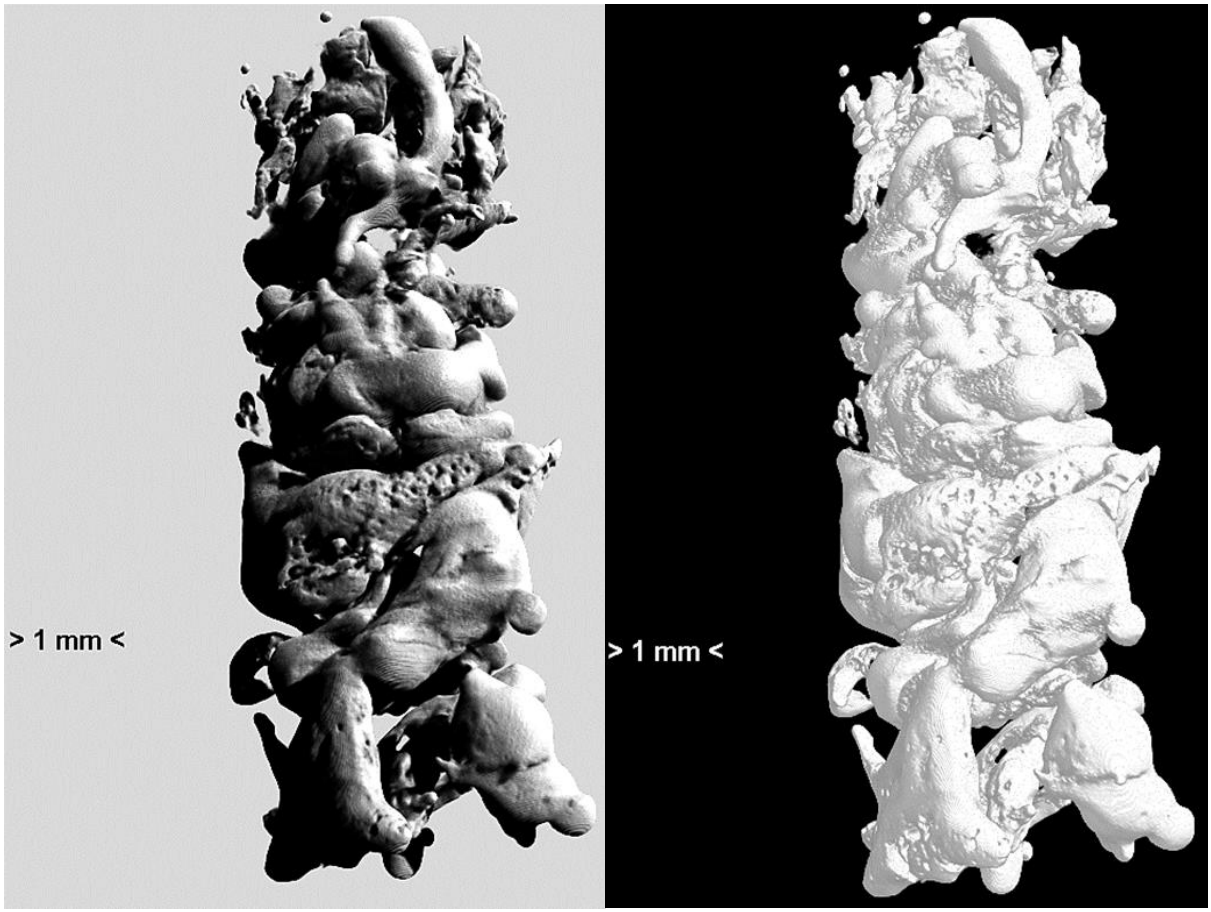

(a) (b)

Fig. 4-9 (a) Raw image and (b) radiography image for Wood's metal debris bed using micro-CT

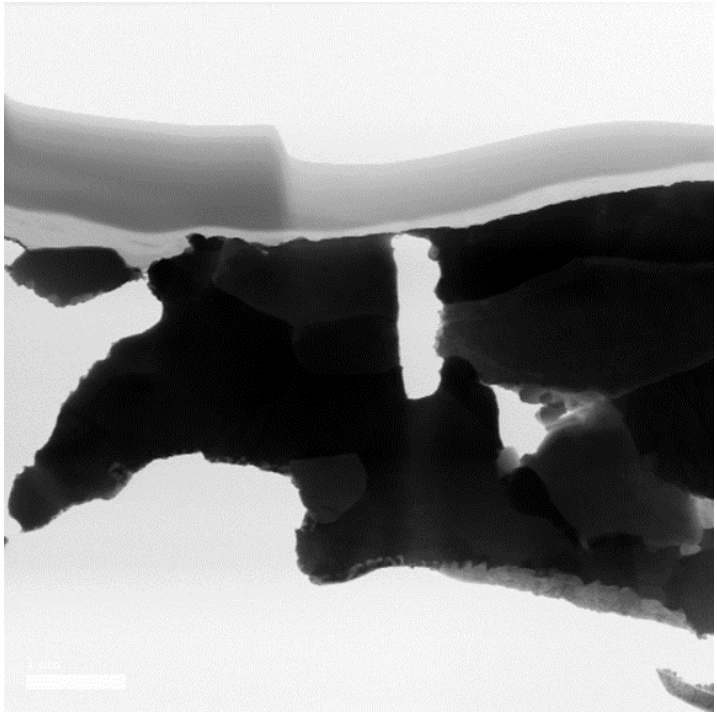

(a)

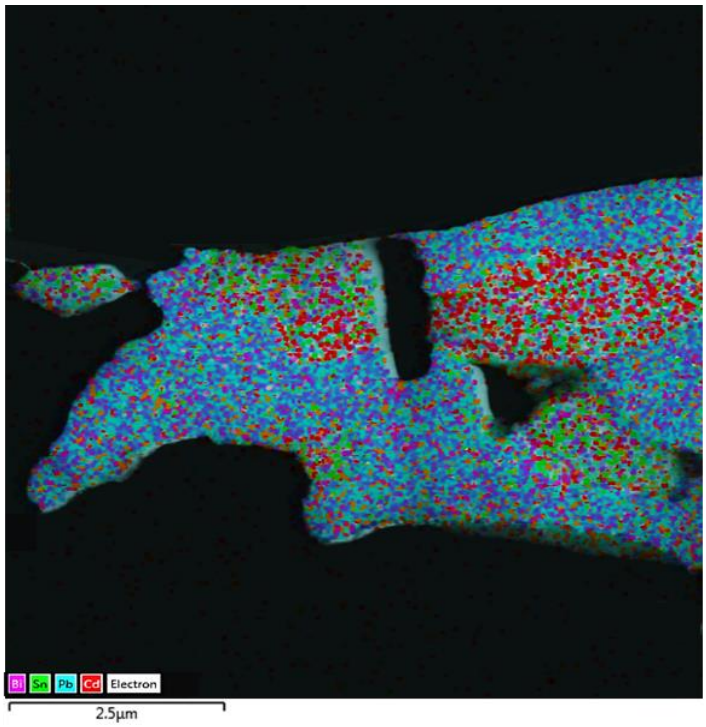

(b)

Fig. 4-10 (a) TEM and (b) EDS image of Wood's metal before quenching experiment

(a)

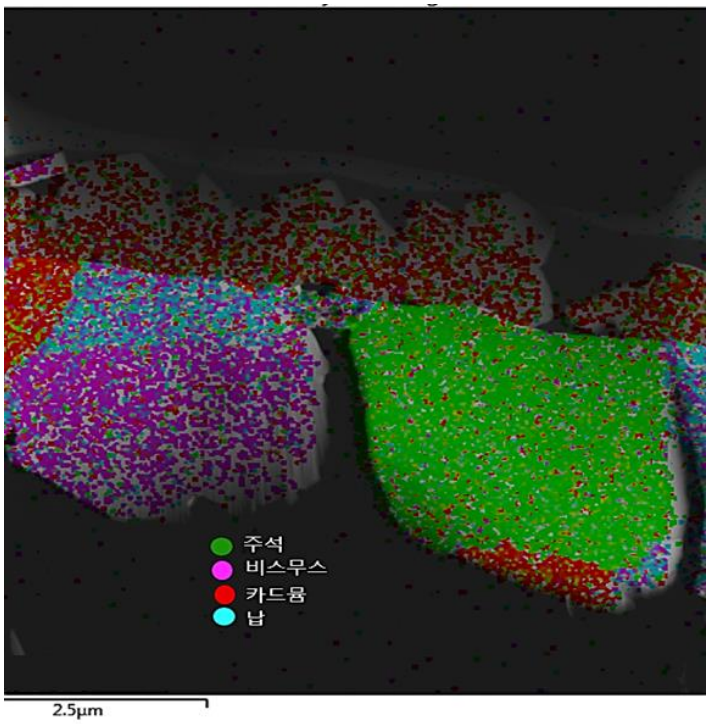

(b)

Fig. 4-11 (a) TEM and (b) EDS image of Wood's metal after quenching experiment ($T_{wood's\ metal}$: 250 °C, T_{water}: 18 °C)

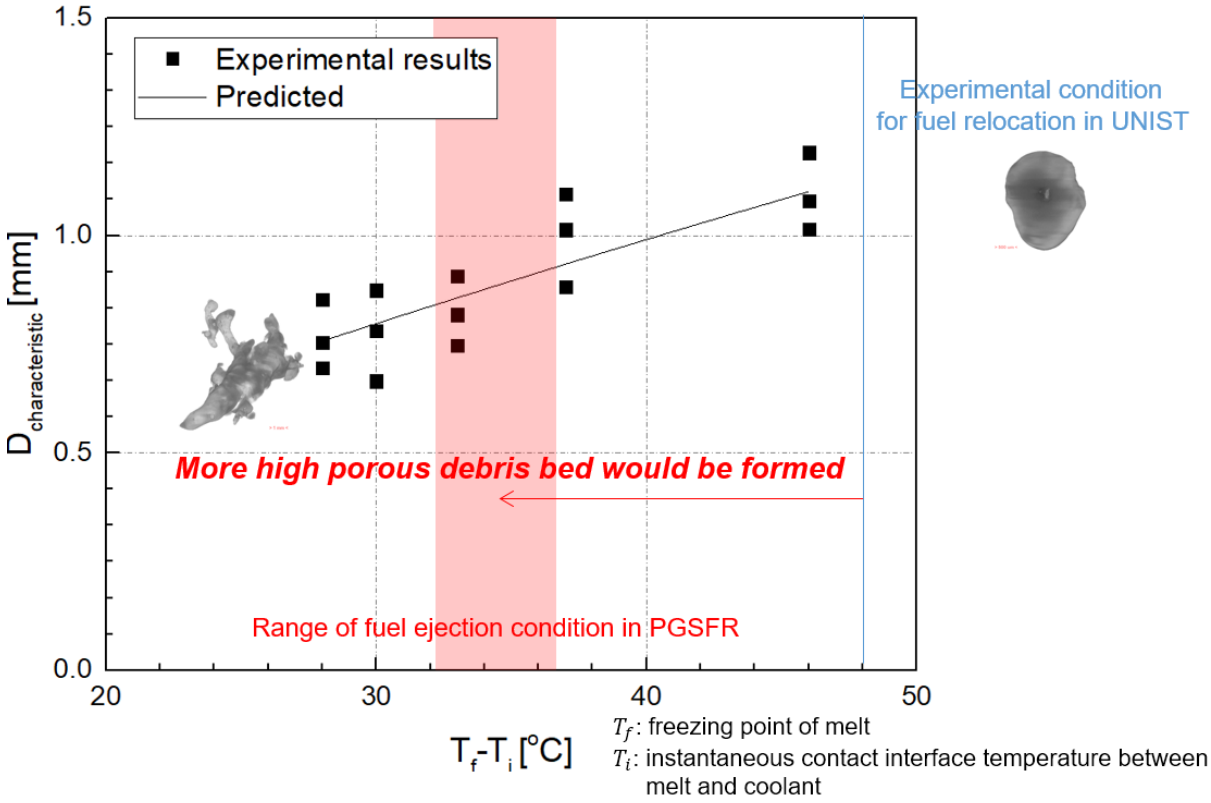

Fig. 4-12 Characteristic diameter of debris with difference between freezing point and instantaneous contact interface temperature between melt and coolant

Chapter 5. CONCLUSIONS AND RECOMMENDATIONS

5.1 Conclusions

In metal-fueled sodium-cooled fast reactor (SFR), molten metal fuel within a subchannel is suggested as an inherent safety strategy in the initiating phase of a hypothetical core disruptive accident (HCDA). This safety strategy provides negative reactivity driven by the melt dispersion, so it could reduce the possibility of occurrence of a severe recriticality. In the initiating phase, the melt could be injected into the subchannel horizontally by the internal pressure of the fuel pin. Complex phenomena occur during intermixing of the melt with the coolant after the horizontal injection of the melt. There is still a lack of fundamental knowledge about the severe accident phenomena and related physics. Therefore, the present study focuses on fuel relocation behavior and debris formation phenomena, which is in specific accident scenario, with experimental approaches.

5.1.1 Fuel relocation behavior

In the initiating phase of the HCDA, occurrence of the recriticality issue is the key safety issue in SFR design with metal fuel. A unique solution for preventing the recriticality issue can be upward dispersion of the melt aimed at an early termination of the accident. Since the melt dispersion conditions differ according to the core region, in the present study, the specific conditions necessary for the molten metal fuel to disperse well were discussed using simulant materials. Upward dispersion of the melt did not occur for a given melt and coolant temperature under the non-boiling condition. Over the range of conditions considered in the study, the behavior of the melt was so static that it was not dispersed at all in the coolant channel. Under the boiling condition, the coolant vapor pressure was built up after the melt injection, in both the coolant-filled and the air-occupied channels. Following the pressure buildup, the melt was dispersed upward sufficiently well. The built-up vapor pressure was one of the driving forces for the upward dispersion of the molten material.

In addition, levitation height where melt was discharged upward was evaluated from experimental results. The experimental parameters as follows: initial melt temperature, initial coolant temperature, melt mass, initial melt pressure, and coolant channel condition. It was found that initial melt pressure was key parameter to determine the levitation height. From the force and energy balance equation, theoretical model for the levitation height was developed. The theoretical model showed well agreement with the experimental results. To consider some force parameter in the theoretical model like friction force of structure, the levitation height in actual metal-fueled SFR would be predicted in HCDA.

5.1.2 Characteristic length of debris

There was high porous debris bed from ex-pin experiment in 19-pin bundle rod structure. The effect of instantaneous contact interface temperature between melt and coolant on debris morphology was investigated. The characteristic length of debris was proposed to represent the debris morphology. It was defined by debris volume over debris surface area. As the characteristic length of debris decreases, the debris bed would have high porous formation. From quenching experiments, it was investigated for physical relationships between the instantaneous contact interface temperature and the characteristic length of debris. That was used to explain the reason why high porous debris would be formed in ULOF condition. In case of metallic fuel, although the debris shape was formed as simple structure which could made low porous debris bed, it has a high porosity of debris bed due to formation of internal pore.

5.2 Recommendations

The fundamental understanding of fuel relocation in initiating phase of HCDA for metal-fueled SFR is important. To improve fuel relocation model in severe accident analysis code, the phenomenological study should be performed. Thus, the observation of fuel relocation behavior would give strong physical insight to study severe accident consequences. The experimental platform to investigate the fuel relocation was setup and it could produce validation data. In addition, the present study proposed simple theoretical model to predict the levitation height where the melt was swept out. The physical relationships were also investigated to account for the debris bed porosity of the metal fuel. Therefore, this study could be used for securing reactor safety for metal-fueled SFR.

References

1. Porter, D.L.; Hilton, C.; Extending sodium fast reactor driver fuel use to higher temperatures. *Proceedings on Evaluation of Uncertainties in Relation to Severe Accidents and Level*, **1988**,
2. Crawford, D.C.; Porter, D.L.; & Hayes S.L.; Fuels for sodium-cooled fast reactors: US perspective. *Nuclear engineering and design*, **1987**, 169, 77-88.
3. Carmack, W.J.; Porter, D.L.; Slezak, S.E.; & Pasedag, W.F.; Metallic fuels for advanced reactors. *Nuclear engineering and design*, **1987**, 169, 89-99.
4. Rouge S.; Dor I., Geffraye G.; Performance of metallic fuels and blankets in liquid-metal fast breeder-reactors, *Workshop on in-vessel core debris retention and coolability*, **1998**.
5. Kittel, J.H.; Frost, B.R.; The integral fast reactor-An overview. *Nuclear engineering and design*, **1997**, 169, 185-195.
6. Rempe, J.L.; Knudson, D.L.; Condie, K.G.; Suh, K.Y.; Cheung, F.B. & Kim, S.B.; Experience with advanced driver fuels in EBR-II. *Nuclear engineering and design*, **1978**, 230, 293-309.
7. Hofman, G.L.; Walters, L.C.; Metallic fast reactor fuels. *Nucl. Eng. Technol*, **1977**, 38
8. Yang, J.; Dizon, M.B.; Cheung, F.B.; Rempe, J.L.; Suh, K.Y. & Kim, S. B.; History of fast reactor fuel development. *Nuclear engineering and design*, **1978**, 236, 1089-1098.
9. Walters, L.C.; Thirty years of fuels and materials information from EBR-II. *Nuclear engineering and design*, **1997**, 169, 59-76.
10. Porter, D.L.; Fuel test plan. *In Proceedings of the 2004 international congress on advances in nuclear power plants-ICAPP'04*, **2004**
11. Pitner, A.L.; Baker, R.B.; Metal fuel test program in the FFTF. *Nuclear Engineering and Design*, **1993**, 258, 176-183.
12. Tokiwai, M.; Yokoo, T.; Nishimura, T.; Horie, M.; & Kinoshita, M.; Metallic fuel core concept and its potential for passive shutdown features. *Proceedings of International conference on fast reactors and related fuel cycles*, **1991.**
13. Pitner, A.L.; Baker, R.B; Metallic fuel test program in the FFTF. *ANL report,* **1976**.
14. Porter, D.L, Tsai, H.; Full-length metallic fast reactor fuel pin test in FFTF (IFR-1)*, INL report,* **1993**.
15. Planchon, H.P.; Singer, R.M.; & Mohr, D.; The experimental breeder reactor II inherent shutdown and heat removal tests-results and analysis. *Nuclear Engineering and Design*, **1986**, 91, 3, 287-296**.**
16. Pahl, R.G.; Porter, D.L; Irradiation behavior of metallic fast reactor fuels. *Nuclear technology*, **1988**, 161, 210-267.
17. Pahl, R.G.; Wisner, R.S.; & Crawford, D.C.; Steady state irradiation testing of U-Pu-Zr fuel to >18^% burnup. *Nuclear Engineering and Design*, **1997**, 169, 1-48.

18. Walter, C.M.; Lahti, J.A.; Compatibility of U-Pu-Fz fuel alloys with potential cladding materials. *Nuclear technology*, **1966**, 152, 162-169.
19. Vishnev, I.; Compatibility between metallic U-Pu-base fuels and potential cladding materials. *J. Eng. Phys. Thermophys*. **1973**, 24, 43–48.
20. Lyon, D.; Reaction of rare earth elements with iron base alloy. *Intern. Adv. Cryog. Eng*. **1965**, 10, 371–379.
21. Pahl, R.G.; Experimental studies of U-Pu-Zr fast reactor fuel pins in the experimental breeder reactor-II. *Int. Nucl. Eng*. **1993**, 16, 414–422.
22. Keiser, D.D.; The development of FCCI zones in irradiated U-Zr and U-Pu-Zr fuel elements with stainless steel cladding. *Nucl. Eng. Technol*, **1996,** 43, 195-204.
23. Keiser, D.D.; Fuel-cladding interaction layers in irradiated U-Zr and U-Pu-Zr fuel elements. *Nucl. Eng. Technol*, **1997**, 51, 3025-3031.
24. Leibowitz, L.; Blomquist, R.A.; Thermal conductivity and thermal expansion of stainless steels D9 and HT9. *Int. J. Heat Mass Transfer*, **1989**, 87, 233107.
25. Cohen, A.B.; Tsai, H.; Fuel-cladding compatibility in U-19Pu-10Zr/HT9-clad at elevated temperatures. *Journal of Nuclear Materials*, **1993**, 250, 720-724.
26. Pahl, R.G.; Lahm, C.E.; Performance of HT9 clad metallic fuel at high temperature. *Journal of Nuclear Materials*, **2003**, 83, 3374.
27. Hayes, S.L.; SAFE: A compute code for the steady state and transient thermal analysis of LMR fuel elements. *Nucl. Eng. Technol*. **1993**, 43, 217–242.
28. Hofman, G.L.; Hayes, S.L.; & Petri, M.C.; Temperature gradient driven constituent redistribution ion U-Zr alloys. *Journal of Nuclear Materials.*, **1996**, 97, 023103.
29. Yeon, S.K.; Hofman, G.L.; & Yacout, A.M.; Migration of minor actinides and lanthanides in fast reactor metallic fuel. *Nuclear Engineering and Design*, **2009**, 239, 941–948.
30. Weast, R.C; CRC handbook of chemistry and physics. CRC Press Online, **2012**, 36, 525-531.
31. Mariani, R.D.; Porter, D.L.; Lanthanides in metallic nuclear fuels, *Journal of Nuclear Material*, **1983**, 26, 389-399.
32. Sadasivan P.; Chappidi P., Unal, C.; Nelson R.; Modelling of constituent redistribution in U-Pu-Zr metallic fuel, *Journal of Nuclear Material*, **1992**, 19, 801-815.
33. Karahan, A.; Buongiorno, J.; Modeling of the steady-state behavior of metallic fuels in liquid metallic fast reactos, *MIT Center for Advanced Energy Studies Reports*, **2009.**
34. Ogata, T.; Diffusion of cerium in uranium-zirconium solid solutions, *Japan Institute of Metals, Materials and Transactions,* **2003**.
35. Kim, T.K.; Taiwo, T.A.; Feasibility study of ultra-long life fast reactor core concept, *Proceedings of PHYSOR 2010,* **2010.**

36. Nishimura, S.; Kinshita, I.; Sugiyama, K. I.; Okada, R.; & Ueda, N; Thermal Interaction Between Molten Metal and Sodium: Examination of the Fragmentation Mechanism of Molten Jet. *Proceedings of International Conference on Nuclear Engineering,* **2002**, 933-942.
37. Nishimura, S.; Kinoshita, I.; Sugiyama, K. I.; & Ueda, N.; Thermal interaction between molten metal jet and sodium pool: effect of principal factors governing fragmentation of the jet. *Nuclear technology*, **2005**, 149, 2, 189-199.
38. Bauer, T.H,; Wright, A.E.; & Robinson, W.R.; Behavior of metallic fuel in TREAT transient overpower tests. *ANL report*. **1998**.
39. Bauer, T.H.; Wright, A.E.; Robinson, W.R.; & Klickman, A.E.; Behavior of metallic fuel in TREAT transient overpower tests, *Proceeding of American Nuclear Society***, 1986**, 306-307.
40. Bauer, T.H.; Wright, A.E.; Robinson, W.R.; Holland, J.W.; & Rhodes, E.A.; Behavior of modern metallic fuel in TREAT transient overpower tests. *Nuclear Technology*, **1990**, 92, 3, 325-352.
41. Robinson, W. R.; Bauer, T.H.; & Wright, A. E., First TREAT transient overpower tests on U-Pu-Zr Fuel: M5 and M6, *ANL report*, CONF-871101-06, **1987**.
42. Pilch, M., Erdman, C.A.; Use of breakup time data and velocity history data to predict the maximum size of stable fragments for acceleration-induced breakup of a liquid drop. *International Journal of Multiphase Flow*. **1987**, 13, 6, 741-757.
43. Kim, T.; Forttner, J.; Harbaruk, D.; Gerardi, C.; & Chang, Y.I.; Experimental studies on eutectic formation between metallic fuel and HT-9M cladding in a single-pin core structure of a sodium-cooled fast reactor. *Journal of Nuclear Materials*, **2018**, 105-118.
44. Kim, T.; Harbaruk, D.; Gerardi, C.; Farmer, M.; & Chang, Y.I.; Experimental studies on metallic fuel relocation in a single-pin core structure of a sodium-cooled fast reactor. *Nuclear Engineering and Design*, **2017**, 322, 204-214.
45. Gabor, J.D.; Purviance, R.T.; & Aeschlimanft, R.W.; Dispersion and thermal interactions of molten metal fuel settling on a horizontal steel plate through a sodium pool. *ANL report*, CONF-890819. **1989**.
46. Gabor, J.D.; Purviance, R.T.; Aeschlimanft, R.W.; & Spencer, B.W.; Characterization of IFR metal fuel fragmentation. *Transaction of American Nuclear Society*, CONF-870601, **1987**, 54.
47. Gabor, J.D.; Purviance, R.T.; Aeschlimann, R.W.; & Spencer, B.W.; Breakup and quench of molten metal fuel in sodium. Report of Argonne National Laboratory, **1988**.
48. Sato, I.; Tobita, Y.; Konishi, K.; Kamiyama, K.; & Toyooka, J.; Safety strategy of JSFR eliminating severe recriticality events and establishing in-vessel retention in the core disruptive accident. *Journal of nuclear science and technology*. **2010**, 48, 4, 556-566.
49. Abe, Y.; Kizu, T.; Arai, T.; & Nariai, H.; Study on thermal-hydraulic behavior during molten material and coolant interaction. *Nuclear engineering and design*. **2004**, 230, 277-291.

50. Matsuo, E.; Abe, Y.; Chitose, K.; Koyama, K.; & Itoh, K.; Study on jet breakup behavior at core disruptive accident for fast breeder reactor. *Nuclear engineering and design*. **2008**, 238,1996-2004.
51. Dinh, T. N.; Bui, V.A.; & Nourgaliev, R.R; Experimental and analytical studies of melt jet-coolant interactions: a synthesis. *Nuclear engineering and design*. **1999**, 189, 1, 299-327.
52. Saito, M.; Experimental study on penetration behavior of water jet into Freon-11 and liquid nitrogen. *National Heat Transfer Conference*. **1988**, 173-183.
53. Fox, R.W.; McDonald, A.T.; & Pritchard, P.J.; Introduction to fluid mechanics. *John Wiley & Sons*. **1985**, 7.
54. Sugiyama, K. I.; Fragmentation mechanism of a single molten-copper drop falling in sodium pool with its melting point. *J. Atomic Energ. Soc,* **2000**, 42, 83-86.
55. Masuba, K.; Imahori, S.; & Isozaki, M.; Experimental study on void development behavior in a simulated coolant channel. *Proceedings of the 6th International Topical Meeting on Nuclear Reactor Thermal Hydraulics*. **2004**, N6P077.
56. Konovalikhin, M.J.; Investigations on melt spreading and coolability in a LWR Severe accident (PhD thesis). *Royal Institute of Technology*. **2001.**
57. Matsuba, K.; Isozaki, M.; Kamiyama, K.; & Tobita, Y.; Fundamental experiment on the distance for fragmentation of molten core material during core disruptive accidents in sodium-cooled fast reactors. *Nuclear safety and simulation*. **2013**, 4, 4.
58. Matsuba, K.; Isozaki, M.; Kamiyama,; & K, Tobita Y. Experimental study on upward fuel discharge during core disruptive accident in JSFR: Results of and out-of-pile experiment with visual observation. *The 19th International Conference on Nuclear Engineering (ICONE19-43993).* **2011**.
59. Matsuba, K.; Isozaki, M.; Kamiyama, K.; Tobita Y.; Mechanism of upward fuel discharge during core disruptive accidents in sodium-cooled fast reactors. *Journal of engineering of gas turbines and power*. **2013**, 135, 032901-1.
60. Kamiyama, K.; Saito, M.; Matsuba, K.; Isozaki, M.; & Sato, I.; Experimental study on fuel-discharge behaviour through in-core coolant channels. *Journal of Nuclear Science and Technology*. **2013**, 50, 6, 629-644.
61. Kamiyama, K.; Konishi, K.; Sato, I.; Toyoka, J.; & Matsuba, K.; An experimental study on heat transfer from a mixture of solid-fuel and liquid-steel during core disruptive accidents in sodium-cooled fast reactors. *The 10th International Topical Meeting on Nuclear Thermal-Hydraulics, Operation and Safety (NUTHOS10-1050).* **2014**.
62. Laufer, J.;New trends in experimental turbulence research. Annual Review of Fluid Mechanics. **1975**, 7, 1, 307-326.
63. Schins, H.; Gunnerson, F. S.; Boiling and fragmentation behaviour during fuel-sodium interactions. *Nuclear engineering and design*, 1986, 91, 3, 221-235.

64. Thakre, S., Manickam, L. & Ma, W.; A numerical simulation of jet breakup in melt coolant interactions. *The 10th International Topical Meeting on Nuclear Thermal-Hydraulics, Operation and Safety (NUTHOS10-1023)*. **2014**.
65. Benz, R.; Schins, H.; Boiling fragmentation of molten stainless steel and copper in sodium. *Nuclear Engineering and Design*, 1982, 72, 3, 429-437.
66. Itagaki, W.; Sugiyama, K. I.; Nishimura, S.; & Kinoshita, I.; Fragmentation of a single molten copper and silver droplets penetrating a sodium pool with solid crust. *Proceedings of 13th Int. Conf. on Nucl. Eng*. **2005**.
67. Schins, H.; Gunnerson, F. S.; Boiling and fragmentation behaviour during fuel-sodium interactions. *Nuclear engineering and design*, **1986**, 91, 3, 221-235.
68. Ishii, M.; Zuber, N. Drag coefficient and relative velocity in bubbly, droplet or particulate flows. *AIChE Journal*, **1979**, 25, 5, 843-855.
69. Sugiyama, K.I.; Sotome, F.; & Ishikawa, M.; Thermal interaction in crusted melt jets with large-scale structures. Nuclear engineering and design, **1999**, 189, 329-336.
70. Epstein, M.; Grolmes, M. A.; Henry, R. E.; & Fauske, H. K.; Transient freezing of a flowing ceramic fuel in a steel channel. *Nuclear Science and Engineering*, **1976**, 61, 3, 310-323.
71. Berthoud, G.; Duret, B.; The freezing of molten fuel: reflections and new results. *Proceeding of In. Fourth international topical meeting on nuclear reactor thermal-hydraulics (NURETH-4)*, **1989**.
72. Berthoud, G.; Relocation of molten fuel determination of the interfacial resistance. *Proceeding of fast reactor safety meetings*, **1994**.
73. Soussan, P.; Propagation and freezing of molten material: interpretation of experimental results. Proceeding of Int. Fast Reactor Safety Meeting, **1990**.
74. Kurz, W.; Fisher, D. J.; Fundamentals of solidification (Vol. 1). *Trans tech publications*, **1986**.
75. Brear, D.; Modeling of fuel freezing for reactor safety analysis. *Proceedings of Fall Meeting of the Atomic Energy Society of Japan*, **1997.**
76. Maschek, W.; Experimental investigations of freezing phenomena of liquid/particle mixtures in the THEFIS facility and their theoretical interpretation. *Proceedings of In. Proc. Int. Fast Reactor Safety Meeting*, **1990**.
77. Pai, B. C., Jones, H.; Effect of experimental variables on casting fluidity and fluid life of liquid tin. Materials science and technology, **1985**, 1, 5, 398-404.
78. Epstein, M.; Henry, R. E.; Grolmes, M. A.; Fauske, H. K.; Goldfuss, G. T.; Quinn, D. J.; & Roth, R. L.; Analytical and experimental studies of transient fuel freezing, *Report of Argonne National Laboratory*, **1976**.
79. Fieg, G.; Henkel, P.; Möschke, M.; Schub, I.; & Werle, H.; Freezing phenomena of flowing melts in nonmelting and melting tubes. Proceedings of In. Science and technology of fast reactor safety. **1987**.

80. Schumacher, P.; Greer, A. L.; Worth, J.; Evans, P. V.; Kearns, M. A.; Fisher, P.; & Green, A. H.; New studies of nucleation mechanisms in aluminum alloys: implications for grain refinement practice. *Materials science and technology*, **1998**, 14, 5, 394-404.
81. Kashyap, K. T.; Chandrashekar, T; Effects and mechanisms of grain refinement in aluminum alloys. *Bulletin of Materials Science*, **2001**, 24, 4, 345-353.

Acknowledgement (감사의 글)

제 인생의 돛이신 지도교수님 방인철 교수님께 가장 감사드립니다. 돛이 있어야만 배가 올바른 방향으로 향하듯, 교수님의 가르침과 믿음으로 인해 제가 학자로서 올바른 방향으로 성장할 수 있었습니다. 교수님께서 주신 소중한 기회가 아니었다면 지금의 저는 없다고 생각합니다. 교수님께 전하는 감사의 글들로 제 마음을 전하기에는 한없이 부족합니다. 교수님 은혜 잊지 않고 앞으로 갚으며 연구자로서 살겠습니다. 그리고 교수님께서 말씀하신 보이지 않는 사명감. 이제는 조금은 알 것도 같습니다. 어디에 있더라도 사명감을 갖고 새로운 것에 도전하는 제자가 되겠습니다.

학위 논문을 심사해주신 이승준 교수님, 윤의성 교수님, 정동욱 교수님, 김윤재 교수님께 감사드립니다. 학위과정 동안 타 학교와의 공동 연구를 통해 스스로의 연구 역량을 향상시킬 수 있었습니다. 공동 연구를 수행하면서 제가 성장할 수 있도록 아낌없는 조언을 주신 정동욱 교수님과 김윤재 교수님께 감사드립니다. 가르침 잊지 않고 더 성장하겠습니다.

학위과정동안 대부분의 시간을 저와 함께한 원자력 열수력 및 안전 연구실 식구들에게 감사드립니다. 대학원 진학에 대한 고민을 함께 해주셨던 이승원 박사님, 김성만 선배님. 새로운 아이디어로 흥미로운 연구를 하시고, 저에게 많은 가르침을 주신 박성대 박사님. 고민에 대해 공감해주시고 조언 해주셨던 강사라 박사님. 때로는 친한 동네 형처럼, 때로는 연구실 선배로서 저를 대해주신 서한 박사님. 선배님들의 격려가 학위과정동안 많은 힘이 되었습니다. 감사합니다. 연구실의 모범이자 리더이신 김경모 박사님. 표현은 못 했지만 형을 닮고 싶습니다. 바른 길이 무엇인지 제시해 주셨던 서석빈 박사님. 형처럼 후배들을 포용하고 싶습니다. 동고동락하며 함께 시간을 보낸 성보 형, 똑부러지는 인국이 형, 동갑으로 동기로서 함께 했던 영신, 든든하고 믿음직한 민호,

친구이지만 연구실 후배였던 한얼이, 열정적인 막내 지용이, 도영이까지 우리 연구실 식구들 덕분에 여기까지 오는데 큰 힘이 되었습니다. 모두에게 감사합니다.

학부 시절 한국원자력연구원 인턴 학생인 저를 가르쳐 주셨던 김형태 박사님. Argonne National Laboratory 연구 파견 동안 저를 챙겨주시고 이끌어 주신 김태일 박사님. 6 개월 간의 ANL 파견 동안 박사님 덕분에 큰 어려움 없이 소중한 경험을 할 수 있었습니다. ANL 에서 함께 문제를 고민하고 디스커션 해주신 Dzmitry, Craig, 그리고 장윤일 박사님. 덕분에 연구자로서 문제를 풀어가는 방법에 대해 배웠습니다. 감사합니다.

20 대를 함께한 내 친구들 성오, 상현이, 명준이. 두 번 다시 돌아오지 않을 20 대를 너희와 함께할 수 있어서 나에겐 더할 나위 없이 소중했고, 앞으로도 같이 옆에서 걸어가자. 학부때부터 함께 많은 추억을 만든 태원이, 철민이, 관윤이형, 승창이, 승현이형, 태호형. 고마워. 그리고 실험장치를 제작해주신 네오시스 사장님 감사합니다.

세상에서 가장 소중한 우리 가족에게 감사합니다. 존경하는 아빠, 사랑하는 엄마, 아끼는 내동생. 애기처럼 저를 챙겨주시고 격려해주시는 외할머니, 그리고 제 박사 졸업식을 누구보다 가장 보고 싶으셨던 하늘에 계신 친할머니. 모두에게 받은 사랑, 앞으로 베풀고 갚겠습니다. 사랑하고, 감사합니다.

지금의 제가 있을 수 있는 건 모두 제 곁에 계신 감사한 분들 덕분입니다. 매사에 겸손하고, 제가 하는 역할에 대한 무게감을 느끼며 책임을 다 하겠습니다. 아무것도 모르던 20 살. 처음 울산으로 향하는 버스를 탔을 때 긴장과 설레임을 아직도 잊을 수 없습니다. 학자로서의 버스를 탄 지금. 또다시 긴장과 설레임을 느낍니다. 올바른 길로 달려나가겠습니다. 모든 분들께 진심으로 감사드리며 이 글을 마칩니다.